International Journal of Antennas and Propagation

Advances in Antenna Technology for Wireless Handheld Devices

Guest Editors: Jaume Anguera, Aurora Andújar, Minh-Chau Huynh, and Charlie Orlenius

Advances in Antenna Technology for Wireless Handheld Devices

International Journal of Antennas and Propagation

Advances in Antenna Technology for Wireless Handheld Devices

Guest Editors: Jaume Anguera, Aurora Andújar, Minh-Chau Huynh, and Charlie Orlenius

Editorial Board

Contents

Hindawi Publishing Corporation
International Journal of Antennas and Propagation
Volume 2013, Article ID 376531, 2 pages
http://dx.doi.org/10.1155/2013/376531

Editorial

Advances in Antenna Technology for Wireless Handheld Devices

Jaume Anguera,[1,2] Aurora Andújar,[1] Minh-Chau Huynh,[3,4] and Charlie Orlenius[5]

[1] *Technology and Intellectual Property Rights Department, Fractus, Barcelona, Spain*
[2] *Electronics and Communications Department, Ramon Llull University, Barcelona, Spain*
[3] *Systems and Concept, Sony Mobile, Redwood City, CA, USA*
[4] *Communications Systems Group, LitePoint Corporation, CA, USA*
[5] *Bluetest AB, Gothenburg, Sweden*

Correspondence should be addressed to Jaume Anguera; jaume.anguera@fractus.com

Received 16 December 2012; Accepted 16 December 2012

Communication between two distant points has been a constant challenge for mankind, from ancient smoke signals, to telegraph, to finally wireless communication through electromagnetic signals. This evolution represents a constant effort to improve the quality and effectiveness of distance communication with ever-evolving techniques to enhance the delivery of contents, from voice to data. Wireless handheld devices are the most representative paradigm of these efforts. Since they first appeared, their size has continuously been shrinking, while their functional capabilities have been increasing, hence creating the never-ending challenge in antenna design. In this regard, the antenna community often has the important role of designing low-profile, small, and multiband antennas capable of being integrated within the handset platform as well as capable to coexist with multiple antenna systems in order to satisfy the strict demands of emergent multifunction wireless devices. Furthermore, the complexity of handheld antenna design is continuously increasing, not only by the pressure of the market needs, but also by the duty of safety regulations which require efficient antennas capable of radiating as much power as possible in free-space conditions, while minimizing the power radiated towards the human head.

Antenna modeling in handset devices, using electromagnetic simulation software, has improved significantly thanks to the progress of computing hardware. Complex environments surrounding the antenna, such as a handset device held beside a human head, and precise details on nearby components, including the presence of a loudspeaker in the antenna volume, can be modeled accurately to predict antenna performance that is closer to reality, without sacrificing simulation speed. This evolution considerably contributes to simplify the antenna design process.

Not only the simulation tools have considerably evolved in the latest years, but also the measurement systems have been forced to evolve for satisfying the emergent communication systems requirements. These recent advances in measurement systems and methodologies have been hot topics in the antenna measurement community for capturing, for instance, radiated performance in the emergent LTE and MIMO antenna systems. These next generation systems have already started to appear in wireless handheld devices in the consumer market. However, new measurement methods need to be developed as these antenna systems are to be used as well as tested in fading environments.

Finally, the commercial success of wireless handheld devices leads to an improvement of the manufacturing techniques and processes. This is not only important for reducing the cost of mass production, but also for enhancing the design performance and size in a controlled fashion.

This special issue contains five papers that gather some of the recent advancements in handset antenna design. In the paper entitled "*Band-notched ultrawide band planar inverted-F antenna,*" an ultrawide planar inverted-F antenna covering the 3.4 GHz–11.2 GHz band with a band-notch at 5.08 GHz–6 GHz is presented. The wideband behavior is obtained by parasitic elements whereas the band-notch is achieved by a W-shaped slot on the top radiating element of the antenna.

The paper "*Compact dual-band dual-polarized antenna for MIMO LTE applications*" proposes an antenna system operating in the LTE bands 700 MHz–862 MHz and 2.5 GHz–2.69 GHz. The design is composed of two compact orthogonal monopoles to perform diversity in mobile terminals such as tablets or laptops.

In the paper, "*Printed internal pentaband WWAN antenna using chip-inductor-loaded shorting strip for mobile phone application*", a compact size on-Board printed antenna using capacitive coupled-fed excitation to generate multiple resonant modes for pentaband WWAN operation (GSM850/900, GSM1800/1900, UMTS2100) is designed.

The paper "*Evaluation of SAR distribution in six-layer human head model*" numerically analyzes a single layer and a six-layer human head model for SAR computation at the 900 MHz frequency.

Finally, in the paper "*Advances in antenna technology for wireless handheld devices*", the evolution of wireless handheld devices, regulations, and challenges in today's smartphones, and handset characterization are reviewed. Finally, recent advancements in antenna technology for wireless handheld or portable devices are presented.

Jaume Anguera
Aurora Andújar
Minh-Chau Huynh
Charlie Orlenius

Hindawi Publishing Corporation
International Journal of Antennas and Propagation
Volume 2013, Article ID 838364, 25 pages
http://dx.doi.org/10.1155/2013/838364

Review Article

Advances in Antenna Technology for Wireless Handheld Devices

Jaume Anguera,[1,2] Aurora Andújar,[1] Minh-Chau Huynh,[3] Charlie Orlenius,[4] Cristina Picher,[1] and Carles Puente[1,5]

[1] *Technology and Intellectual Property Rights Department, Fractus, 08190 Barcelona, Spain*
[2] *Electronics and Communications Department, Universitat Ramon Llull, 08022 Barcelona, Spain*
[3] *Systems and Concept, Sony Mobile, Redwood City, CA 94085, USA*
[4] *Bluetest AB, Lindholmsallén 10, 417 55 Gothenburg, Sweden*
[5] *Department of Signal Theory and Communications, Universitat Politècnica de Catalunya, 08034 Barcelona, Spain*

Correspondence should be addressed to Jaume Anguera; jaume.anguera@fractus.com

Received 24 August 2012; Accepted 27 November 2012

Academic Editor: Mandeep Singh Jit Singh

The constant evolution of wireless handheld devices together with the apparition of multiple wireless communication systems fosters the antenna community to design new radiating and measurements systems capable of satisfying the market demands. It is an object of the present paper to provide an overview of the evolution that wireless handheld technology has experienced in the last years. In this sense, a description of the evolution of wireless handheld devices, regulations, challenges in today's smartphones, and handset characterization is reviewed. Finally, recent advances in antenna technology for wireless handheld or portable devices are presented.

1. Introduction

Communication between two distant points has been a constant challenge for mankind, from ancient smoke signals, to telegraph, to finally wireless communication through electromagnetic signals. This evolution represents a constant effort to improve the quality and effectiveness of distance communication with ever-evolving techniques to enhance the delivery of contents, from voice to data. Wireless handheld devices are the most representative paradigm of these efforts. In this regard, the antenna community often has an important role focused on designing low-profile, small, and multiband antennas together with multiple antenna systems capable of satisfying the strict demands of emergent multifunction wireless devices. Furthermore, the complexity of handheld antenna design is continuously increasing, not only by the pressure of the market needs but also by the duty of safety regulations which require efficient antennas capable of radiating as much power as possible in free-space conditions, while minimizing the power radiated towards the human head.

Antenna modeling in handheld devices, using electromagnetic simulation software, has improved significantly by allowing the simulation of the antenna behavior in complex environments surrounding the antenna. Thus, current electromagnetic software allows the simulation of handheld antennas regarding not only the human presence (such as human head and hand) but also the presence of nearby components (such as cameras, batteries, displays, and speakers).

At the same time, recent advances in measurement systems and methodologies have become hot topics in the antenna measurement community for capturing radiated performance in emergent LTE and MIMO antenna systems.

Finally, with the commercial success of wireless handheld devices comes the important role of good manufacturing techniques. This is not only important for reducing the cost of mass production, but also for enhancing the design performance and size in a controlled fashion.

The paper is divided into the following sections. Section 2 describes the evolution of handheld mobile telephones and generations, the apparition of new frequency bands, the industrial design influence on antennas, requirements and

regulations, and finally antenna design challenges in today's smartphones. Section 3 explains the most relevant electromagnetic parameters to characterize antennas for wireless handheld devices such as radiation efficiency, impedance mismatch, signal branch correlation, diversity gain, MIMO capacity, Total Radiated Power (TRP), Specific Absorption Rate (SAR), Total Isotropic Sensitivity (TIS) or Total Radiated Sensitivity, Average Fading Sensitivity (AFS), and Data bit throughput (TPUT). In addition, Section 3 shows how these parameters can be measured in a reverberation chamber. Section 4 summarizes recent advances in the field of antennas for wireless handheld devices. In particular, Section 4 describes antenna technology for designing antennas at low frequencies such as FM, for short-range wireless applications, and finally for mobile communications. For this last section, several antenna design techniques are explained such as coupled monopoles and PIFAs combined with slots. In addition, a technique robust to human loading is presented based on an array of small monopoles. Section 4 further discloses the use of broadband matching networks to enhance the bandwidth of an antenna element in order to increase the number of operating bands. It is also focused on techniques to add intelligence in the ground plane for enhancing bandwidth and efficiency. Finally, a novel antenna technology based on small nonresonant ground plane boosters is described. The proposal is focused on exciting the ground plane radiation modes that the inherent ground plane of any handset platform performs at mobile frequencies. This technology removes the need of including large antenna elements featuring quarter-wavelength dimensions, thus enabling the integration of multiple antenna elements and multiple functionalities and services in the wireless platform.

2. Evolution of Handheld Mobile Telephones

The evolution of handheld mobile telephones throughout history has been captivating. The first telephone call using a handheld device dates back to the 1970s [1]. Since the 1980s, handheld telephone devices have become a commodity for everyone and the mobile market has not stopped expanding since then. The exponential increase in the number of subscribers pushes research and development in wireless communication to deliver technologies capable of accommodating that growth. These technologies have evolved to a great extent and have included going from analog to digital, and going from using one frequency band to multiple frequency bands, as well as many others. This constant evolution led to the recent deployment of the latest generation radios onto the consumer market: the Long-Term Evolution (LTE) technology.

Operators of consumer wireless handheld devices recently started to deploy the LTE wireless technology for the next-generation smartphones. Before going through the challenges engineers have to face in developing antennas for LTE-capable phones, it is important to look at the previous generations of mobile handheld devices to describe the general challenges in antenna design, some of which still remain in the current design challenges. The following sections talk about the challenges that exist in antenna design for wireless mobile handsets.

2.1. Wireless Mobile Generations. The first generation (1G) wireless communication technology was introduced back in the early 1980s. It used an analog standard. A few commercially used 1G standards included NMT (Nordic Mobile Telephone) and AMPS (Advanced Mobile Phone System). NMT network first used a frequency band in the 450-MHz region, called NMT-450. Due to the subscribers' demand, it expanded its network to the 900-MHz region (NMT-900), since it could carry more channels at that frequency band than its previous band. The AMPS standard used in the United States was deployed in the 800-MHz frequency region. The subsequent generation radios, for example, 2G, 3G, and 4G, started in the 1990s. These newer generations were drastically different in the sense that they were all using digital standards. There were many advantages to replacing analog with digital standards. One of the advantages is that digital standards could accommodate more users, which was necessary.

Even though the 2G standards, such as GSM, D-AMPS, and CDMAOne, have been superseded by their newer generations, they still remain widely used networks in all the parts of the world. The third generation (3G) network appeared on the market in early 2000, and the latest LTE network was offered in 2010. These later standards were tailored to improve data services. The following sections describe what influences antenna design and what challenges antenna engineers have to face in the development of mobile handset devices.

2.2. Increase in the Number of Frequency Bands. Wireless communication standards sometimes come with a new set of frequency bands. Fortunately, some bands of newer generations overlap previous generations, which releases some of the burden on the antenna design when a new generation standard comes into the picture. Looking back from the first generation to the current generation, the number of frequency bands kept increasing. Antennas for the first generation handheld devices were designed back in the 1980s to work in one frequency band. As the number of frequency bands increased with newer generations, the need for multiband antenna designs became necessary. Furthermore, as the mobile market became more and more popular and global travel became more accessible to the general population, there was a need for making devices with roaming capability. This was necessary in order for subscribers of one market region to be able to use the same device in other regions with similar standards but different operating frequency bands. As an example of today's US mobile devices, a phone operating in North America has the main bands operating from 824 MHz to 894 MHz and from 1850 MHz to 1990 MHz for both GSM (2G) and UMTS (3G) standards. Furthermore, an additional band is now needed for the LTE standards in the 700-MHz band. The phone would generally have roaming capability at operating bands used in the rest of the world, precisely, GSM 900, GSM 1800,

Figure 1: Mobile handheld phone examples through all the generations.

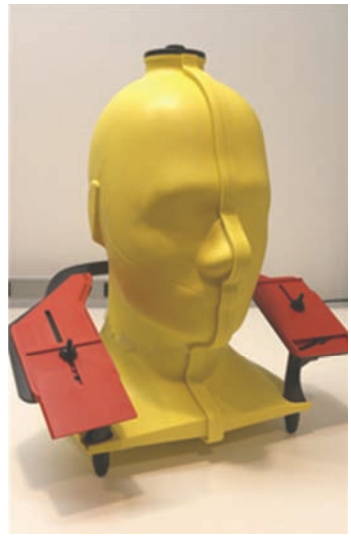

Figure 2: A model of the specific anthropomorphic mannequin (SAM) head.

UMTS B I, and B VIII. The frequency band of coverage of these roaming bands are from 880 MHz to 960 MHz (GSM 900 and UMTS B VIII), 1710 MHz to 1880 MHz (GSM 1800), and 1920 MHz to 2170 MHz. Therefore, there is a need for designing multiband antennas that can operate in these bands with good performance.

2.3. Industrial Design Influence on Antennas. For some people, a mobile telephone handset is a device that serves only as a way of communication and they do not care whether it is big or small, thin or thick, shiny or mat. For some other people, industrial design is an important factor when it comes to using consumer electronics devices. The look and feel of their phones are important factors in making their purchasing decision.

Prior to the early 2000s, antennas in mobile handsets were designed externally. They were mostly monopole-type, retractable or not, or helical stub antennas protruding from the top of the phones (Figure 1). Industrial design did not have much influence or impose great limitations for antenna design. In the early 2000s, antenna design for mobile handsets completely changed its course and internal design became the next design evolution, as it was very appealing in terms of industrial design. However, new design challenges started to haunt engineers from many disciplines, including RF, audio, and of course antenna engineers. As expected, the integration of antennas inside the phone created interference and noise problems that had to be controlled. Furthermore, antenna design was now limited within the shape of the phone. Nonetheless, these challenges were surpassed with the help of new technologies and the fantastic creative mind of antenna engineers.

2.4. Requirements and Regulations. Requirements are an important part of mobile handset designs. Operators rely on their sets of specifications to make sure that the phones they sell work well in their network. Phone manufacturers have to make sure that they meet operator's requirements. Up to the 3rd generation wireless standards, antenna performance only was measured by two quantities: TRP and TIS. TRP is a measure of how much power is radiated by the antenna when it is connected to a transmitter. TIS is defined as a measure of the smallest power that can be input to the receiver so that the receiver can still maintain a reliable communication link. For example, the communication link reliability for the GSM standard is defined using a bit-error-rate (BER) level at 2.4%.

Operator's requirements have evolved over the years. There are several reasons why this evolution occurred. Ultimately, operators, as well as phone manufacturers, know that the phones need to perform well under the real environment condition of the user holding the phone against his or her head. However, it is not possible for operators to rely on performance measurement from phone manufacturers using a human head and hand grip of a real person as each person's head and hold would differ from one to another. A focus group was needed to investigate on how to come up with a standardized model of a human head and hand. One such organization is the CTIA—The Wireless Association [2]. A subgroup in this organization was created to come up with a set of a standardized head and hand for the purpose of obtaining consistent and reliable performance measurement in a controlled lab environment. While this work was under study, operators had to rely on measured TRP and TIS in a free-space condition.

The phantom head model, called SAM (Specific Anthropomorphic Mannequin), was first introduced in 2002 (Figure 2). The material inside the plastic shell has specific electrical properties, that is, dielectric constant and conductivity that are modeled closely to the real human head. Modeling the hand was more difficult and it took longer to get to the final set of phantom hands (Figure 3).

Operators from around the world had different requirements and, when they decided to adopt new measurement conditions for their requirements, it was not at the same time. Antenna designers had to face the challenge of designing antennas with performance that had to meet various operators' requirements with different environment conditions.

Figure 3: Examples of phantom hand models.

Figure 4: SAR measurement system. The wireless handheld device radiating RF power is attached to a phantom cheek. A probe measures the electrical field generated by the device inside a phantom filled with liquids emulating the human tissue at the frequencies of interest.

In certain phone designs where the antenna is external or when there is enough antenna volume for the internal antenna design, it is not a problem to meet all operators' requirements. When the design is limited due to industrial or mechanical designs, then antenna variants for different markets are needed, each one of them meeting the operator's requirements of their market while the over-the-air (OTA) performance in the roaming market can be relaxed a little bit.

A good example of antenna design change due to a requirement modification is when the operator AT&T changed the cellular antenna requirements from free-space to talk position (with the phone placed against the phantom head). In order to come up with an attractive handset design and still meet operator's OTA performance requirements and other regulations, Motorola came out with a thin phone with the cellular antenna in the bottom of the phone. Placement of the antenna in the bottom of the phone allowed them to design a thin form-factor handset and still meet the operator's requirement with great performance in the low band (824–894 MHz). That year marked the change in antenna location in antenna design.

Requirements are specific to operators. Handset manufacturers must also meet the broadcasting and RF emission regulations that are specific to countries. For example, the Federal Communication Commission (FCC) [3] has duties of regulating RF emissions in the United States. A few regulations pertaining to mobile phone radiated emission and antennas include SAR (Specific Absorption Rate) compliancy, HAC (Hearing Aid compliancy), and GPS E911 requirements.

SAR relates to the near E-field effects of the antennas (Figure 4). FCC regulations mandate that all phones used in the United States must meet a SAR limit of 1.6 W/Kg averaged over a volume of 1 gram of tissue [4]. In some other countries, the SAR limit is 2 W/kg averaged over a volume of 10 grams of tissue [4]. The SAR requirement can be a show stopper for phone manufacturers. They must meet the regulations or else the phones cannot be released to the market. Antenna designers have to make sure that such regulations are met. One way to reduce the SAR value is to decrease radiated power. This is done by reducing the transmit power or detuning the antenna impedance so that antenna performance is degraded. However, this technique of SAR reduction would impact the OTA performance and may cause a failure to meet the operators' OTA requirements. Fortunately, there are other techniques. The general idea is to reduce the E-field towards the head. One example that helps reduce SAR in the low band (850 MHz band) is moving the antenna located on the top of the phone to the bottom. A phone with good OTA performance and a thin form factor design would have a very difficult time to meet the SAR limit if the cellular antenna was placed on the top of the phone. This is another important factor of the antenna location.

Regulations in the United States for interference with hearing aid devices due to wireless mobile handsets were imposed on phone manufacturers and operators around 2006 [5]. There are two kinds of interference related to HAC: T-Coil and RF emission. Interference due to T-coil is taken care of by acoustics engineers and relates to the coupling effect between the coil in the handset earspeaker and that of the hearing aid. Antenna engineers have to deal with the RF emission interference, precisely the near E- and H-fields emanating from the cellular antenna around the earspeaker of the phone. These fields are measured within a 5 cm by 5 cm squared area centered 15 mm above the phone earspeaker [6]. They are required to be below a certain strength level in order to be compliant. Just like the SAR problem, antenna engineers have to find ways to reduce the near fields around the earspeaker without affecting the OTA performance of the phones.

Another antenna challenge relating to regulations pertains to the Enhanced 911, or E911. This mandate from the FCC organization was created to assure that, when calling 911 for an emergency, the user can be geographically located with a certain amount of accuracy within 30 seconds after dialing 911 in the United States. In order to locate a user this fast, a standalone GPS system is not enough. The system needs some assistance from the network to acquire the required location accuracy within a small amount of time. This system is called assisted-GPS (aGPS). Regardless of whether the system is standalone or assisted, the most important parameter in the system is antenna performance. The GPS antenna has to be designed in such a way that, under the use-case condition,

its radiation pattern has a good coverage of the sky, where the GPS satellites are. Even though the aGPS system generally works with ease under the open-sky environment, that is, no obstruction between the sky and the system, the difference between good and bad antenna design can be seen when it comes to testing it in the urban and indoor environments.

There are other requirements and regulations specific to operators and countries, but the ones just previously described are the challenging ones that antenna engineers have to deal with during the concept design phase and development of antenna systems in wireless mobile handsets.

2.5. Antenna Design Challenges in Today's Smartphones. The previous sections highlighted some challenges that antenna engineers have had to face in antenna design for phones. These challenges are not getting easier in today's mobile handheld devices. Smartphones are becoming a universal device that subscribers want to have. These devices are packed with a great amount of applications. They are no longer just a simple phone. Examples of such applications include data communications such as internet browsing, movie streaming, email access, navigation system, remote control, geotagging in photoshooting, and a payment system. All these applications need the use of an antenna built in the smartphone, whether it is a cellular, Bluetooth, WiFi, GPS, NFC, or FM antenna. The obvious challenge is to design all the necessary antennas inside a compact device. Placement of these antennas is crucial to the design as coupling between antennas needs to be minimized. Another design challenge in compact devices is the additional NFC antenna needed for near-field communication such as the payment system, FeliCa, in Japan. This NFC antenna is conventionally made of a coil resonating at 13.56 MHz. The coil is generally designed on a ferrite sheet to minimize Eddie current created by the coil on any metal surface underneath the NFC antenna. Big coils and ferrite materials can often cause performance degradation in other antennas located nearby, which can complicate other antenna designs as space can become more limited.

As mentioned in the previous section, creating a controlled environment for testing over-the-air performance in labs needs to be close to the real use-case environment. Operators are now starting to adopt and create requirements for OTA phone performance testing in the talk position, including the phantom hand (Figure 5). Even though one hand-grip testing does not represent the entire spectrum of hand grips from real users, it is still one step closer to capturing performance effects of a real use-case condition. This new requirement forces antenna engineers to pay attention to the effect of the hand on the antenna performance so that a system can be designed to satisfy the requirement.

The next-generation smartphones that are LTE-capable further increase the level of challenge involved in antenna design. For an LTE system in phones, a second antenna, for receive diversity, is needed, along with a primary cellular antenna. Both antennas are operating in the same frequency band. That is an additional antenna to design in a small device that is already populated with multiple antennas. For

Figure 5: Over-the-air phone testing in the talk position, including the phantom hand.

MIMO design, antenna efficiency, antenna isolation, gain imbalance, and correlation between the two antennas are important parameters in designing antennas for the LTE systems. In MIMO systems, optimal system gain is obtained if the two antennas are totally uncorrelated, have similar gain performance, and are uncoupled. Increasing the antenna space can help reach optimal performance. However, in phone design, space is limited. Fortunately, operator requirements can tolerate the secondary receive antenna having an antenna efficiency level of about 3 to 6 dB below that of the primary. This is helpful for the secondary antenna design as its efficiency does not have to be as good as that of the primary antenna. However, isolation and correlation remain the challenging tasks to work on.

Correlation is mostly dependent upon the far-field antenna pattern. Radiation pattern characteristics at frequencies of 1500 MHz and higher are generally dependent upon the antenna location. This means that, at higher frequency, the radiation patterns of the two antennas can be very different with enough distance separation between them and therefore it is generally not an issue in meeting the operators' requirements at LTE bands higher than 1500 MHz. The challenge still remains for LTE bands at frequencies below 1000 MHz. This is because the radiation patterns at these frequencies have somewhat similar characteristics, no matter where the antennas are placed within the real estate of the phone design. The reason to this similarity in characteristics is because the PCB, or ground of the antenna, is the main radiating element at frequency below 1000 MHz for a typical phone length. Operators target an envelope correlation coefficient (ECC) of 0.5 as their requirement.

Isolation is also a challenge in smartphones at frequencies below 1000 MHz due to antenna small electrical distance separation. If not designed well, the overall efficiency of both antennas can degrade dramatically and instead of designing a system that gives additional processing diversity gain performance, one can end up with a system that has a similar or worse performance to a conventional system with one antenna.

LTE systems are data centric. At this stage, voice is not supported on the LTE network. Voice-over-LTE (VoLTE) is still in the test phase and is not yet deployed. Therefore, there is no simultaneous data communication over LTE and voice communication. For a 3G UMTS smartphone that has

additional LTE bands, simultaneous data and voice can only be done in 3G. So, if a phone call is received and a user answers during a data connection over the LTE network, then data connection has to fall back to a slower speed in the 3G UMTS network. One operator, that is, Verizon Wireless in the United States, takes it one step further to have a design that is capable of having simultaneous voice in the CDMA network and data communication over their LTE network. The reason for this design is that their CDMA network does not allow simultaneous voice and data communication. One antenna is designed for voice in the 850- and 1900-MHz bands, and for the receive diversity for the LTE band at 750 MHz. The other antenna is designed to be the primary transmit/receive antenna for data communication at the LTE band and EVDO CDMA bands. This is a complex and challenging system to design for a smartphone and to meet not only all the operators' OTA requirements but also the SAR limit for simultaneous transmission, which is still at 1.6 W/kg average over 1 gram of tissue.

An overview of the challenges and issues antenna engineers have to face during the concept and development phases of wireless mobile handsets was discussed. From the beginning of the history of mobile phones, the challenge level for designing antennas has never decreased. There has always been a constant increase in the number of challenges from one generation to the next. In the midst of all this, the extraordinary creativity of the antenna designers has helped them overcome all the challenges that have led from the design of a wireless mobile device with a large external single-band antenna design to a small and slim device with multiband and multiantenna systems.

3. Verifying Designed Performance: Handset Antenna Characterization

Antenna characterization has experienced a rapid development through the last couple of decades, and a large part of antenna measurement development has been caused by the introduction of handset antennas. For traditional antennas, such as those used for radars, point-to-point links, or macrocell base stations, the radiation pattern is of great importance. Those types of antennas are specifically designed to direct energy in a certain direction and avoid spilling energy in other directions.

Handset types of antennas are by nature electrically small, which means that they exhibit more or less omnidirectional radiation patterns due to the small size of the radiating element. This is not necessarily a bad thing; handset antennas are used in an arbitrary orientation with signals arriving to the device from arbitrary directions, and there is a benefit in collecting as much of this energy as possible. Therefore, designing handset antennas towards a specific radiation pattern is of less interest. Hence the parameters used to characterize handset antennas have somewhat different focus than those used for the traditional types of antennas mentioned above.

Another shift in antenna characterization is ongoing right now. This shift is caused by the introduction of multielement antennas, which are used to facilitate antenna diversity or MIMO communication. Still, the same basic characteristics as for single-element handset antennas are important, but these are complemented with additional parameters to validate the antennas functionality in the modern communication system.

3.1. Figure-of-Merits for Wireless Handheld Devices. There are several figure-of-merits (FOMs) which are interesting for characterization of wireless handheld devices.

The FOMs can be divided into passive and active parameters, where the former are antenna only parameters, and the latter include radio circuitry. This division reflects another fundamental difference between the two groups of FOMs, which is that the passive antenna parameters are component values, whereas the active parameters are composite values combining performance of several components into a single value.

3.1.1. Passive Antenna Parameters. Commonly used passive antenna parameters are

(a) radiation efficiency [7],

(b) impedance mismatch [7],

(c) signal branch correlation [8],

(d) diversity gain [8],

(e) MIMO capacity [8].

The first two are traditional antenna parameters applicable to all types of small antennas, whereas the latter three are relevant for multielement antennas (MEAs). This does not mean that the two former parameters are less important for MEAs. On the contrary, radiation efficiency is still the most important design parameter for electrically small antennas.

Radiation efficiency of an antenna is basically the ratio of power radiated from the antenna to the delivered power to the antenna feed, which means that it is a description of the internal losses of the antenna element. This means that the radiation efficiency goes directly into the link budget of the communication system and therefore has a direct impact on the performance of the system.

Radiation efficiency is often paired with impedance mismatch as the most useful design parameters for antennas in wireless handheld devices. Total radiation efficiency (sometimes also called antenna efficiency) is a combination of these two, defined as the product of the radiation efficiency and the efficiency due to mismatch.

It is applicable to talk about radiation efficiency also in the case of MEAs. The most proper way to characterize the efficiency of each element of an MEA is to look at its performance when the other elements are present, in order to fully account for loss due to mutual coupling between elements. Such radiation efficiency that accounts for mutual coupling can be referred to as Embedded Element Efficiency, where the embedded prefix denotes the presence of other nearby antenna elements.

Signal branch correlation is applicable to antennas with two or more branches and is a measure of how uncoupled the

antenna elements are. It is calculated as the cross correlation between the signals received on two separate antenna ports. The signal branch correlation, as well as radiation efficiency and impedance mismatch, is example of component parameters, that is, parameters directly showing the performance of a certain part of the communication system.

Diversity gain and MIMO capacity, the two latter passive parameters in the list above, are actually composite parameters determined by the first three passive antenna parameters just mentioned: radiation efficiency, mismatch, and correlation. In the literature, there are a few definitions of diversity gain to be found, and it is important to apply these definitions in a correct way in order to draw justified conclusions from a set of data. The basic difference between different diversity gain definitions is how the radiation efficiency is embedded in the parameter. The three basic definitions of diversity gain are Apparent Diversity Gain, Effective Diversity Gain, and Actual Diversity Gain, where the difference is the reference from which the diversity gain is calculated [8]. The reference can either be one of the diversity branches (Apparent Diversity Gain), an ideal single reference antenna (Effective Diversity Gain), or any practical antenna to be replaced (Actual Diversity Gain).

Note that the passive parameters discussed here are integral quantities, based on the assumption of a statistically isotropic multipath environment surrounding the antenna. This type of environment is especially useful for handset antenna characterization, not only due to the similarity to the environment where most handsets are used, but also due to that a handset is arbitrarily oriented due to individual preferences of the users. This environment can be referred to as Rich Isotropic MultiPath environment (RIMP) [9].

In some cases, there is interest in creating the integrated parameters over other types of spatial distributions. An example of this is the Mean Effective Gain parameter which can be described as radiation efficiency weighted with respect to a certain angular distribution of incoming waves to the antenna under test [10].

An extreme in the sense of spatial distributions is the pure Line-of-Sight environment, where there is a single signal component arriving at the antenna under test. This is the direct opposite of the RIMP environment mentioned above, meaning that these two environments complement each other. The difference between these two environments is how they impact a multiantenna system such as diversity or MIMO. An example of a LOS parameter is the LOS diversity gain [11].

3.1.2. Active Antenna Parameters. Commonly used active antenna parameters are

(f) Total Radiated Power (TRP) [7],

(g) Specific Absorption Rate (SAR),

(h) Total Isotropic Sensitivity (TIS) or Total Radiated Sensitivity (TRS),

(i) Average Fading Sensitivity (AFS) [12],

(j) Data bit throughput (TPUT) [13].

Figure 6: Anechoic chamber having a gate with 31 probes to electrically measure the radiation in one plane radiated by the device under test. The device under test is rotated so as to have the full 3D data.

The three first parameters of active antenna parameters listed above can at this point all be considered traditional characterization parameters for wireless devices. Both TRP and TIS can be directly related to the total radiation efficiency of the device antenna and are therefore commonly used parameters to characterize the radiation efficiency of devices without a direct external cable connection to its antenna. SAR is a bit different from other antenna parameters described in this section of the paper, since it is not a pure over-the-air parameter but a measure of the absorption rate of power in simulated human brain tissue.

TIS is originally a single antenna parameter but it is possible, when measuring TIS in a multipath scattering environment as the reverberation chamber, to extend the measurement to include multielement antenna performance. That is, exactly the same measurement procedure as used for single element TIS will include the performance improvement offered by the multielement implementation, as long as the measurement is performed in a multipath scattering and with the multiple signal combination activated in the device.

The last parameter, data bit throughput, has attracted considerable interest in MIMO-OTA discussions in the antenna community over the past few years, mainly because of its close link to end-user experience. The basic principle behind this type of throughput measurement is to create a scattering environment in which the unit experiences fading and sample the data throughput over time to get a statistical value of what data bit rate the unit can support given a certain average available power. The measurement chamber needs in this case to work as a spatial channel emulator, and there are several ways of achieving this either with existing measurement setup (like reverberation chambers), or modifications of existing chambers (like anechoic chambers).

Data bit throughput is essentially equal to an error rate measurement taken over a fading sequence, whether it is bit

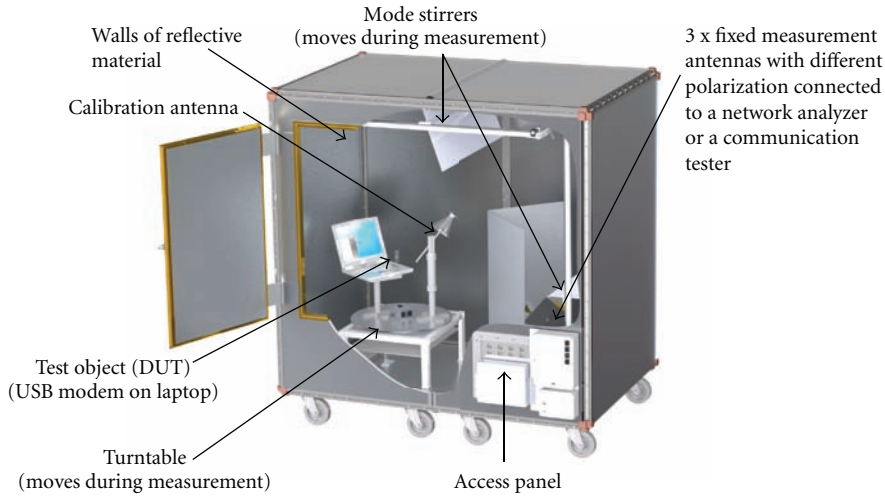

Figure 7: Reverberation chamber configured for measurements of antennas for wireless handheld devices.

error rate (BER), packet error rate (PER), frame error rate (FER), or block error rate (BLER). The process of sampling the error rate specifically during a fading sequence has been referred to as Average Fading Sensitivity (AFS) and is then very similar to how data throughput measurements are performed today. It is interesting to note that there is a relationship between the AFS and TIS value of a device.

3.2. Measurement Methods of Antennas for Wireless Handheld Devices. There are two dominating range types for small antenna measurements; anechoic chambers and reverberation chambers. Although many of the parameters accessible through measurements in these two chamber types are identical, the methods themselves work in diametrically opposite ways.

In an anechoic chamber, everything but the direct signal from the measurement antenna to the antenna under test is removed, hence the name of anechoic chamber; no echoes exist in the measurement setup. To measure any integral parameter, the antenna under test is rotated to cover all different angles of arrival at the antenna. The integral parameters described above are then calculated from the information given in each angular direction (Figure 6).

The reverberation chamber on the other hand is fully reflective and creates a field with many angles of arrival present at the same time, that is, a lot of echoes but no direct signal path. As the so-called mode stirrers are moved, signals will combine in different ways, and over a full stirring sequence all angles of arrival will be equally probable. Hence the integral parameters described above can be extracted as a direct result of a measurement sequence. Figure 7 shows an example of how a reverberation chamber looks like.

Figure 8 shows the schematic setup for anechoic and reverberation chamber measurements, respectively. Note that the instrumentation is similar between the two methods.

With the current trend of creating fading channels to test handset antennas, there is much work ongoing to modify the anechoic chamber to facilitate multipath fading in the originally pure LOS environment. The proposed method means placing a ring or sphere of probes in the anechoic chamber and feed signals through these antennas so that a specific fading profile is created in the center of the test volume. The drawback with this modification is that the chamber has to be converted back to a normal anechoic chamber, that is, removing the additional probes, before traditional antenna parameters can be measured, so most of MIMO-enabled anechoic chambers are likely to be dedicated to MIMO testing only.

Reverberation chambers have an inherent multipath fading due to its reflective nature, and therefore MIMO OTA measurements can be performed without any other modifications than adding fixed measurement antennas to facilitate the MIMO signaling.

Figure 9 shows the schematic setups for MIMO OTA measurements in reverberation and modified anechoic chambers. Note that both measurement setups are equipped with channel emulator to control the fading. In modified anechoic chamber, the channel emulator is essential in order to create the fading, and it is done by feeding prefaded signals on each of the probes in the chamber. In the reverberation chamber the channel emulator is optional due to its inherent fading, but the channel emulator gives a wider range of possible power delay profiles in the measurement setup.

Table 1 shows a compilation of the different measurement methods and which figures of merit used for design of small antennas are applicable for each method.

4. Antenna Technology for Wireless Handheld Devices

The massive incorporation of wireless handheld devices such as mobile phones in our lives has changed their functionality conception. Nowadays, mobile phones are not only used to communicate, but they also offer a big range of services such as digital camera, video player, internet connectivity, geolocalization, TV services, or FM radio. In this regard,

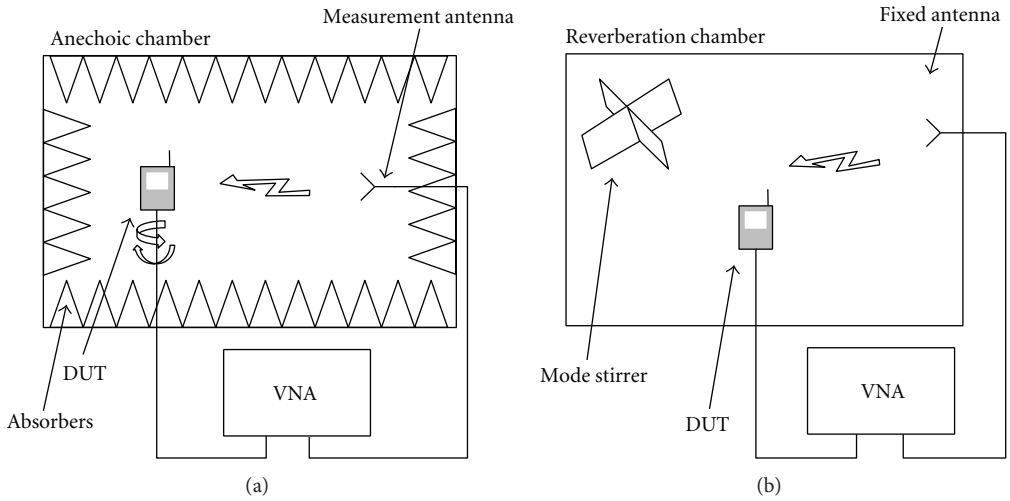

Figure 8: Example measurement setups for passive (cable-fed) testing of antennas for wireless handheld devices. For active device testing the DUT is replaced by a functional handset, and the vector network analyzer (VNA) is replaced by a base station simulator.

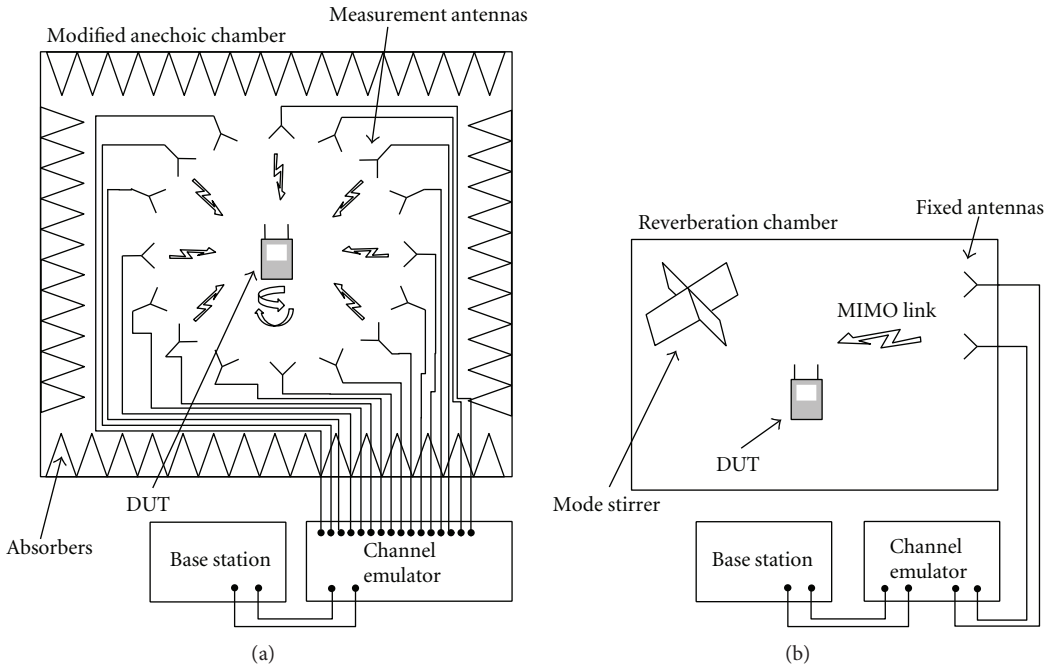

Figure 9: Example measurement setups for active MIMO testing of antennas for wireless handheld devices.

antenna industry as well as academic areas are being forced to evolve constantly to obtain small and multiband antennas capable of radiating efficiently in such a hostile environment. On one hand, the volume constraints in wireless handheld devices produced by the reduction of the available space due to the existence of multiple components (such as displays, batteries, speakers, and shieldings) must be considered for optimizing the antenna performance. On the other hand, user interaction also needs to be taken into account from two perspectives. Firstly, the amount of power absorbed by the human body, especially the head and hand, has to be minimized. Secondly, the antenna needs to be robust to such human interaction which causes power absorption and/or detuning effects. Minimizing power losses is an important aspect since they produce higher battery consumption and eventually call drops.

With the objective of reviewing several antenna applications that can be found in current or emergent wireless handheld devices, this section is divided into three main parts. Firstly, antennas for reception applications are discussed, in particular for FM reception (88–108 MHz). Secondly, a brief discussion on antennas for short-range wireless applications is presented, and finally a summary of some advances in the field of handset antennas is disclosed.

Table 1: Measurement methods for characterization of antennas for wireless handheld devices and applicable figures of merit for respective method.

FOM	Table ref.	Reverberation chamber	Anechoic chamber	Multi-probe MIMO setup in anechoic chamber
Radiation efficiency	a	Yes	Yes	No
Impedance mismatch	b	Yes	Yes	No
Signal branch correlation	c	Yes, calculated direct from received signals	Yes, calculated from radiation patterns	Yes, calculated direct from received signals
Diversity gain	d	Yes, direct from received signal distributions	Yes, calculated from radiation patterns	Yes, direct from received signal distributions
MIMO capacity	e	Yes, from received signal statistics	Yes, from radiation patterns	Yes, from received signal statistics
TRP	f	Yes	Yes	No
SAR	g	No	No	No
TIS or TRS	h	Yes	Yes	No
TIS/TRS including diversity reception	h	Yes	No, no multipath fading in anechoic chamber	No
Average fading sensitivity (AFS)	i	Yes	No, no multipath fading in anechoic chamber	Yes
Data bit throughput (TPUT)	j	Yes	No, no multipath fading in anechoic chamber	Yes

4.1. Broadcast Antennas: FM. The main challenge of designing antennas for providing operation in the FM service mainly relies on size limitations. Regarding the FM service, a conventional monopole antenna ($\lambda/4$) operating at FM frequencies is 75 cm length, which is too long for being integrated in a handset phone. In order to overcome this limitation, some mobile phone manufacturers incorporate the FM antenna in the wire of the headsets, but this solution goes against having a fully integrated wireless handheld device. Other solutions found in the literature propose the use of active schemes [13], thus resulting in an undesired increment of the battery consumption. In order to solve the aforementioned shortcomings this section explains two techniques for designing internal antennas at the FM band based on

(i) nonresonant elements [14–16],

(ii) reusing a PIFA antenna operating at mobile communication services [17, 18].

4.1.1. Nonresonant Elements. The authors of [15, 16] describe the problem of designing a resonant antenna such as a spiral at the FM band taking into account the reduced space of a PCB (Printed Circuit Board). Since the available space is limited, coupling between antenna tips forces the need of increasing the total length in order to attain the desired resonance, thus resulting in a length larger than $\lambda/4$. For example, to attain resonance at 100 MHz in a 40 mm × 20 mm × 5 mm antenna volume, a length of 2262 mm is needed, which becomes larger than a quarter of a wavelength at this operating frequency ($\lambda/4$ = 750 mm) [16]. Moreover, due to the aforementioned volume constraints, the width of the antenna has to be thin. Such constraint in the design width can considerably increase ohmic losses, thus producing a poor radiation. In order to solve these limitations, the proposed idea substitutes a resonant antenna by a nonresonant antenna inspired in the Hilbert geometry with a high-Q inductive element that brings the antenna to resonance. With this approach, better efficiency is obtained (around 20 dB more). Although the efficiency for the nonresonant element is around 1%, this result is still acceptable for FM reception for two reasons. First, the transmit power for FM broadcast tower is in the order of KW. Second, the free-space loss for FM is not as critical as other telecommunication services such as cellular communications (GSM); for example, at 100 MHz, the free-space loss is approximately 20 dB less than at 900 MHz. As a result, more power is available in the air. With this condition, a small compact antenna for FM reception inspired in the fractal geometry of the Hilbert curve is proposed, which becomes suitable for being integrated in current wireless handheld devices thanks to its reduced dimensions of just 30 mm × 10 mm × 1 mm (Figure 10).

Besides the common electromagnetic parameters such as SWR (Standing Wave Ratio), radiation patterns, and efficiency, another figure of merit is proposed to evaluate the performance of antennas for FM reception. It consists of demodulating the RF signal to an audio signal. This procedure is presented in Section 4.1.2 where the performance of the proposed Hilbert antenna is compared to the performance of a $\lambda/4$ monopole concluding that the Hilbert solution offers a similar audio quality of the received signal with the advantage of its reduced size and its integration capabilities.

4.1.2. Reusing a Mobile Antenna. This section introduces a solution for integrating an FM receiver antenna in a wireless

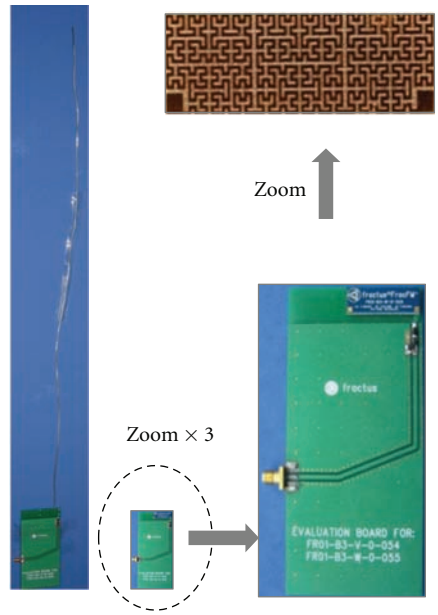

FIGURE 10: External wire (75 cm length) and internal FM Chip Hilbert antennas (30 mm × 10 mm) integrated within a typical smartphone platform [19–21].

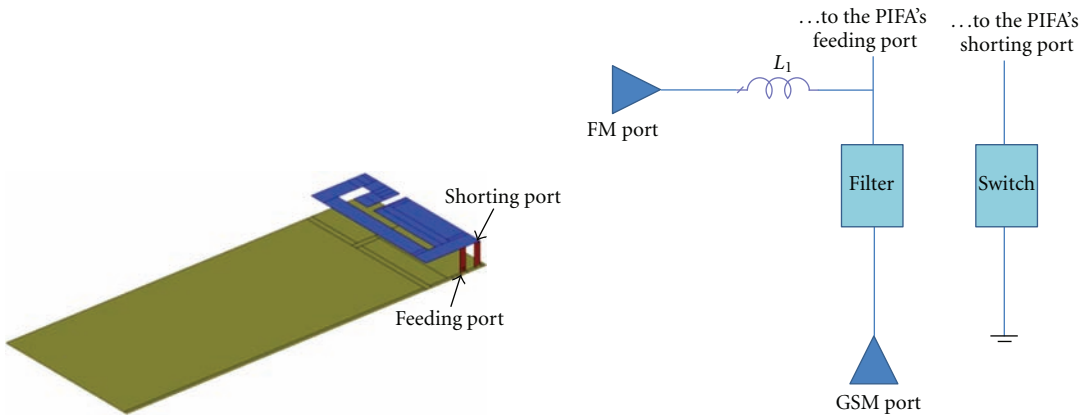

FIGURE 11: (a) 3D view of the PIFA. Ground plane size is 100 mm × 40 mm and PIFA is 38 mm × 15 mm × 6 mm; (b) proposed matching network including a switching circuit, a filter, and a series inductor.

handheld device that goes one step beyond. The proposed technique is focused on reusing an existing antenna operating at cellular bands. In this sense, a PIFA (Planar Inverted F Antenna) designed to operate at two GSM standards (900 and 1800 MHz) (Figure 11(a)) can be reused to become operative at the FM band [15]. The PIFA behaves as a nonresonant element at FM frequencies. The required 75 cm length needed to behave as a $\lambda/4$ monopole is far from the PIFA's dimensions. Therefore, a high series inductor is added in order to compensate for the capacitive behavior of the PIFA at FM frequencies (Figure 11(b)).

The PIFA has a feeding port and a port which short-circuits the antenna with the ground plane. In order to guarantee a good response in the FM band, the shorting connection must be removed because the distance between ports is electrically small at these frequencies, producing a short-circuited antenna with poor electromagnetic performance at the FM band [18]. To guarantee good radiation in the desired frequency bands (FM and GSM900/1800), a matching circuit is needed (Figure 11(b)). The PIFA used here does not need any matching network at GSM frequencies but a 1000 nH series inductor is required at FM. Both ports are isolated by means of a filter and the series inductor. The filter is designed to only reject the FM signal at the GSM port because the GSM signal in the FM port is already rejected due to the series inductor that presents high impedance at GSM frequencies. Finally, a switching circuit is needed in the short port in order to disconnect the antenna from the ground plane when it is operating at FM band.

In [13], it was demonstrated that a high received power does not mean necessarily a better signal quality. In some cases, a low received power offers satisfactory audio

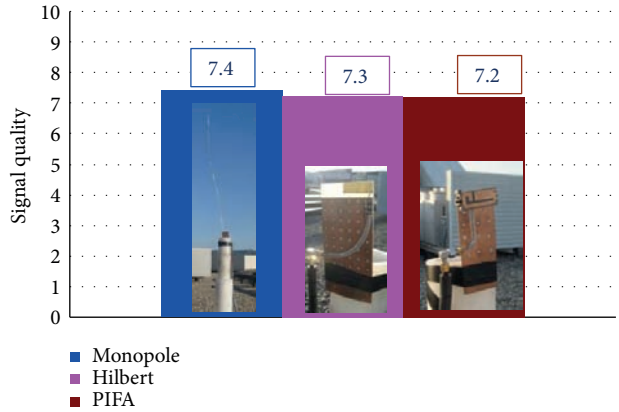

Figure 12: Marks obtained through the quality evaluation after averaging 28 FM channels.

reception, whereas a high received power presents low SNR (Signal-to-Noise Ratio) leading to a decrement of the quality audio reception. For this reason, a subjective procedure [19] for evaluating the demodulated signal quality has been carried out regarding the PIFA, the 75 cm length monopole, as well as the previous fractal-inspired Hilbert-based monopole [20, 21].

This procedure consists in quantifying the quality of the FM signal received by the antenna being tested. The signal quality indicator is ranked from 0 to 10 depending on the quality of the FM channel heard by the user [19].

Despite having the highest received power, the monopole's final evaluation does not differ from the other ones. The final mark for the $\lambda/4$ monopole is 7.4, the final mark for the Hilbert antenna is 7.3, and finally the PIFA's mark is 7.2 (Figure 12), having the advantage that this antenna can also operate in the mobile communication bands.

It is interesting to outline that human body has been also taken into account concluding that, in some position such as holding the device with the hand, the overall efficiency is improved by 10 dB [22, 23]. This improvement is due to the fact that at this low frequency ranges, the human body acts as a dielectric antenna with a size comparable to the wavelength of operation, thus becoming an efficient radiator (a human body of 1.7 m at 100 MHz is 0.56λ).

In conclusion, the PIFA offers the same satisfactory performance as the reference monopole and it ensures the integration of the FM antenna in wireless handheld devices. Moreover, other handset antenna techniques, such as the slotted ground planes (as described in the following sections), can be used in combination with the PIFA to obtain a heptaband antenna (FM, GSM 850/900/1800/1900, UMTS, and Bluetooth/Wi-Fi).

One of the major advantages of the proposed technique is that no extra antenna is needed because the existing mobile antenna is reused.

4.2. Short-Range Wireless. Short-range wireless generally refers to those applications characterized in that they have

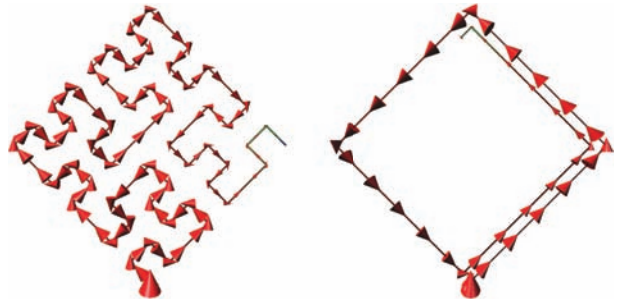

Figure 13: Current vector distribution of the antennas at the resonance frequency of f = 84.5 MHz.

small transmitted power (order of mW), indoor operation, range of meters, and limited bandwidth (about 4% for Bluetooth application). Examples of short-range wireless systems are Bluetooth, WiFi, ZigBee, and RFID. The vast majority of wireless handheld devices incorporate a short-range wireless antenna for Bluetooth/WLAN services. Antenna size is again an important aspect to consider since the center frequency of operation for Bluetooth is 2.45 GHz, meaning that a $\lambda/4$ antenna is 30 mm. Such antenna size is still large, considering the device's space limitation due to displays, batteries, speakers, as well as the need of integrating other multiple antennas such as the ones intended for mobile communication. Therefore, the challenge relies on making the antenna as small as possible to simplify its integration in a wireless handheld device while preserving its electromagnetic performance.

In order to face the challenge of antenna miniaturization for short-range wireless applications, two categories described extensively in the literature are proposed:

(i) geometry based,

(ii) material based.

On one hand, geometry-based antenna relies on designing antenna geometries capable of taking the maximum profit of the available space. An example is found in space-filling geometries [24–36]. On the other hand, material-based antennas are focused on using high dielectric materials such as ceramics capable of providing the required miniaturization [37].

The suitability of space-filling geometries in the design of small antennas has been broadly investigated. In this case, small antennas like the Hilbert monopole are described extensively in the literature [24–36], to demonstrate that an antenna can become electrically smaller as the iteration increases. Using this type of miniaturization technique, it is possible to reduce the electrical size of a conventional quarter-wave monopole up to a factor of 11 [24].

To analyze the benefits of the Hilbert curve in designing small antennas, a comparison with a spiral antenna is carried out [31, 36] (Figure 13). Two antennas are designed to resonate at the same frequency of 84.5 MHz occupying the same footprint and having the same wire width. Although the spiral needs less wire for resonating at 84.5 MHz, the

Figure 14: SMD space-filling-based antenna for 2.4-2.5 GHz applications. Antenna is 4.1 mm × 2 mm × 1 mm (4.1 mm is 0.033λ at 2.45 GHz).

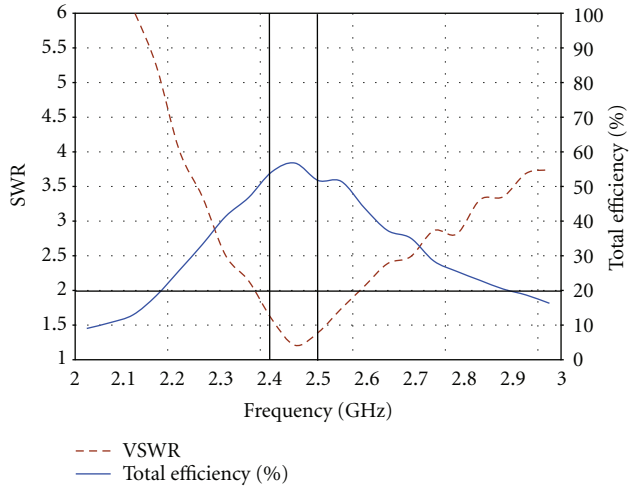

Figure 15: Measured SWR and total efficiency for the 2.4-2.5 GHz antenna shown in Figure 14.

bandwidth of the Hilbert antenna is 1.62 larger for the same radiation efficiency.

Thanks to its miniaturization properties, space-filling based antennas are suitable to make efficient, small, and multiband antennas. Some examples for short-range wireless applications (e.g., wireless headsets, cellular handsets, Bluetooth USB, and serial Dongles) are already adopted in industry (Figure 14).

Space-filling geometry-based antennas have been proven to be efficient radiators showing that, not only size and wire length but also geometry plays a role in the performance of a small antenna. A small antenna featuring 4.1 mm × 2 mm × 1 mm for 2.4-2.5 GHz operation shows a total efficiency more than 50% making it attractive for many wireless handheld devices (Figure 15).

4.3. Mobile Communications. This section discusses some antenna techniques for mobile communications. In the first part, some antenna types are presented based on monopoles, and combination of PIFA (Planar Inverted F Antenna) and slots. Second, an antenna architecture robust to hand loading is discussed. Third, the benefit of manipulating the ground plane is analyzed. Fourth, a particular matching network for enhancing the bandwidth is studied, and finally a novel antenna technology based on the use of compact elements for exciting the ground plane of wireless handheld device is presented.

4.3.1. Radiators. Nowadays, internal antennas such as patch/PIFAs and monopoles are the most common designs for handsets [37–42]. For PIFAs, several well-known techniques are used to provide dual-band or multiband operations such as shaping the radiating path or using slotted ground planes. This fact increases the complexity of the design and makes difficult their integration in slim platforms since, to guarantee good performance, the PIFA antenna has to be arranged at a certain height with respect to the ground plane, hence occupying a considerable volume (≈4500 mm^3). Monopole antennas are an alternative design to provide multiband operation in slim platforms mainly due to its low profile characteristics [43]. In this section two kinds of radiators are briefly discussed. The first one employs monopole antennas. The mechanism to obtain multiband and enough bandwidth is achieved by a structure based on driven parasitic elements. The second radiator combines a PIFA with a slot to make a modular design in the sense that the number of bands is controlled independently from each radiator.

Coupled Monopoles. The use of monopole antennas in wireless handheld devices has increased in the recent years thanks to its low-profile characteristics that simplify their integration in wireless platforms. Many designs have appeared in the literature and industry with the aim of covering the largest number of frequency bands as possible without reducing the antenna performance [44–50].

A multiband behavior (GSM850/900/1800/1900 and UMTS) is obtained with a technique using parasitic elements coupled to a primary driven element. At the same time, the proposal maximizes the space on the PCB to integrate other cellular components [51, 52]. The proposed antenna has also a planar profile which is attractive for slim platforms (Figure 16). The driven element is located closer to the ground plane, separated at a distance from the parasitic elements. The ground plane area located at the right side of the antenna provides a useful space to integrate some typical elements of this kind of devices, such as a camera or a speaker. On the other hand, the design takes into account the most critical variables when defining the operating frequency ranges. These variables are the element lengths and the gap between them, which determines their coupling effect. Furthermore, the location of the elements determines the correct behavior, especially at the low frequency bands (GSM850/GSM900).

Coupling between the driven and a parasitic element allows the apparition of an impedance loop in the Smith chart. By properly controlling the coupling between both elements, the performance can be wideband or multiband. Electrical models can be used to give a physical insight into the coupling mechanism [52]. In this particular case a first parasitic element is tightly coupled to the driven element to obtain two separated bands (Figure 16). Another

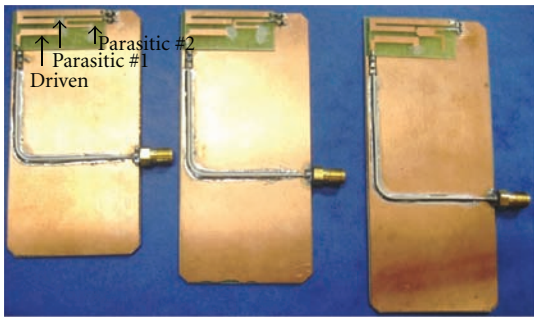

Figure 16: Prototypes regarding a ground plane of 45 mm × 90 mm, 100 mm, and 110 mm. The driven element is fed through a 50Ω transmission line.

parasitic element (parasitic #2, Figure 16) is weakly coupled to the driven to obtain a wideband at the upper region. It is interesting to outline that similar effect is found in microstrip antennas formed by a driven and a parasitic element. Therefore, the use of electric models is useful to understand the behavior of the impedance performance of antennas.

The design features a footprint of 35 mm × 15 mm and 1 mm height achieving pentaband behavior for GSM850, GSM900, GSM1800, GSM1900, and UMTS.

Combination of PIFA and Slots. PIFA and slots have been widely studied in the literature [38, 53, 54]. Basically, the PIFA needs a 3D volume to radiate efficiently whereas the slot antenna can be completely flat. However, due to the ground plane, the space underneath the antenna cannot be reused to place other handset components (such as a speaker, a battery, and shieldings) since they would affect significantly the antenna performance. In order to combine the benefits of PIFAs and slot antennas (planar structures), a concept that combines a PIFA with a slot antenna is discussed here. Other kinds of combination such as monopole and slot antennas using a self-complementary structure have been proposed in [55].

An illustration on how the concept works is shown next [56, 57]. Figure 17(a) depicts a slot in a ground plane having 100 mm × 40 mm. In this case, the slot is excited around 1900 MHz which results in a $\lambda/4$ slot antenna. The obtained bandwidth covers GSM1800-UMTS at SWR $\leq$ 3. Figure 17(b) shows a 900 MHz PIFA on the same ground plane. The feeding mechanism is in the same position used to excite the previous slot. Both designs are combined, that is, the PIFA and the slot share the same feeding mechanism (Figure 17(c)). The antenna combines both reflection coefficients (Figure 17(d)). To increase the bandwidth at the second band, slot width may be increased [58].

Since the PIFA has only one branch, the space can be reused to allocate more branches and therefore increasing the number of bands [56]. For this technique it can be concluded that

(a) number of bands = number of PIFA bands + number of slot bands,

(b) bands due to the PIFA and the slot can be adjusted independently.

This concept is based on a parallel excitation of a PIFA-slot that becomes particularly useful to design multiband handset antennas where the number of frequency bands is given by the sum of the bands given by each radiator. Moreover, said bands can be controlled independently which adds an additional degree of freedom to the design.

Thanks to the slot radiator, the PIFA volume can be reused to add more bands. With this structure, an extra band centered at S-DBM has been added to finally design a pentaband prototype including GSM900, 1800, 1900, UMTS, and S-DMB [56]. The total antenna volume is 39 mm × 11 mm × 2 mm (h). Results for total efficiency taking into account several components (battery, display, speaker, camera, and phone covers) are satisfactory and make this concept attractive for the new generation of low-profile multiband handset phones.

4.3.2. Robust Architectures to Hand Loading. The challenge for the antenna community is not only to design small-multiband antennas but also make them robust to human interaction, that is, to minimize the radiation toward the human body and make the antenna behavior independent, for instance, from the hand loading that detunes and absorbs the radiated power [59–62].

Several techniques have appeared in the literature. In [63], two strips are located at the edges of the PCB to make the system robust to hand loading. Some schemes propose the compensation of the finger effect by an antenna selection which requires a switching mechanism that involves an increment in the battery consumption [64, 65].

A technique named distributed antenna system is presented here to provide robustness to the hand-loading effect. The technique proposes a handset antenna architecture based on an array of small monopoles strategically arranged along a PCB in order to provide robustness to the human loading effect and, in particular, to the finger loading effect (Figure 18) [66–68].

It is well know from microwave theory that an array of in-phase radiating elements presents the same return loss at the input port of the feeding system as the return loss of the single element. However, if a phase delay is introduced, for example, to achieve a certain beam tilting, the bandwidth may be enhanced at the input port due to the nonconstructive sum of all the reflections coming from each radiator. This principle of array theory is applied here in order to obtain not only a broadband antenna, but also a more insensitive system to finger loading effect than the one using a single element.

The proposed system is completely passive, which in terms of simplicity and battery consumption is considerably advantageous.

Electric models have been used to give a physical insight on the broadbanding mechanism of the distributed antenna systems [69].

A prototype having a single monopole, another prototype comprising two monopoles, and a third one integrating three small monopoles combined in a single port are built and

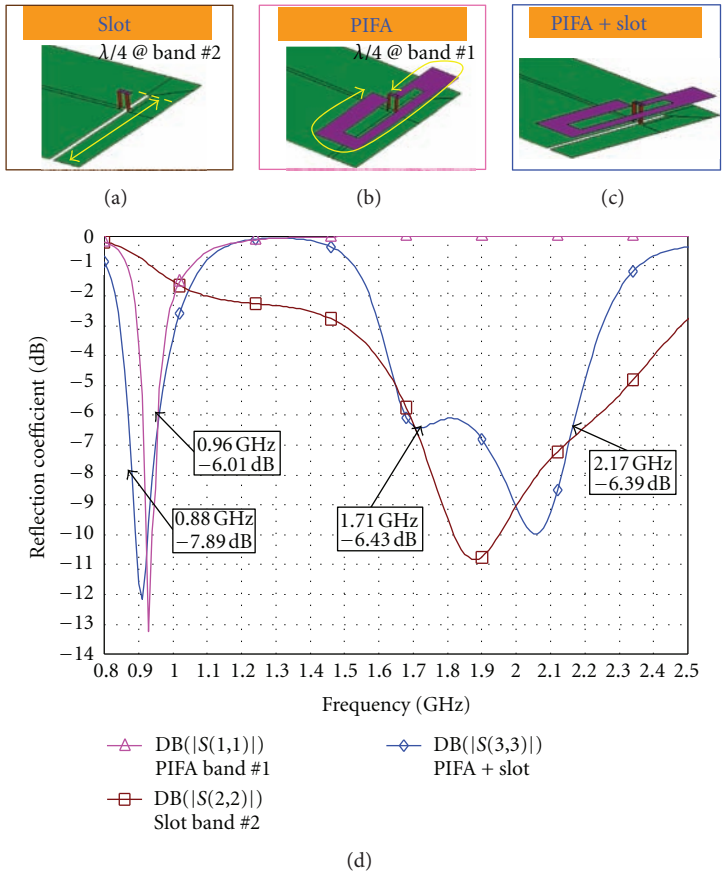

Figure 17: Sequence showing the antenna concept. (a) A slot on the ground plane is tuned at 1900 GHz (band #2); (b) PIFA is tuned at 900 MHz (band #1); (c) parallel excitation of both antennas (PIFA + slot); (d) reflection coefficient of the antenna system. Ground plane is 100 mm × 40 mm for all cases.

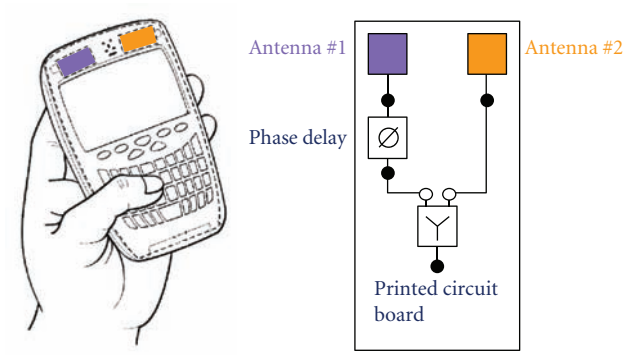

Figure 18: Illustration of a distributed antenna system having two elements placed at different locations of a handset device.

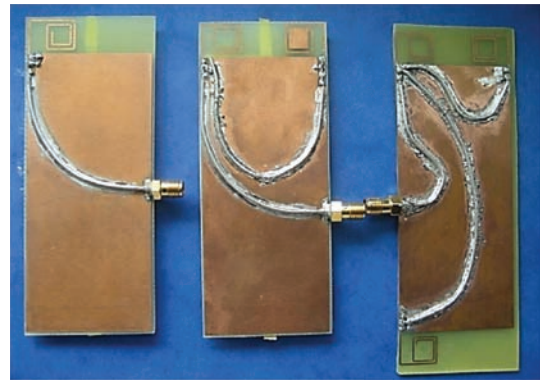

Figure 19: Single monopole (left); an array of two monopoles (middle); an array of three monopoles (right). Ground plane is 90 mm×40 mm printed on an FR4 substrate 1 mm thick. Monopoles are 13 mm × 11 mm.

measured in order to demonstrate the effectiveness of the proposal (Figure 19) [68]. The bandwidth (SWR ≤ 3) for the system with three monopoles is broader than that attained by the other prototypes. The bandwidth is 15.6%, 23.6%, and 34.0% for the single, two, and three antenna cases, respectively. It is worth to note that the three prototypes operate across the GSM850-GSM900 mobiles services. However, it should be taken into account that the array with three antennas operates also from 700 MHz to 824 MHz where neither the array of two antennas nor the single antenna present a good reflection coefficient. This is particularly useful for providing operation in the emergent communication standards, such as LTE700.

To determine the robustness to human loading, a hand phantom is used (Figure 20). The hand phantom is filled

(a) (b)

Figure 20: (a) Common holding position during a call; (b) the hand phantom emulating the real situation illustrated in (a).

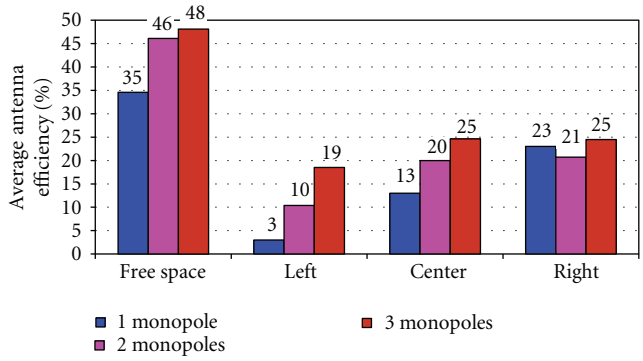

Figure 21: Comparisons of the measured average antenna efficiency (824–960 MHz) in free space and regarding hand loading for the proposed antenna systems depicted in Figure 19 and regarding the three positions of the finger.

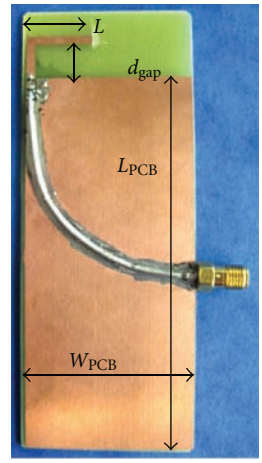

Figure 22: L-shaped monopole printed on a ground plane. The dimensions of the monopole antenna are $L = 23$ mm with a strip width of 2 mm, and it is located in the shorter edge of a PCB at a distance $D_{gap} = 4$ mm from the ground plane. The PCB dimensions are $L_{PCB} = 90$ mm and $W_{PCB} = 40$ mm.

with liquids emulating the electromagnetic properties of the human hand at the frequencies of interest [70]. Different experiments with the finger located 1 mm away from the antenna have been carried out considering three distinct positions: left, middle, and right. The palm is 20 mm spaced from the ground plane in order to characterize a realistic scenario when the user is holding the phone. For the three monopoles, the same scheme is used (the bottom monopole does not suffer from the finger loading effect).

For the single antenna, the finger in the right position is critical since the finger totally covers the antenna, whereas for the left position the finger is far away (Figure 21). It should be outlined that these experiments consider a critical scenario in which the finger is only 1 mm above the antenna.

For the array of two elements, efficiency is better for all cases except for the left position where the single antenna does not suffer from the finger effect since it is far away. However, in the best case of the single antenna, antenna efficiencies for the single and the array of two elements are quite comparable. The advantage of the array of two elements is demonstrated for the other cases, where the efficiency is above the efficiency of the single antenna case.

For the array of three elements, the advantages are even better since it presents the best results among the three prototypes. For example, for the right case, the efficiency in the 824–960 MHz frequency range is 2.5 dB higher than the array using two elements and 7.9 dB higher than the single antenna case, showing that this technique may be useful to mitigate the efficiency drop due to the finger loading that can be directly related to a decrement of the battery duration, reduction of coverage, and eventually call drops.

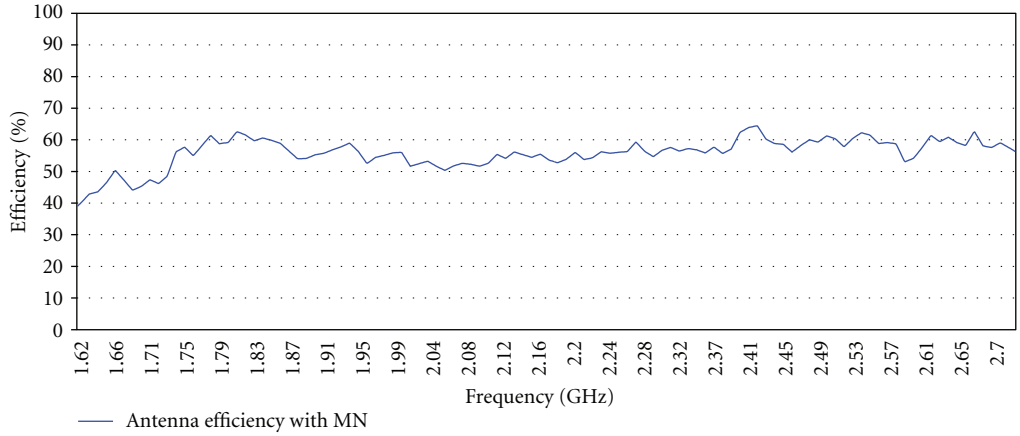

Figure 23: Measured antenna efficiency of the L-monopole shown in Figure 22. Broadband matching network consisting of a shunt $L = 3.3$ nH and a shunt $C = 1.3$ pF.

A distributed handset antenna system using three small monopoles has been described featuring enough bandwidth to cover the communication standards in the range of 686 to 970 MHz. This concept uses an array of monopoles with a proper phase shift to improve the bandwidth compared with a single antenna element. Moreover, the proposed system is robust to the finger effect because, when one element is interfered by the finger, there are still two more elements that efficiently contribute to the radiation. Finally, it should be emphasized that the proposed distributed system is completely passive, being advantageous in terms of simplicity and battery consumption.

4.3.3. Matching Networks. In combination with antenna techniques, matching networks play a significant role not only in tuning the band location but also in providing greater bandwidth [71–75]. A technique consisting of a simple circuit is discussed to enhance the bandwidth of a simple antenna by a factor of about 2.45 times for SWR = 3 [72, 73].

Matching networks using lumped components are widely used in many commercial handset devices. In many situations, the use of a matching network helps to fine tune the operating bands. Here, a technique for broadening the inherent bandwidth of a handheld antenna is reviewed. Basically, the technique consists in adding an LC shunt circuit that allows creating an impedance loop of proper size to be inscribed inside the circle of a given target SWR [73].

A circuit analysis shows that the bandwidth of an antenna featuring an input impedance similar to that produced by an RLC series circuit around the central operating frequency can be improved by a theoretical factor of 2.45 regarding an SWR = 3 [73]. To demonstrate the potential of this technique, a single L-shaped monopole featuring an RLC series input impedance along the central frequency of operation is matched with a broadband matching network (Figure 22). Bandwidth and efficiency measurements demonstrate that this single element of reduced dimensions can be operative at GSM1800, GSM1900, UMTS, LTE2100, LTE2300, and LTE2500 (Figure 23).

Measured radiation patterns are stable across the frequency range of operation being omnidirectional and having a minimum along the long axis of the PCB. Measured directivities range from 2.8 to 4.4 dB. As a result, a BW enhancement of at least one half of Fano's limit [76] is achieved with a simple two-stage matching network. As a practical example a monopole with an inherent BW_0 of 14.21% SWR $\leq$ 3 has been improved to achieve a BW_f of 52.4% SWR $\leq$ 3 with an average measured antenna efficiency of 56.5%.

As a conclusion, matching networks and in particular the proposed broadband matching network allows increasing the bandwidth of the antenna element without the necessity of increasing the antenna size.

4.3.4. Intelligence in the Ground Plane. The efforts on the antenna design have been mainly addressed to the antenna geometry and not to the ground plane, since its relevance in the radiation process was underestimated. Accordingly, the antenna element was typically a self-resonant element that provided an efficient radiation independently from the ground plane structure. Nevertheless, the ground plane is progressively acquiring relevance since several studies have demonstrated its strong contribution to the radiation properties [77–90].

The future generations of mobile phones will need to operate over as much frequency bands as possible, such as LTE700, GSM850, GSM900, DCS1800, PCS, UMTS, LTE2300, LTE2500, among others. It has been shown that a ground plane length of 0.4λ effectively excites the ground plane which improves bandwidth and efficiency [37].

Thus, the antenna design is mainly determined by the PCB dimensions, which are fixed by the size of the handset or wireless device. A further important limitation is the antenna height, which should be small enough as for allowing the emergent generation of ultraslim phones. Moreover, such new mobile phones also incorporate extra-large number of extra services, such as photo-video cameras, big displays to watch television, and several speakers for high-fidelity audio

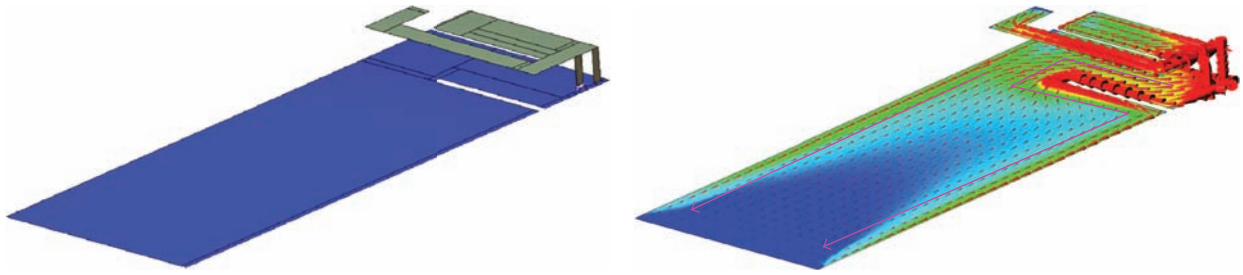

(a) (b)

Figure 24: (a) Introducing slots in the ground plane to electrically lengthen the current path. (b) Continuous arrows are a qualitative representation of the main current distribution for 900 MHz which is distributed along the long edges of the PCB. PCB is 100 mm × 40 mm.

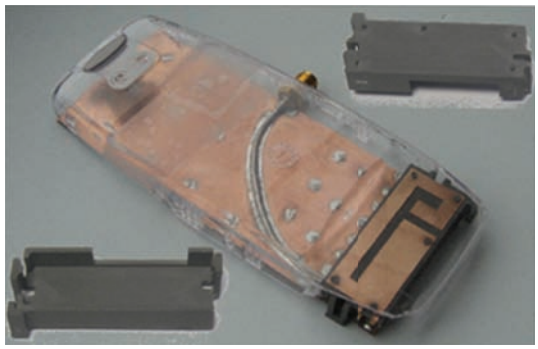

(a)

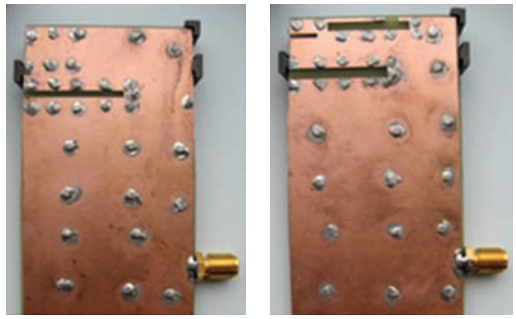

(b) (c)

Figure 25: Manufactured antenna prototypes: (a) dual-band PIFA and rear view of the, (b) quad-band, PIFA, and (c) the hexaband PIFA. In (a) the carrier to attach the metal plate and the plastic cover are also shown.

which undesirably contribute to the reduction of the available space to fit the antenna. Therefore new techniques are needed in order to attain the maximum performance with an antenna that occupies the smallest possible space. Three techniques to manipulate the ground plane are revisited:

(i) use of slot to lengthen the ground plane,

(ii) use of a conductive strip to lengthen the ground plane,

(iii) use of traps to electrically reduce the ground plane.

Lengthen the Ground Plane by Using Slots. To effectively enlarge the ground plane, slots can be used. The idea is illustrated in Figure 24 where the slot is used to tune the ground plane mode (enlarging the current path) at the low frequency range (900 MHz) while placed underneath the antenna area to act as a parasitic element at higher frequencies (1800–2100 MHz).

Prototypes of three PIFA antennas, namely, a dual-band PIFA without slots, a quad-band PIFA with one slot, and the proposed hexaband PIFA with multiple slots on the ground plane, have been constructed and studied (Figure 25) [88]. The simulation software IE3D was used for optimizing the design parameters.

In this concept, a slotted ground plane is used to improve the bandwidth at both low and high frequency regions without increasing the volume of the antenna. On one hand, at low frequencies, the slot is below resonance but forces the ground plane mode to be excited so as to increase the bandwidth at low frequencies; on the other hand, the slots are comparable to $\lambda/4$ at high frequencies, and therefore they enhance the bandwidth (Figure 26). This solution does not excite directly the slots as the case with PIFA and slots explained in Section 4.3.1 but by coupling being the PIFA the driven element.

The placement of a component (speaker) over the slot (without any metallic contact between the speaker and the ground plane) does not affect the antenna performance at low frequencies. However, it is critical at high frequencies when the component is close to the open edge of the slot [88]. The effect is minimized at the center and at the short end of the slot. Also, the SAR has been evaluated for this concept and the ones using slots in the ground plane. Results show that this concept presents a similar SAR to that of the PIFA on the bare PCB with the advantage that more bands are covered with the slotted ground plane solution [89].

This new design has been compared with the same design without the slots. Results show that the bandwidth and, as a consequence, the total efficiency are improved, obtaining a radiator useful for multiband handset applications.

Lengthen the Ground Plane by Using Conductive Strips. As discussed above, the ground plane plays an important role in the electromagnetic behavior of a handset antenna. The next technique uses a conductive strip on the ground plane to effectively produce an electromagnetic enlargement capable

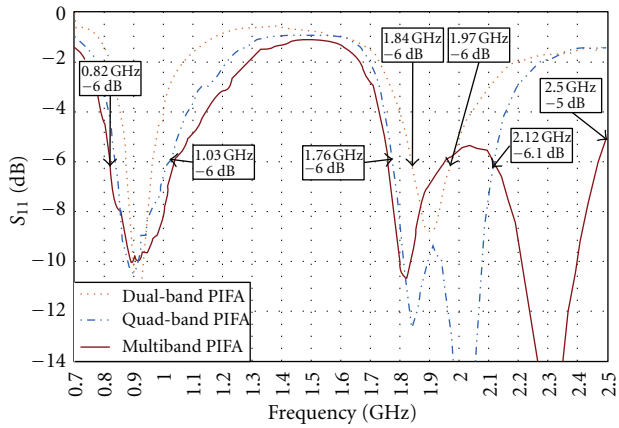

Figure 26: Measured reflection coefficient for the three studied prototypes. It can be seen how the proposed multiband design can operate at least over the GSM850, GSM900, DCS, PCS, UMTS, and Bluetooth bands.

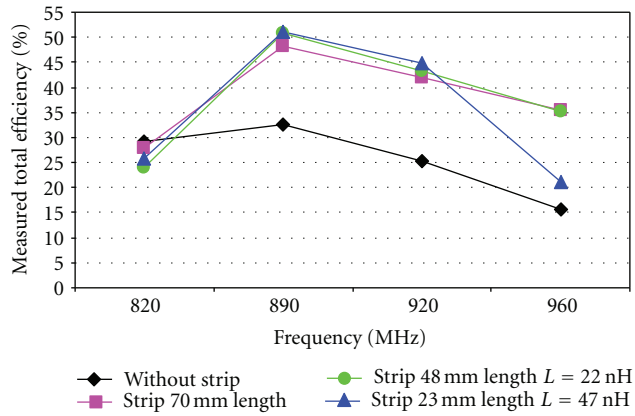

Figure 28: Measured total efficiency without the strip and with the strip considering loading inductors for the case shown in Figure 27. The case having L of 22 nH and 48 mm length effectively enhances the efficiency across the 820–960 MHz band.

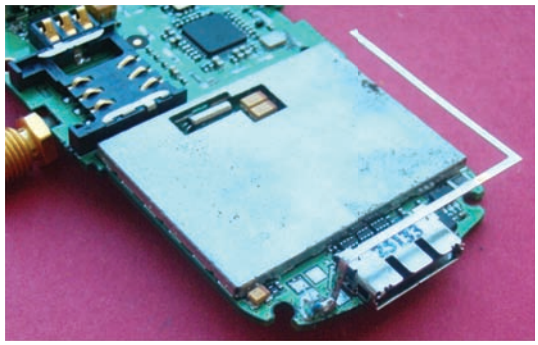

Figure 27: Conductive strip on a real handset PCB.

of tuning the resonant frequency of the fundamental mode to lower values close to 900 MHz (Figure 27). Basically, to make the ground plane larger, a strip at the opposite edge of the antenna location is used. Such a strip is designed to tune the ground plane mode [91]. As a result, the bandwidth and efficiency are increased. The length of the strip can be reduced by inductive loading and/or dielectric loading. Physical insight is given by electrical models [91] and using radar cross-section analysis [92].

Other authors have used the strip to mitigate the hand loading effect [63]. In [93], a mechanism to control near electrical and magnetic fields is used for hearing-aid compatibility.

To give a better perspective of the efficiency improvement, four case studies are selected (Figure 27): handset phone without strip, with the strip, with the strip length having 48 mm and 23 mm, and with the respective loading inductor. On one hand, it is clearly shown how the efficiency is improved at the low frequency region (Figure 28). The unloaded strip and the inductive loaded strip having 48 mm length perform very similar demonstrating the benefit of the inductance loading. The 23 mm case improves the efficiency peak but the efficiency drops at 960 MHz. In summary, the strip with 48 mm length improves the efficiency across the band. In particular, the improvement at 960 MHz is very significant: 3.5 dB. On the other hand, the strip does not alter the performance in the high frequency region [91].

As a conclusion, this technique is useful to improve the bandwidth and efficiency at the low frequency region where the ground plane is smaller than 0.4λ, which is approximately the optimum length to excite the fundamental mode of the ground plane and, thus, to maximize the bandwidth and efficiency.

Reducing the Ground Plane Using Stubs. In some platforms such as, for example, clamshell type handsets, the ground plane is large in open position. Moreover, if the antenna is placed at one edge instead of that in the hinge, it may excite a particular mode that results in a radiation pattern with many lobes and a minimum in the horizontal plane. In this regard, the present technique consists in reducing the electrical length of the ground plane by adding a trap (Figure 29) [94]. In [95], the technique of using traps increases the bandwidth at the high frequency region. In effect, at this frequency, a typical length of a bar-type handset of 100 mm is $0.63\lambda_0$ at 1900 MHz, being larger than $0.4\lambda_0$. Therefore, the strip forces the ground plane to be $0.4\lambda_0$ in length at such frequencies. Similar effects can be obtained by introducing a slot in the ground plane [96].

When the antenna is placed at one edge of a clamshell platform, the radiation in the horizontal plane does not present a maximum radiation due to a multilobe pattern. By adding the trap which is a short-ended $\lambda/4$ stub at the central frequency of operation, the current is blocked due to the high impedance of the stub. In this way, the current is minimized. As a result, the higher order mode has been removed at the ground plane that supports a fundamental mode which radiates with a maximum in the horizontal plane.

4.3.5. Ground Plane Boosters. Wireless device manufacturers regard the volume dedicated to the integration of the radiating structure and in particular the antenna element, as being

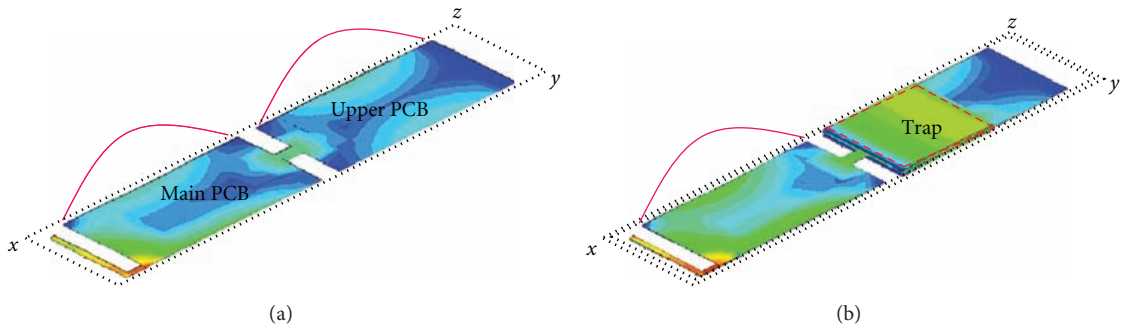

Figure 29: Simulated current distribution at 1.82 GHz without and with a shortening mechanism consisting of a short circuit plate of $\lambda/4$ at 1.82 GHz. The continuous line is a qualitative approach of the currents on the ground plane. For (a), a current mode having two sinusoids is supported causing a multi-lobe pattern. For (b), the current in the upper PCB board has been mitigated due to the trap.

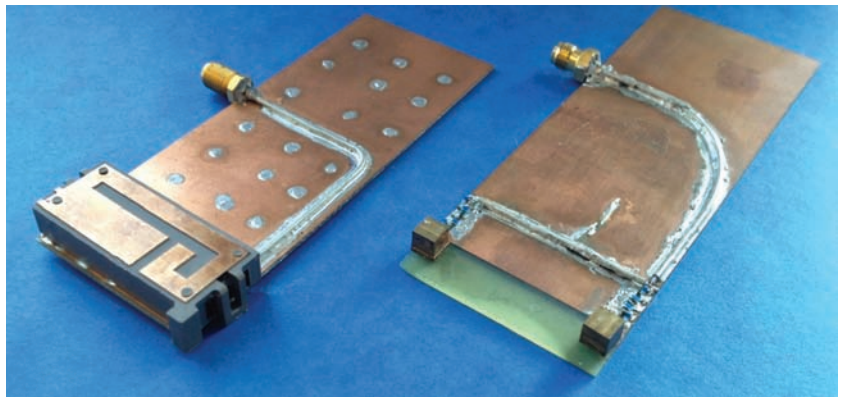

Figure 30: Comparison of a PIFA antenna and the solution based on ground plane boosters for operation at GSM850/900, DCS, PCS, and UMTS. The volume of the PIFA is 4600 mm^3, whereas the compact solution is only 250 mm^3.

a toll to pay in order to provide wireless capabilities to the handheld or portable device.

The new technique named ground plane booster antenna technology provides very compact elements, easy to integrate, and able to be used as standard elements [97–106]. This technique is based on the concept of using the ground plane as the main radiator. An element, called ground plane booster, is in charge of properly exciting the efficient radiation modes that the inherent ground plane of any wireless platform features at mobile frequencies. Its proper location together with a radiofrequency system allows multiband operation with significant small dimensions (e.g., only 250 mm^3 to obtain multiband performance at GSM850, 900, 1800, 1900, and UMTS), thus making the new architecture attractive to emergent multifunction wireless devices.

Other different approaches have appeared in the literature. In [107] two antenna structures based on coupling elements designed to transfer energy to the ground plane mode are presented. They are intended for covering the communication standards GSM900 and GSM1800 separately by means of a single-resonant matching circuit based on distributed matching elements. Other reference based on coupling elements is given in [108], where an antenna structure consisting in two coupling elements and two resonant circuits is proposed. The proposal achieves a quad-band behavior. Nevertheless, the coupling elements presented for covering each frequency region (624 mm^3 and 64 mm^3, resp.), and especially the one in charge of providing operability in the low frequency region, still present a considerable volume compared to the 250 mm^3 disclosed herein for providing pentaband operation. In [98, 100], the pentaband behavior is achieved by means of two ground plane boosters and two matching networks capable to provide multiband operation at each frequency region (Figure 30).

A wireless device employing very small elements would be advantageous as it would make the integration of the radiating structure into the wireless handheld device easier. The volume freed up by the absence of the antenna element would enable smaller and/or thinner devices, or even to adopt radically new form factors which are not feasible today due to the presence of an antenna element. Furthermore, by eliminating precisely the element that requires customization, a standard solution is obtained which only requires minor adjustments to be implemented in different wireless devices.

Accordingly, the present solution replaces the self-resonant antenna element by nonresonant ground plane boosters (Figure 31). In this case, a challenge appears since the ground plane resonance is not coupled to the antenna resonance. Thus, the present technique is focused on providing multiband wireless handheld device architecture based on

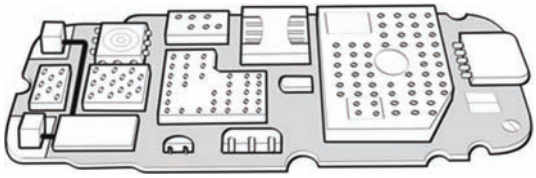

Figure 31: Schematic of a handset phone including two ground plane boosters located at the short edge of the PCB.

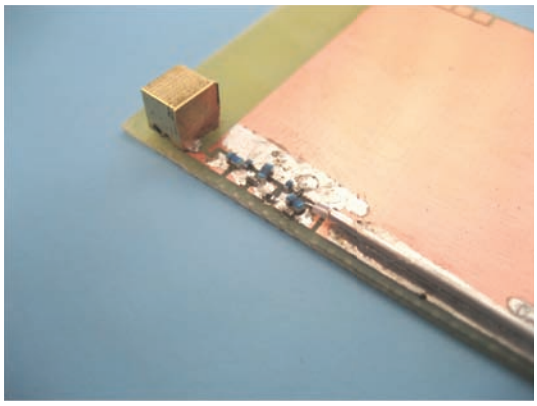

Figure 32: Single-band prototype including the reactance cancellation inductor and the broadband matching network.

the proper excitation of the ground plane without the need of an antenna element [97–100]. This technique demonstrates that no handset antenna is required for effectively exciting the radiation modes of the ground plane. The novel architecture introduced here only requires small ground plane boosters featured by a high quality factor ($Q \approx 2250$ for the low frequency region and $Q \approx 265$ for the high frequency region) and extremely poor stand-alone radiation properties in combination with a matching network for providing simultaneous operability in the main communication standards (GSM850/900, DCS, PCS, and UMTS) [100].

However, the proper excitation of the predominant mode is not enough for providing pentaband behavior and a matching network is required in order to guarantee operability in the aforementioned communication standards. For the present example, each ground plane booster uses a reactance element to cancel out the reactance and a broadbanding circuit as the one described in Section 4.3.3 to achieve enough bandwidth to cover the required standards. Such a broadbanding circuit follows the principles explained in Section 4.3.3 (Figure 32). Also, a combiner is used to merge the two port solution into a single input/output port (Figure 33).

In this sense, the conventional handset antenna featured by a considerable volume ($\approx 4550\,\text{mm}^3$) has been replaced by two low-volume nonresonant ground plane boosters ($250\,\text{mm}^3$) and a matching topology with a systematic design. These elements are in charge of properly exciting the efficient radiation mode of the ground plane, which presents high radiation efficiency and low Q at the frequencies of interest, especially in the low frequency region (GSM850/900). The

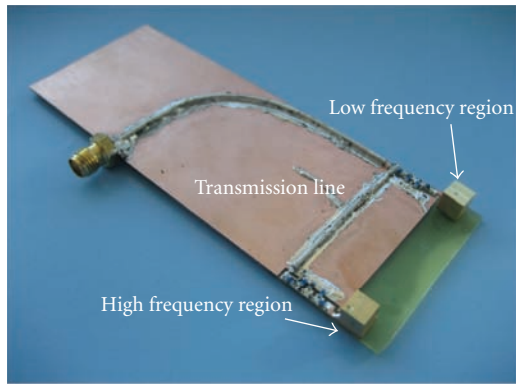

Figure 33: Pentaband prototype designed including the reactance cancellation inductor, the broadband matching network, and the notch filters required for providing isolation between both frequency regions.

systematic matching network design enables the operability in the desired frequency regions. The radiation contribution provided by such small boosters is negligible and they should not be considered as antennas. Consequently their integration in the handset platform removes the need of including a dedicated antenna in the wireless handheld device [97–106].

The effects of head absorption and SAR have been compared to other technologies such as PIFA using slots in the ground planes and the coupled monopoles presented in this paper, resulting in a technique more robust to the effects of the head [109].

This proposal becomes an alternative to current antenna technology and appears as a promising standard solution for being integrated in emergent multifunctional wireless devices since the available space in handset platforms for integrating new functionalities is further increased while the radiating performance is preserved. New advances in this field show the possibility of adding new bands such as LTE700 and LTE2100/2300/2500.

5. Conclusions

The apparition of new wireless communications systems with new platforms makes the antenna design a difficult challenge since not only more antennas are needed to operate at new bands but also the antennas require multiband operation and small size to be integrated into the wireless handheld devices.

However, the characterization of the antennas is as important as their design. The antennas integrated in wireless handheld devices operate in singular environments, like for example, the presence of the human body and the multipath signal propagation, which add additional challenges. These particular environments force the antenna community to characterize the integrated antennas in wireless handheld device to attain efficient antenna systems for this kind of situations. On one hand, head and hand phantoms are used to analyze the effect that the human body has on the electromagnetic performance of the antennas and also how the radiation

of the antennas affects the human body. This characterization facilitates the understanding of the antenna behavior which at the end serves to make robust antenna systems. On the other hand, the multipath environment fosters new measurements systems such as reverberation chambers which can emulate a real propagation environment.

Finally, smaller and multiband radiating systems are required to allow the integration of other handset components such as, for example, big displays which are a common feature of current smartphones and an important factor for the final user. In this regard, the ground plane boosters presented herein offer an alternative to current antenna technologies, since they significantly reduce the volume occupied by the radiating system while preserving the electromagnetic performance. An example of two ground plane boosters having a size of only 5 mm × 5 mm × 5 mm has been proved to operate at GSM850, GSM900, GSM1800, GSM1900, and UMTS. Therefore, the ground plane boosters become a promising technology for the new generation of wireless handheld devices.

Acknowledgments

The authors would like to thank the following institutions for their financial support: Spanish Ministry of Industry, Commerce, and Tourism and ACC1Ó.

References

[1] "Motorola Executive Helped spur Cellphone Revolution," *Wall Street Journal*, p. A10, 2009.

[2] http://www.ctia.org.

[3] http://www.fcc.gov.

[4] "Safety levels with respect to human exposure to radio frequency electromagnetic fields, 3 kHz to 300 GHz," ANSI/IEEE C95. 1.

[5] Guidelines for Limiting Exposure to Time-Varying Electric, Magnetic, and Electromagnetic Fields (up to 300 GHz), International Commission on Non-Ionizing Radiation Protection (ICNRP).

[6] "American national standard for methods of measurement of compatibility between wireless communications devices and hearing aids," ANSI C63.19-2007.

[7] M. Andersson, A. Wolfgang, C. Orlenius, and J. Carlsson, "Measuring performance of 3GPP LTE terminals and small base stations in reverberation chambers," in *Long Term Evolution: 3GPP LTE Radio and Cellular Technology*, chapter 12, CRC Press, New York, NY, USA, 2009.

[8] P. S. Kildal and K. Rosengren, "Correlation and capacity of MIMO systems and mutual coupling, radiation efficiency, and diversity gain of their antennas: simulations and measurements in a reverberation chamber," *IEEE Communications Magazine*, vol. 42, no. 12, pp. 104–112, 2004.

[9] P. S. Kildal, C. Orlenius, and U. Carlberg, "MIMO LTE OTA measurements in reverberation chamber: rich isotropic reference environment makes agreement with theoretical system model," in *Proceedings of the 6th European Conference on Antennas and Propagation (EuCAP '12)*, Prague, Czech Republic, March 2012.

[10] T. Taga, "Analysis for mean effective gain of mobile antennas in land mobile radio environments," *IEEE Transactions on Vehicular Technology*, vol. 39, no. 2, pp. 117–131, 1990.

[11] J. Carlsson, U. Carlberg, and P. S. Kildal, "Diversity gains in random line-of-sight and rich isotropic multipath environment," in *Proceedings of the Loughborough Antennas and Propagation Conference (LAPC'12)*, pp. 1–4, Leicestershire, UK, November 2012.

[12] C. Orlenius, P. S. Kildal, and G. Poilasne, "Measurements of total isotropic sensitivity and average fading sensitivity of CDMA phones in reverberation chamber," in *Proceedings of the IEEE Antennas and Propagation Society International Symposium and USNC/URSI Meeting*, pp. 409–412, Piscataway, NJ, USA, July 2005.

[13] A. Skarbratt, J. Åsberg, and C. Orlenius, "Over-the-air performance testing of wireless terminals by data throughput measurements in reverberation chamber," in *Proceedings of the 5th European Conference on Antennas and Propagation (EUCAP '11)*, pp. 615–619, Rome, Italy, April 2011.

[14] P. Lindberg and A. Kaikkonen, "Built-in handset antennas enable FM transceivers in mobile phones," RF Design Magazine, 2007.

[15] J. Anguera, D. Aguilar, J. Vergés, M. Ribó, and C. Puente, "Handset antenna design for FM reception," in *Proceedings of the IEEE Antennas and Propagation Society International Symposium*, San Diego, Calif, USA, 2008.

[16] D. Aguilar, J. Anguera, M. Ribó, and C. Puente, "Small handset antenna for FM reception," *Microwave and Optical Technology Letters*, vol. 50, no. 10, pp. 2677–2683, 2008.

[17] J. Anguera, C. Borja, C. Picher, and A. Andújar, "Wireless device providing operability for broadcasting standards and method enabling such operability," Patent application WO/2010/145825.

[18] C. Picher, J. Anguera, A. Andújar, C. Borja, C. Puente, and S. Kahng, "Reuse of the mobile communication antenna for FM reception," in *Proceedings of the 5th European Conference on Antennas and Propagation (EuCAP '11)*, pp. 324–327, Rome, Italy, April 2011.

[19] C. Borja, J. Anguera, C. Puente, and J. Vergés, "How much can be reduced the internal FM antenna of mobiles phones?" in *Proceedings of the 4th European Conference on Antennas and Propagation (EuCAP '10)*, Barcelona, Spain, April 2010.

[20] J. Anguera and A. Sanz, "Wireless portable device including internal broadcast receiver," Patent application WO, 2007/128340.

[21] C. Puente, E. Rozan, and J. Anguera, "Space filling miniature antennas," Patent application WO 01 54225.

[22] J. Vergés, J. Anguera, C. Puente, and D. Aguilar, "Analysis of the human body on the radiation of FM handset antenna," *Microwave and Optical Technology Letters*, vol. 51, no. 11, pp. 2588–2590, 2009.

[23] A. Pladevall, C. Picher, A. Andújar, and J. Anguera, "Some thoughts on human body effects on handset antenna at the FM band," *Progress in Electromagnetics Research M*, vol. 19, pp. 121–132, 2011.

[24] J. Anguera, C. Puente, E. Martínez, and E. Rozan, "The fractal Hilbert monopole: a two-dimensional wire," *Microwave and Optical Technology Letters*, vol. 36, no. 2, pp. 102–104, 2003.

[25] C. Puente, E. Rozan, and J. Anguera, "Space filling miniature antennas," Patent application WO0154225.

[26] D. Gala, J. Soler, C. Puente, C. Borja, and J. Anguera, "Miniature microstrip patch antenna loaded with a space-filling transmission line based on the fractal Hilbert curve," *Microwave and Optical Technology Letters*, vol. 38, no. 4, pp. 311–312, 2003.

[27] J. Anguera, *Fractal and broadband techniques on miniature, multifrequency, and high-directivity microstrip patch antennas [Ph.D. thesis]*, Department of Signal Theory and Communications, Universitat Politècnica de Catalunya, 2003.

[28] J. Anguera, C. Puente, C. Borja, and J. Soler, "Fractal-shaped antennas: a review," *Wiley Encyclopedia of RF and Microwave Engineering*, vol. 2, pp. 1620–1635, 2005.

[29] K. J. Vinoy, K. A. Jose, V. K. Varadan, and V. V. Varadan, "Resonant frequency of Hilbert curve fractal antennas," in *Proceedings of the IEEE Antennas and Propagation Society International Symposium*, vol. 3, pp. 648–651, Boston, Mass, USA, July 2001.

[30] K. J. Vinoy, K. A. Jose, V. K. Varadan, and V. V. Varadan, "Hilbert curve fractal antenna: a small resonant antenna for VHF/UHF applications," *Microwave and Optical Technology Letters*, vol. 29, no. 4, pp. 215–219, 2001.

[31] S. R. Best, "A comparison of the performance properties of the Hilbert curve fractal and meander line monopole antennas," *Microwave and Optical Technology Letters*, vol. 35, no. 4, pp. 258–262, 2002.

[32] S. R. Best, "A comparison of the resonant properties of small space-filling fractal antennas," *IEEE Antennas and Wireless Propagation Letters*, vol. 2, pp. 197–200, 2003.

[33] J. M. González-Arbesú, S. Blanch, and J. Romeu, "Are space-filling curves efficient small antennas?" *IEEE Antennas and Wireless Propagation Letters*, vol. 2, pp. 147–150, 2003.

[34] S. R. Best and J. D. Morrow, "The effectiveness of space-filling fractal geometry in lowering resonant frequency," *IEEE Antennas and Wireless Propagation Letters*, vol. 1, pp. 112–115, 2002.

[35] S. R. Best and J. D. Morrow, "On the significance of current vector alignment in establishing the resonant frequency of small space-filling wire antennas," *IEEE Antennas and Wireless Propagation Letters*, vol. 2, pp. 201–204, 2003.

[36] I. Sanz, J. Anguera, A. Andújar, C. Puente, and C. Borja, "The Hilbert monopole revisited," in *Proceedings of the 4th European Conference on Antennas and Propagation (EuCAP '10)*, Barcelona, Spain, April 2010.

[37] K. L. Wong, *Planar Antennas for Wireless Communications*, Wiley-Interscience, New York, NY, USA, 2003.

[38] T. Taga and K. Tsunekawa, "Performance analysis of a built-in planar inverted-F antenna for 800 MHz band portable radio units," *IEEE Journal on Selected Areas in Communications*, vol. 5, no. 5, pp. 921–929, 1987.

[39] C. R. Rowell and R. D. Murch, "A compact PIFA suitable for dual-frequency 900/1800-MHz operation," *IEEE Transactions on Antennas and Propagation*, vol. 46, no. 4, pp. 596–598, 1998.

[40] D. Manteuffel, A. Bahr, and I. Wolff, "Investigation on integrated antennas for GSM mobile phones," in *Proceedings of the ESA Millennium Conference on Antennas & Propagation (AP '00)*, Davos, Switzerland, April 2000.

[41] C. Puente, C. Borja, J. Anguera, and J. Soler, "Multilevel antennas," Patent application WO0122528.

[42] M. Martínez-Vázquez, O. Litschke, M. Geissler, D. Heberling, A. M. Martínez-González, and D. S. Sánchez-Hernández, "Integrated planar multiband antennas for personal communication handsets," *IEEE Transactions on Antennas and Propagation*, vol. 54, no. 2, pp. 384–391, 2006.

[43] C. Y. Chiu, P. L. Teng, and K. L. Wong, "Shorted, folded planar monopole antenna for dual-band mobile phone," *Electronics Letters*, vol. 39, no. 18, pp. 1301–1302, 2003.

[44] K. L. Wong, G. Y. Lee, and T. W. Chiou, "A low-profile planar monopole antenna for multiband operation of mobile handsets," *IEEE Transactions on Antennas and Propagation*, vol. 51, no. 1, pp. 121–125, 2003.

[45] K. L. Wong and C. H. Huang, "Printed loop antenna with a perpendicular feed for penta-band mobile phone application," *IEEE Transactions on Antennas and Propagation*, vol. 56, no. 7, pp. 2138–2141, 2008.

[46] K. L. Wong and S. C. Chen, "Printed single-strip monopole using a chip inductor for penta-band WWAN operation in the mobile phone," *IEEE Transactions on Antennas and Propagation*, vol. 58, no. 3, pp. 1011–1014, 2010.

[47] H. Kanj and S. M. Ali, "Compact multiband folded 3-D monopole antenna," *IEEE Antennas and Wireless Propagation Letters*, vol. 8, pp. 185–188, 2009.

[48] J. Ma, Y. Z. Yin, J. L. Guo, and Y. H. Huang, "Miniature printed octaband monopole antenna for mobile phones," *IEEE Antennas and Wireless Propagation Letters*, vol. 9, pp. 1033–1036, 2010.

[49] H. W. Hsieh, Y. C. Lee, K. K. Tiong, and J. S. Sun, "Design of a multiband antenna for mobile handset operations," *IEEE Antennas and Wireless Propagation Letters*, vol. 8, pp. 200–203, 2009.

[50] C. T. Lee and K. L. Wong, "Planar monopole with a coupling feed and an inductive shorting strip for LTE/GSM/UMTS operation in the mobile phone," *IEEE Transactions on Antennas and Propagation*, vol. 58, no. 7, pp. 2479–2483, 2010.

[51] J. Anguera, A. Condes, J. Soler, and C. Puente, "Coupled multiband antennas," Patent application WO 04/025778.

[52] S. Risco, J. Anguera, A. Andújar, A. Pérez, and C. Puente, "Coupled monopole antenna design for multiband handset devices," *Microwave and Optical Technology Letters*, vol. 52, no. 2, pp. 359–364, 2010.

[53] C. I. Lin and K. L. Wong, "Printed monopole slot antenna for internal multiband mobilephone antenna," *IEEE Transactions on Antennas and Propagation*, vol. 55, no. 12, pp. 3690–3697, 2007.

[54] C. H. Wu and K. L. Wong, "Hexa-band internal printed slot antenna for mobile phone application," *Microwave and Optical Technology Letters*, vol. 50, no. 1, pp. 35–38, 2008.

[55] N. Takemura, "Inverted-FL antenna with self-complementary structure," *IEEE Transactions on Antennas and Propagation*, vol. 57, no. 10, pp. 3029–3034, 2009.

[56] J. Anguera, I. Sanz, J. Mumbrú, and C. Puente, "Multiband handset antenna with a parallel excitation of PIFA and slot radiators," *IEEE Transactions on Antennas and Propagation*, vol. 58, no. 2, pp. 348–356, 2010.

[57] J. Anguera and C. Puente, "Shaped ground plane for radio apparatus," Patent application WO 2006/070017.

[58] S. K. Sharma, L. Shafai, and N. Jacob, "Investigation of wide-band microstrip slot antenna," *IEEE Transactions on Antennas and Propagation*, vol. 52, no. 3, pp. 865–872, 2004.

[59] C. H. Li, E. Ofli, N. Chavannes, and N. Kuster, "Effects of hand phantom on mobile phone antenna performance," *IEEE Transactions on Antennas and Propagation*, vol. 57, no. 9, pp. 2763–2770, 2009.

[60] M. Pelosi, O. Franek, M. B. Knudsen, G. F. Pedersen, and J. B. Andersen, "Antenna proximity effects for talk and data modes in mobile phones," *IEEE Antennas and Propagation Magazine*, vol. 52, no. 3, pp. 15–27, 2010.

[61] J. Ilvonen, O. Kivekäs, J. Holopainen, R. Valkonen, K. Rasilainen, and P. Vainikainen, "Mobile terminal antenna performance with the user's hand: effect of antenna dimensioning and location," *IEEE Antennas and Wireless Propagation Letters*, vol. 10, pp. 772–775, 2011.

[62] W. Yu, S. Yang, C. L. Tang, and D. Tu, "Accurate simulation of the radiation performance of a mobile slide phone in a hand-head position," *IEEE Antennas and Propagation Magazine*, vol. 52, no. 2, pp. 168–177, 2010.

[63] J. M. Jung, S. J. Kim, K. H. Kong, J. S. Lee, and B. Lee, "Designing ground plane to reduce hand effects on mobile handsets," in *Proceedings of the IEEE Antennas and Propagation Society International Symposium*, Honolulu, Hawaii, USA, June 2007.

[64] R. Valkonen, S. Myllymäki, A. Huttunen et al., "Compensation of finger effect on a mobile terminal antenna by antenna selection," in *Proceedings of the International Conference on Electromagnetics in Advanced Applications (ICEAA '10)*, pp. 364–367, Sydney, Australia, September 2010.

[65] J. Ilvonen, R. Valkonen, O. Kivekäs, P. Li, and P. Vainikainen, "Antenna shielding method reducing interaction between user and mobile terminal antenna," *Electronic Letters*, vol. 47, no. 16, pp. 896–897, 2011.

[66] J. Anguera and C. Puente, "Distributed antenna system robust to human loading effects," Patent application WO 2007/141187.

[67] J. Anguera, A. Camps, A. Andújar, and C. Puente, "Enhancing robustness of handset antennas to finger loading effects," *Electronics Letters*, vol. 45, no. 15, pp. 770–771, 2009.

[68] J. Anguera, A. Andujar, Y. Cobo, C. Picher, and C. Puente, "Handset antenna array to mitigate the finger loading effect," in *Proceedings of the 5th European Conference on Antennas and Propagation (EUCAP '11)*, pp. 611–614, Rome, Italy, April 2011.

[69] A. Andújar, J. Anguera, Y. Cobo, and C. Picher, "Distributed antenna systems for wireless handheld devices robust to hand loading," *IEEE Transactions on Antennas and Propagation*, vol. 60, no. 10, pp. 4830–4837, 2012.

[70] "Basic standard for the measurement of specific absorption rate related to human exposure to electromagnetic fields from mobile phones (300 MHz–3 GHz)," CENELEC-European Committee for Electrotechnical Standardization Std, EN 50 361, 2001.

[71] J. S. Lee, G. C. Kang, B. Jung et al., "Triple band internal antenna using matching circuits," in *Proceedings of the IEEE Antennas and Propagation Society International Symposium and USNC/URSI Meeting*, vol. 1A, pp. 442–445, July 2005.

[72] J. Anguera, C. Puente, C. Borja, G. Font, and J. Soler, "A systematic method to design single-patch broadband microstrip patch antennas," *Microwave and Optical Technology Letters*, vol. 31, no. 3, pp. 185–188, 2001.

[73] A. Andújar, J. Anguera, and C. Puente, "A systematic method to design broadband matching networks," in *Proceedings of the 4th European Conference on Antennas and Propagation (EuCAP '10)*, Barcelona, Spain, April 2010.

[74] Y. Li, B. Derat, D. Pasquet, and J. C. Bolomey, "Matching limits for a dual-band mobile phone antenna," in *Proceedings of the IEEE International Symposium on Microwave, Antenna, Propagation, and EMC Technologies for Wireless Communications (MAPE '07)*, pp. 656–659, Hangzhou, China, August 2007.

[75] Y. Li, T. Cantin, B. Derat, D. Pasquet, and J. C. Bolomey, "Application of resonant matching circuits for simultaneously enhancing the bandwidths of multi-band mobile phones," in *Proceedings of the IEEE International Workshop on Antenna Technology: Small and Smart Antennas Metamaterials and Applications (iWAT '07)*, pp. 479–482, Cambridge, UK, March 2007.

[76] R. M. Fano, "Theoretical limitations on the broadband matching of arbitrary impedances," *Journal of the Franklin Institute*, vol. 249, no. 2, pp. 139–154, 1950.

[77] T. Y. Wu and K. L. Wong, "On the impedance bandwidth of a planar inverted-F antenna for mobile handsets," *Microwave and Optical Technology Letters*, vol. 32, no. 4, pp. 249–251, 2002.

[78] M. C. Huynh and W. Stutzman, "Ground plane effects on planar inverted-F antenna (PIFA) performance," *IEE Proceedings: Microwaves, Antennas and Propagation*, vol. 150, no. 4, pp. 209–213, 2003.

[79] K. L. Wong, J. S. Kuo, and T. W. Chiou, "Compact microstrip antennas with slots loaded in the ground plane," in *Proceedings of the 11th International Conference on Antennas and Propagation (IEE Conference Publication No. 480)*, vol. 2, pp. 623–626, Manchester, UK, April 2001.

[80] P. Vainikainen, J. Ollikainen, O. Kivekäs, and I. Kelander, "Resonator-based analysis of the combination of mobile handset antenna and chassis," *IEEE Transactions on Antennas and Propagation*, vol. 50, no. 10, pp. 1433–1444, 2002.

[81] R. Hossa, A. Byndas, and M. E. Bialkowski, "Improvement of compact terminal antenna performance by incorporating open-end slots in ground plane," *IEEE Microwave and Wireless Components Letters*, vol. 14, no. 6, pp. 283–285, 2004.

[82] A. Byndas, R. Hossa, M. E. Bialkowski, and P. Kabacik, "Investigations into operation of single- and multi-layer configurations of planar inverted-F antenna," *IEEE Antennas and Propagation Magazine*, vol. 49, no. 4, pp. 22–33, 2007.

[83] M. F. Abedin and M. Ali, "Modifying the ground plane and its effect on planar inverted-F antennas (PIFAs) for mobile phone handsets," *IEEE Antennas and Wireless Propagation Letters*, vol. 2, pp. 226–229, 2003.

[84] B. Sanz-Izquierdo, J. Batchelor, and R. Langley, "Multiband printed PIFA antenna with ground plane capacitive resonator," *Electronics Letters*, vol. 40, no. 22, pp. 1391–1392, 2004.

[85] J. Anguera, I. Sanz, A. Sanz et al., "Enhancing the performance of handset antennas by means of groundplane design," in *Proceedings of the IEEE International Workshop on Antenna Technology: Small Antennas and Novel Metamaterials (iWAT '06)*, pp. 29–32, New York, NY, USA, March 2006.

[86] M. Cabedo, E. Antonino, V. Rodrigo, and C. Suárez, "Análisis Modal de un Plano de Masa Radiante Doblado y con una Ranura para Terminales Móviles," in *Proceedings of the 21st National Symposium URSI '06*, Oviedo, Spain, 2006.

[87] J. Anguera, I. Sanz, A. Sanz, T. Condes, C. Puente, and J. Soler, "Multiband PIFA handset antenna by means of groundplane design," in *Proceedings of the IEEE Antennas and Propagation Society International Symposium*, Albuquerque, NM, USA, July 2006.

[88] A. Cabedo, J. Anguera, C. Picher, M. Ribó, and C. Puente, "Multiband handset antenna combining a PIFA, slots, and ground plane modes," *IEEE Transactions on Antennas and Propagation*, vol. 57, no. 9, pp. 2526–2533, 2009.

[89] C. Picher, J. Anguera, A. Andújar, C. Puente, and S. Kahng, "Analysis of the human head interaction in handset antennas with slotted ground planes," *IEEE Antennas and Propagation Magazine*, vol. 54, no. 2, pp. 36–56, 2012.

[90] C. Picher, J. Anguera, A. Cabedo, C. Puente, and S. Kahng, "Multiband handset antenna using slots on the ground plane: considerations to facilitate the integration of the feeding transmission line," *Progress in Electromagnetics Research C*, vol. 7, pp. 95–109, 2009.

[91] J. Anguera, A. Andújar, and C. Puente, "A mechanism to electrically enlarge the ground plane of handset antennas: a bandwidth enhancement technique," *Microwave and Optical Technology Letters*, vol. 53, no. 7, pp. 1512–1517, 2011.

[92] J. Anguera and A. Andújar, "Ground plane contribution in wireless handheld devices using radar cross section analysis," *Progress in Electromagnetics Research M*, vol. 26, pp. 101–114, 2012.

[93] J. Holopainen, J. Ilvonen, O. Kivekäs, R. Valkonen, C. Icheln, and P. Vainikainen, "Near-field control of handset antennas based on inverted-top wavetraps: focus on hearing-aid compatibility," *IEEE Antennas and Wireless Propagation Letters*, vol. 8, pp. 592–595, 2009.

[94] J. Anguera and C. Puente, "Handset with electromagnetic bra," Patent application WO 2005/083833.

[95] P. Lindberg and E. Öjefors, "A bandwidth enhancement technique for mobile handset antennas using wavetraps," *IEEE Transactions on Antennas and Propagation*, vol. 54, no. 8, pp. 2226–2233, 2006.

[96] C. T. Lee and K. L. Wong, "Internal WWAN clamshell mobile phone antenna using a current trap for reduced ground plane effects," *IEEE Transactions on Antennas and Propagation*, vol. 57, no. 10, pp. 3303–3308, 2009.

[97] J. Anguera, A. Andújar, C. Puente, and J. Mumbrú, "Antennaless wireless device," Patent application WO2010/015365, 2009.

[98] J. Anguera, A. Andújar, C. Puente, and J. Mumbrú, "Antennaless wireless device capable of operation in multiple frequency regions," Patent Application WO2010/015364, 2009.

[99] J. Anguera and A. Andújar, "Antennaless wireless device comprising one or more bodies," Patent application WO 2011/095330.

[100] A. Andújar, J. Anguera, and C. Puente, "Ground plane boosters as a compact antenna technology for wireless handheld devices," *IEEE Transactions on Antennas and Propagation*, vol. 59, no. 5, pp. 1668–1677, 2011.

[101] A. Andújar, J. Anguera, C. Puente, and C. Picher, "Wireless device capable of multiband MIMO operation," Patent application WO 2012/017013.

[102] A. Andújar and J. Anguera, "Compact radiating array for wireless handheld or portable devices," Patent Application US 61/661, 885, 2012.

[103] J. Anguera, C. Picher, A. Andújar, and C. Puente, "Concentrated antennaless wireless device providing operability in multiple frequency regions," Patent application US 61/671906, 2012.

[104] A. Andújar and J. Anguera, "On the radiofrequency system of ground plane booster antenna technology," *Electronics Letters*, vol. 48, no. 14, pp. 815–817, 2012.

[105] A. Andújar and J. Anguera, "Multiband coplanar ground plane booster antenna technology," *Electronic Letters*, vol. 48, no. 21, pp. 1326–1328, 2012.

[106] A. Andújar and J. Anguera, "Magnetic boosters for multi-band operation," *Microwave and Optical Technology Letters*, vol. 55, no. 1, pp. 65–75, 2013.

[107] J. Villanen, J. Ollikainen, O. Kivekäs, and P. Vainikainen, "Coupling element based mobile terminal antenna structures," *IEEE Transactions on Antennas and Propagation*, vol. 54, no. 7, pp. 2142–2153, 2006.

[108] S. Ozden, B. K. Nielsen, C. H. Jorgensen, J. Villanen, C. Icheln, and P. Vainikainen, "Quad-band coupling element antenna structure," U.S. Patent 7, 274, 340, 2007.

[109] A. Andújar, J. Anguera, C. Picher, and C. Puente, "Ground plane booster antenna technology: Human head interaction: functional and biological analysis," in *Proceedings of the 6th European Conference on Antennas and Propagation (EuCAP '12)*, pp. 2745–2749, Prague, Czech Republic, 2012.

Hindawi Publishing Corporation
International Journal of Antennas and Propagation
Volume 2013, Article ID 580872, 8 pages
http://dx.doi.org/10.1155/2013/580872

Application Article

Evaluation of SAR Distribution in Six-Layer Human Head Model

Asma Lak[1] and Homayoon Oraizi[2]

[1] *Young Researchers Club, Bushehr Branch, Islamic Azad University, Bushehr, Iran*
[2] *Iran University of Science and Technology, Tehran, Iran*

Correspondence should be addressed to Asma Lak; lak.asmae@gmail.com

Received 4 May 2012; Revised 2 August 2012; Accepted 16 October 2012

Academic Editor: Aurora Andújar

The interaction between human head model and electromagnetic field sources is studied. The head models are composed of one and six layers. The six layers are skin, fat, bone, dura (the outer membrane of brain and spinal cord), CSF (colony stimulating factor), and brain. An antenna as a source of exposure is simulated too. The E-field strength distribution in both one- and six-layer human models is shown to estimate the intensity of E-field penetration in human head. Like standard models, the antenna is situated near the head model at a distance of 5 mm. The local and average SARs (specific absorption rates) are simulated at 900 MHz in both human head models. The results are then compared between the two models. The HFSS software is used for all the simulations. The paper wants to show that the initial model (one layer) is not a good model, because the real human head tissue is not equivalently modeled. It seems that the values of one-layer model are not reliable, so the paper considers the better and more similar human head model and compares these two models.

1. Introduction

It is well known that high frequency EM fields can damage human and other biological tissues by damaging molecular structure and rising of body temperature. The biological effects of radiofrequency fields and living systems can be evaluated at various levels including the molecular, subcellular, organ, or whole body environments. According to [1, 2], bioeffects from radiofrequency fields are classified into three categories: that is, high-level effects (thermal), intermediate-level effects (athermal), and low-level effects (nonthermal). Thermal effects are energy depositions higher than the natural human thermoregulatory capacity. The studies show some effects due to nonthermal and athermal sources such as: blood brain barrier, morphology, immune system, gene and chromosomal morphology, enzyme activity, and tumour promotion. More information can be seen in [3–5]. In this paper dosimetry and SAR are defined. So the human head model (one and six layers) and an antenna as an exposure source are simulated in HFSS software. For validation of results two antenna types are used, dipole and PIFA. The results for SAR and E-field strength for these two models are shown and compared. Because of some limitations the standard phantom models are made of one layer. For example, because of the gel or liquid materials, it is not easy to model all tissues. For example, the human head is a multilayer tissue, and its modelling is very hard. These phantoms are not good models for the human tissue, because the real properties of tissues are different from each other. Also, the human head does not have equivalent electrical properties. So the Six-layer phantom model is the better model of human head to simulate.

2. Measurements of EM Field Absorption

In this part the dosimetry is introduced. Some parameters have been used to measure EM fields. The SAR as a quantity for EM measurement at radiofrequency spectrum is defined and finally the electrical properties of tissues, that is, conductivity and permittivity, are described.

2.1. Definition of Dosimetry. According to [7] the relationship between exposure levels and electromagnetic energy deposited in the body is called "electromagnetic dosimetry." On the other hand, the electromagnetic dosimetry describes the relationship between the induced fields in biological bodies and distribution of an electromagnetic field in free

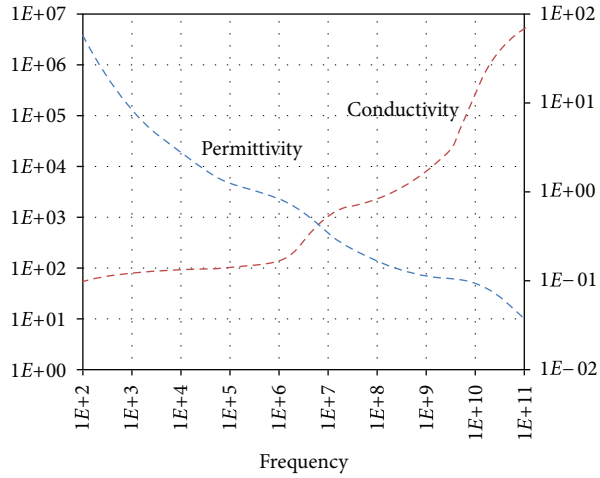

Figure 1: Dielectric properties spectrum of a high water content tissue [3].

space. Dosimetry information is very important to protect humans from probable electromagnetic field health hazards.

2.2. Specific Absorption Rate. By the widespread wireless device applications, such as mobile phones, the persons, and operators living and working in near electromagnetic sources, the biological effects of exposure to these electromagnetic fields are an important subject. The safety standards, such as the Federal Communication Commission (FCC), the International Commissions on Nonionizing Radiation Protection (ICNIRP), and National Radiological Protection Board (NRPB), are established for human protection and safety from electromagnetic fields. The specific absorption rate (SAR) is used to quantify the energy absorbed in tissues at radiofrequency spectrum, which is expressed in units of watts per kilogram. SAR is defined as the ratio of the absorbed power to the absorbing mass [7, 8]. The total power absorbed in the human body is

$$P_{\text{abs}} = \int_V \frac{1}{2}\,\sigma |E|^2 dV, \tag{1}$$

where σ is the conductivity of tissue, E is the electric field intensity, and V is the volume of the biological tissue. SAR is defined as

$$\text{SAR} = \left(\frac{\sigma}{2\rho}\right) E_i^2, \tag{2}$$

where σ is the conductivity of tissue, E is is the electric field intensity and ρ is the mass density of the tissue.

2.3. Human Tissues. Human body tissues have different values of dielectric properties, that is, permittivity and conductivity [9]. These properties are functions of several variables, such as frequency, geometry and size of tissue, and water contents. For example, the dielectric constant of a high water content tissue is shown in Figure 1, as a function of frequency.

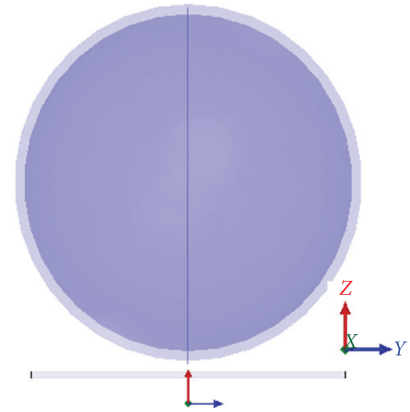

Figure 2: One-layer human head model defined in HFSS software.

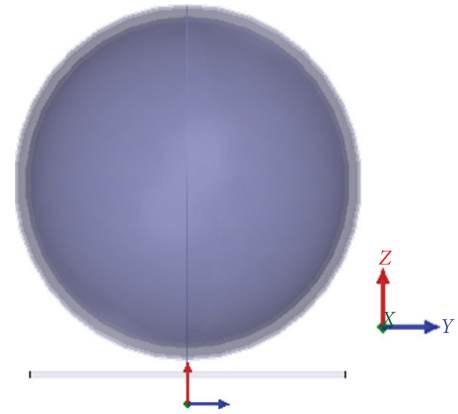

Figure 3: Six-layer human head model defined in HFSS software.

3. Simulations

Many researchers have simulated, measured, and evaluated the probable biological effects of EM fields on the human and other living systems. Several researchers have simulated the human body models, specially the human head and have evaluated the effective parameters on SAR [11–14].

3.1. Phantoms. Measurements of SAR and EM fields in the human body are not possible; consequently, the phantoms have been designed to model the human body at normal body temperatures. They have many shapes, such as spherical and human-like bodies. The liquids or gels as materials to tissues are placed in phantoms and exposure source is situated near them. One robot arm will then measure the E or H field by a probe placed at various locations near the model. A computer processor calculates the SAR. These measurement systems have several problems.

3.2. Modelling by HFSS Software. Because of the available commercial systems, the common models for SAR measurements are a thin bowl (a 5 mm thickness shell with 4.6 relative permittivity) containing fully the head (brain) tissue equivalent materials. Figure 2 shows this commercial model.

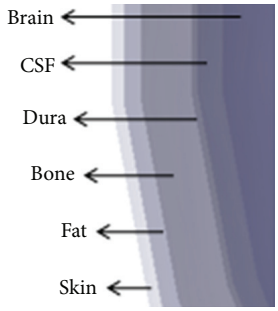

Figure 4: The perspective of Six-layer human head model [6].

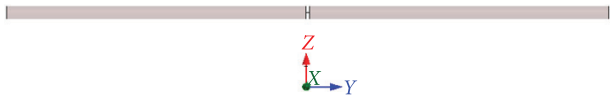

Figure 5: Dipole antenna.

Table 1: Specifications of one-layer head.

Tissue	Permittivity	Conductivity (S/m)	Thickness (mm)
Head equivalent material	41.5	0.9	85
Shell	4.6	0	5

Table 2: Other specifications of model.

Dipole length	149 mm
power	1 Watt
SAR line*	180 mm

*SAR line is a line that HFSS software measures the SAR around it.

Then a six-layer human head model has been tried instead of a one-layer common phantom model, because it models the real human head in a much better way as shown in Figure 3. This new model is composed of six spheres, similar to a six-layer model for the human head, that is, skin, fat, bone, dura, CSF, and brain as shown in Figure 4.

Tables 1, 2, and 3 show the model properties and dimensions in HFSS simulations.

3.3. Source Exposure. A dipole antenna has been used as the exposure source as shown in Figure 5. The antenna is situated at 5 mm distance from the head models in both one- and six-layer models. The simulations have been done at frequency 900 MHz. The length of antenna is 149 mm, its radius is 1.8 mm and the frequency of operation is 900 MHz.

3.4. Characteristics of Models. All specifications of the one- and six-layer human head model and dipole antenna are shown in Tables 1 to 3.

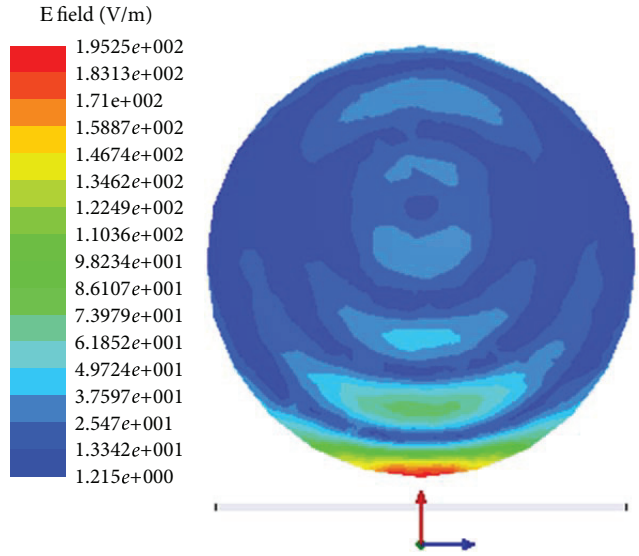

Figure 6: E-field strength distribution in one-layer human head model at 900 MHz.

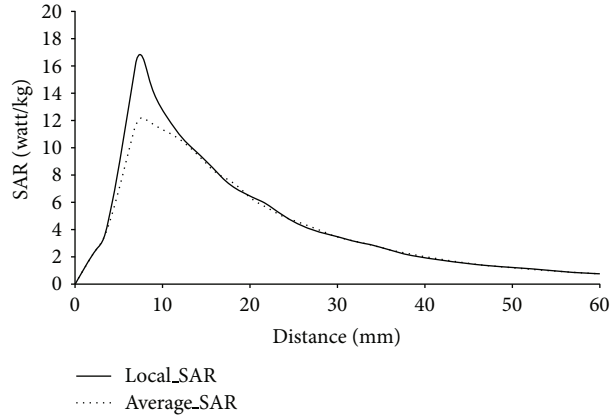

Figure 7: Head model as a function of the distance between the dipole and the head model.

Table 3: Tissue properties and thickness of six-layer human head model [6].

Tissue	Permittivity	Conductivity (S/m)	Thickness (mm)
Skin	40.7	0.65	1
Fat	10	0.17	0.14
Bone	20.9	0.33	0.41
Dura	40.7	0.65	0.5
CSF	79.1	2.14	0.2
Brain	41.1	0.86	81

4. Results

In this section the results of human head model in one and six layer and antenna model both dipole and PIFA are shown. Also the results for SAR and electric fields strength are compared.

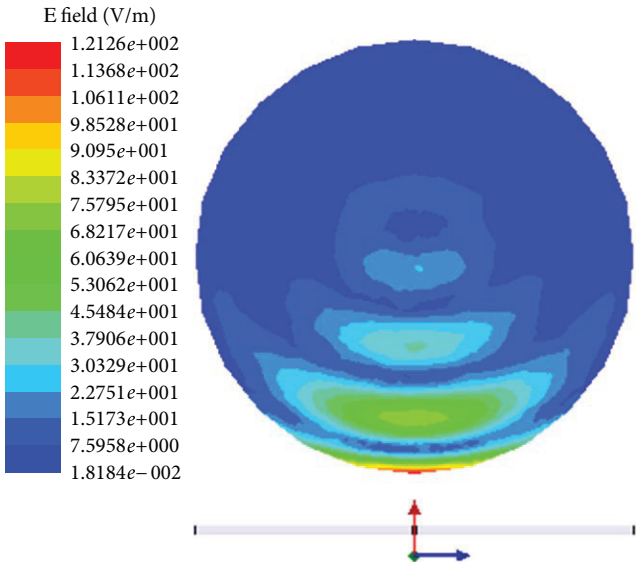

Figure 8: E-field strength in brain tissue at 900 MHz.

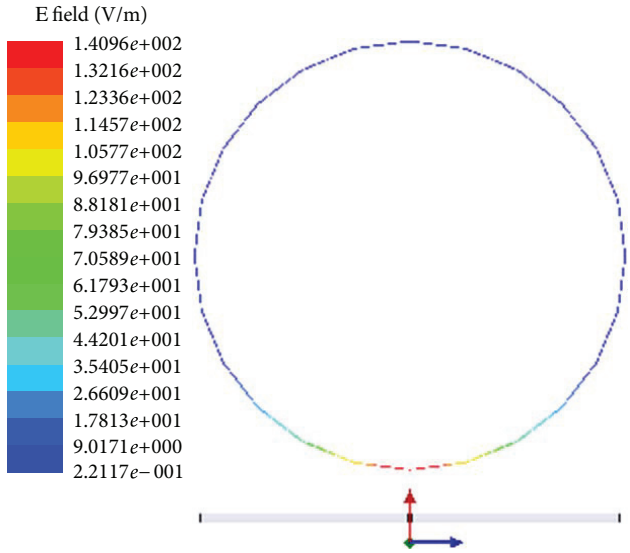

Figure 10: E-field strength in Dura tissue at 900 MHz.

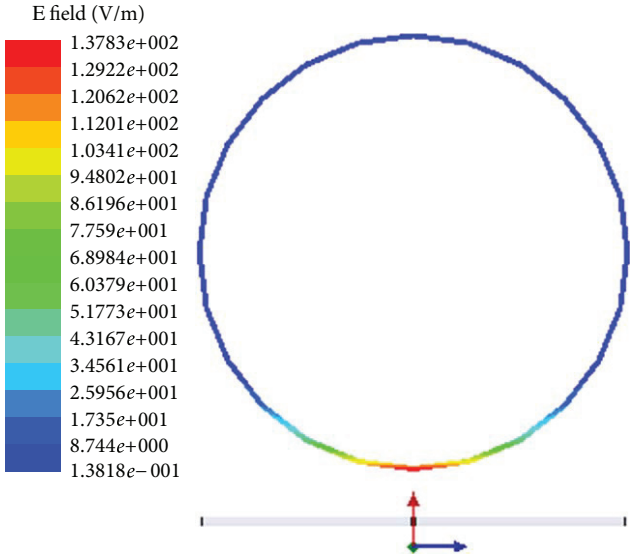

Figure 9: E-field strength in CSF tissue at 900 MHz.

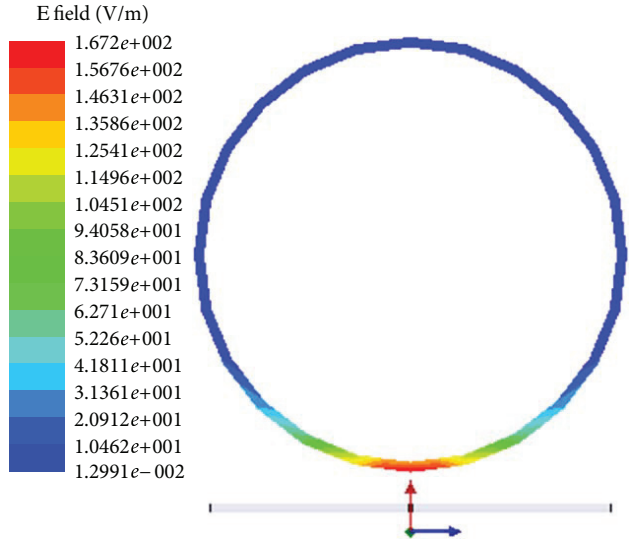

Figure 11: E-field strength in bone tissue at 900 MHz.

Table 4: E-field strength in six-layer model, dipole antenna.

Tissue	E-field strength (V/m)
Skin	1.80×10^2
Fat	1.77×10^2
Bone	1.67×10^2
Dura	1.40×10^2
Csf	1.37×10^2
Brain	1.21×10^2

4.1. "One-Layer" Human Head Model with Dipole Antenna at 0.9 GHz. This model consists of a shell with 5 mm thickness and a sphere with 85 mm radius as the head equivalent materials. According to (2), the SAR has a direct relationship to the E-field strength. Because of the importance of the electric field in SAR calculations, the E-field strength distribution in the one-layer head model is shown in Figure 6. The maximum value is at the nearest point to the source exposure (red colour). The local and average SAR as a function of the distance between the dipole and the head model is shown in Figure 7.

4.2. "Six-Layer" Human Head Model with Dipole Antenna at 0.9 GHz. The E-field distribution in the six-layer model is simulated and shown in Figures 8, 9, 10, 11, 12, and 13. The E-field strength is simulated in all the six layers, by the aforementioned procedure.

The result of simulations is shown in the Table 4. As shown the E-field strength is decreasing by the distance

Table 5: Compression between SAR in two models (one- and six-layer model by Dipole antenna).

Max SAR (Watt/Kg)	Layer	Conductivity	Local SAR	Average SAR
One layer + dipole	Shell	0	0	0
	Head equivalent material	0.9	$1.8 \times 10^{+1}$	$1.2 \times 10^{+1}$
Six layers + dipole	Skin	0.65	$1.39 \times 10^{+2}$	$2.2 \times 10^{+1}$
	Fat	0.17	$3.57 \times 10^{+1}$	7.77
	Bone	0.33	$5.06 \times 10^{+1}$	$2.05 \times 10^{+1}$
	Dura	0.65	$6.6 \times 10^{+1}$	7.83
	CSF	2.14	$2.16 \times 10^{+2}$	$7.75 \times 10^{+1}$
	Brain	0.86	$8.8 \times 10^{+1}$	$4.5 \times 10^{+1}$

Table 6: E-field strength in six layers (PIFA antenna).

Tissue	E-field strength (V/m)
Skin	7.99×10^{-1}
Fat	7.8×10^{-1}
Bone	7.4×10^{-1}
Dura	6.4×10^{-1}
CSF	6.2×10^{-1}
Brain	5.2×10^{-1}

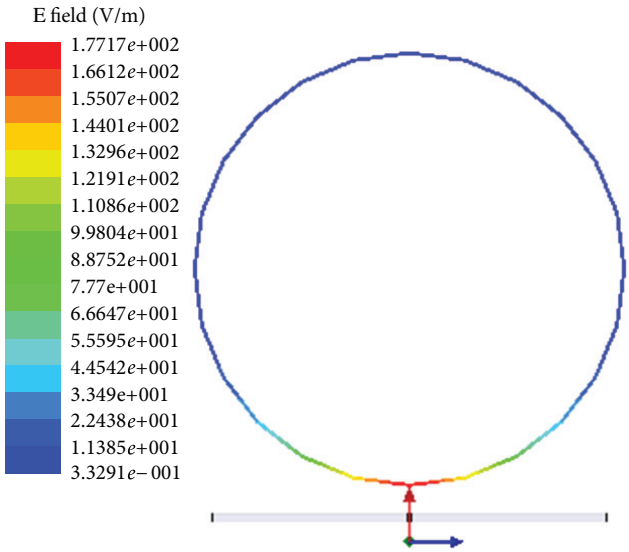

Figure 12: E-field strength in fat tissue at 900 MHz.

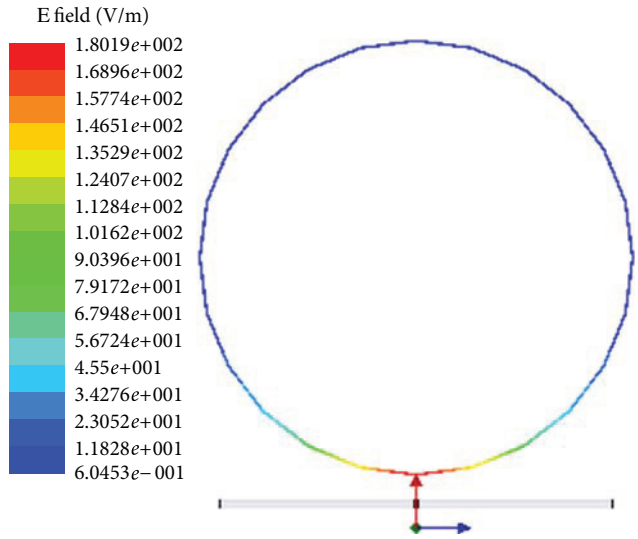

Figure 13: E-field strength in skin tissue at 900 MHz.

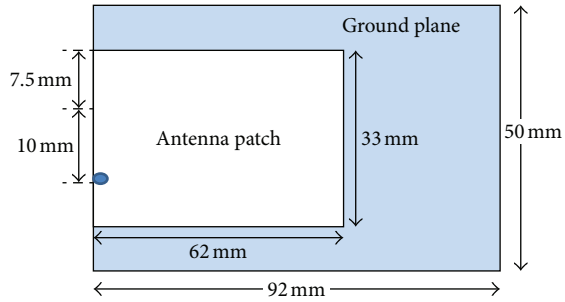

Figure 14: The structure of PIFA antenna at 0.9 GHz [10]. *Height of the antenna patch from the ground plane is the 7.5 mm.

from the source, consequently the maximum value of E-field strength in the brain tissue as an internal layer is the lowest.

The comparison of SAR between one- and six-layer head models are given in Table 5.

The values show that the maximum of SAR strength in the six layers is more than one layer. It says that the standard model (that is used in standard systems) may be not suitable and complete and does not show the accurate model of human tissues.

4.3. "Six-Layer" Human Head Model with PIFA Antenna at 0.9 GHz. For further consideration of the problem, simulation is repeated for head model, but with PIFA antenna at 900 MHz [10]. The geometry of antenna is shown in Figures 14, 15, and 16. The other specifications of the model are according to Table 1. The results for the E-field strength and SAR simulations are shown in Figures 17, 18, 19, 20, 21, and 22.

The results show that the E-field strength is decreasing by increasing the distance from the source: consequently, the maximum value of E-field strength in the brain tissue at the internal layer is the lowest. The results for PIFA antenna are similar to those of dipole antenna, with regards

Table 7: Compression between SAR in two models (one- and six-layer model by PIFA antenna).

Max SAR (watt/Kg)	Layer	Conductivity	Local SAR	Average SAR
One layer + PIFA	Shell	0	0	0
	Head equivalent material	0.9	1.27×10^{-4}	0.83×10^{-4}
Six layers + PIFA	Skin	0.65	2.4×10^{-3}	1.27×10^{-3}
	Fat	0.17	1.4×10^{-3}	0.9×10^{-3}
	Bone	0.33	1×10^{-3}	0.99×10^{-3}
	Dura	0.65	1.5×10^{-3}	0.52×10^{-3}
	CSF	2.14	5×10^{-3}	3.2×10^{-3}
	Brain	0.86	2×10^{-3}	1.47×10^{-3}

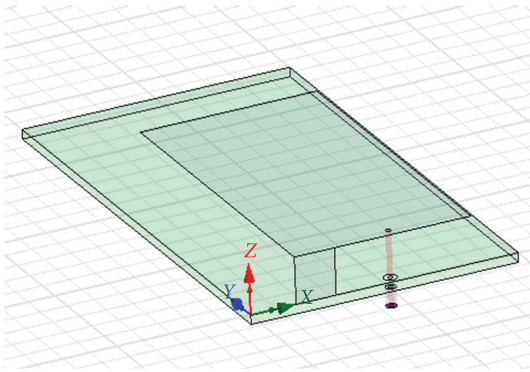

Figure 15: PIFA antenna at 900 MHz.

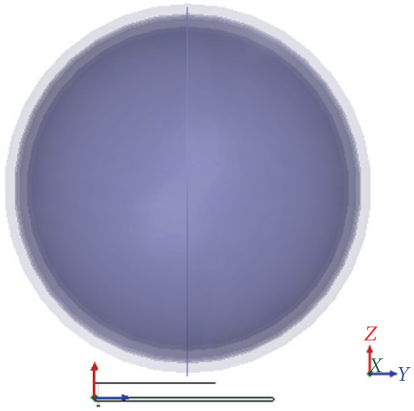

Figure 16: Six-layer human head model with PIFA antenna.

to the decreasing values of SAR with increasing the distance between the source and head. Table 6 shows the results for PIFA antenna.

Table 7 shows the SAR maximum strength values in one- and six-layer model by PIFA antenna as a source exposure. According to these results it has been seen that the SAR values in these simulation depend on the distance from antenna and conductivity value of tissues. For example in one-layer model shell is the nearer layer to the exposure source, so although it has lower conductivity, the SAR is more than head equivalent material. Also in six-layer model the SAR is varied by conductivity and distance from the exposure source too.

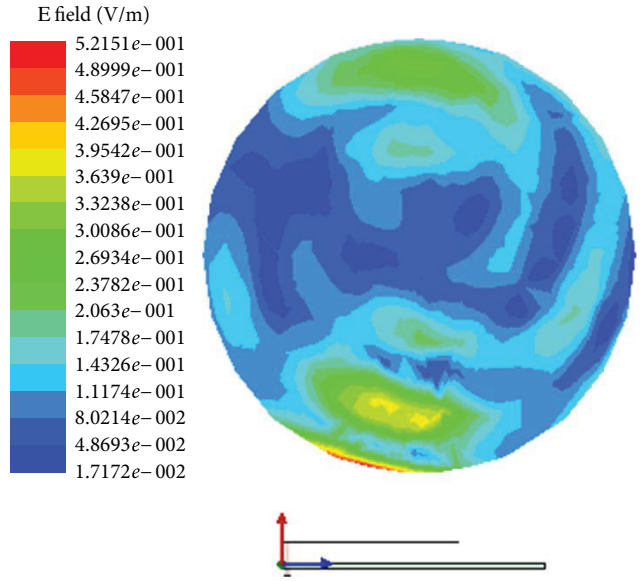

Figure 17: E-field strength in brain tissue at 900 MHz.

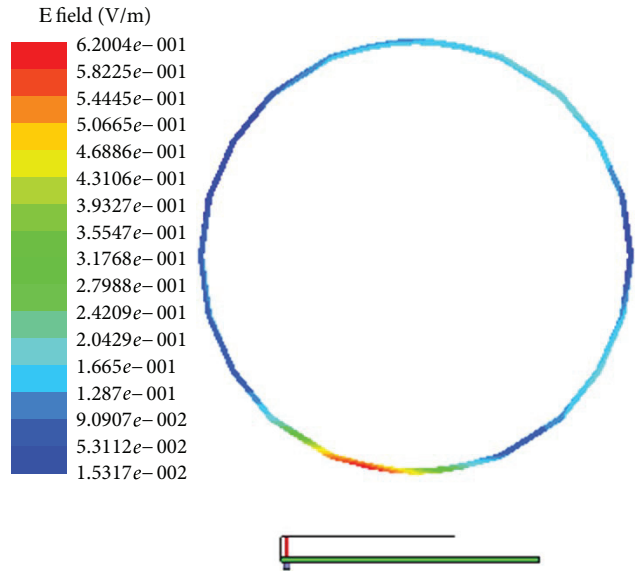

Figure 18: E-field strength in CSF tissue at 900 MHz.

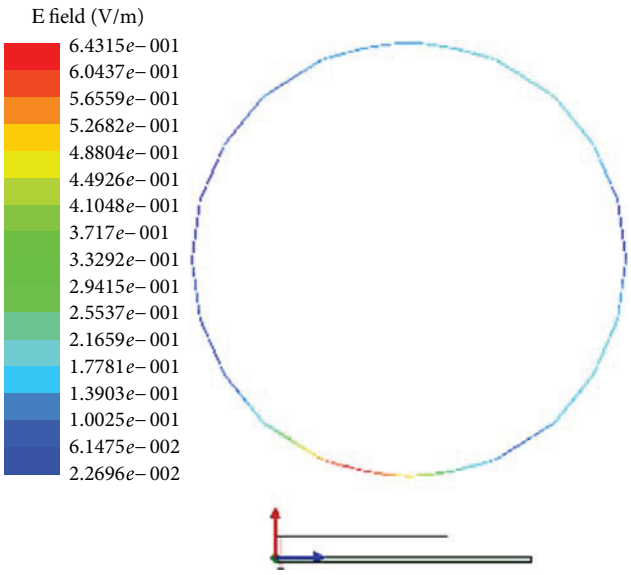

Figure 19: E-field strength in Dura tissue at 900 MHz.

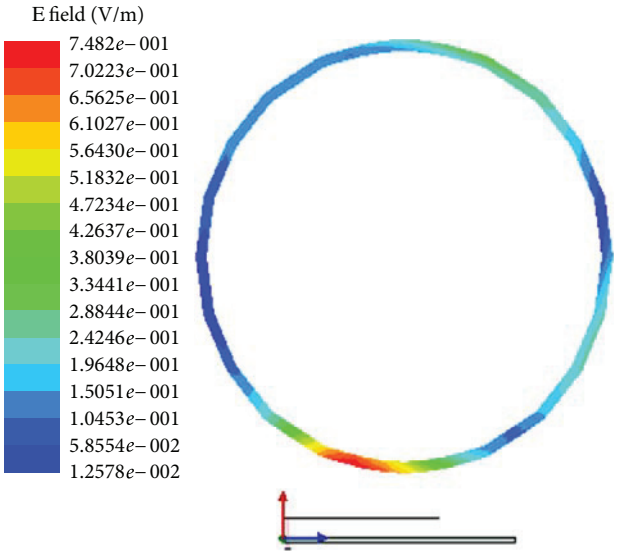

Figure 20: E-field strength in bone tissue at 900 MHz.

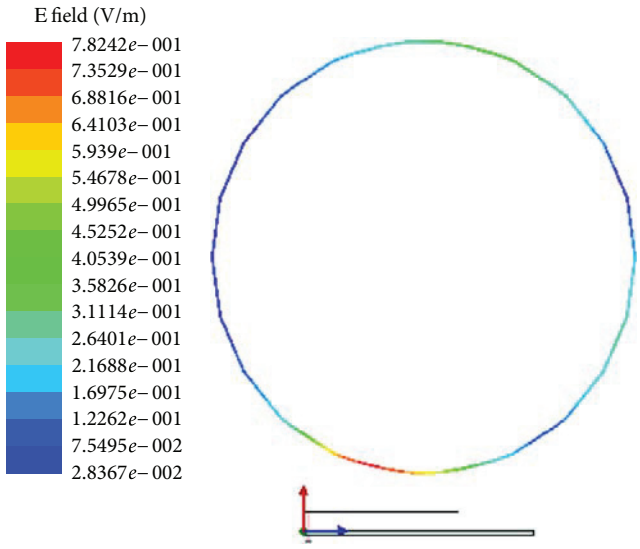

Figure 21: E-field strength in fat tissue at 900 MHz.

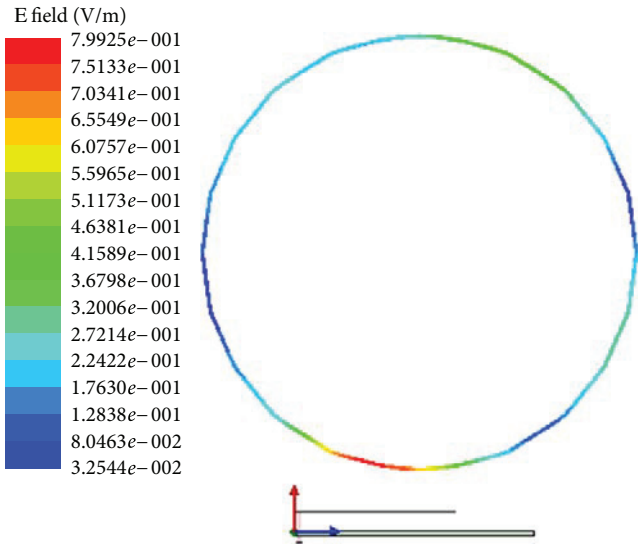

Figure 22: E-field strength in skin tissue at 900 MHz.

For example, dura and skin have same conductivity but the skin is the nearer layer to antenna, so it has more SAR.

The penetration of fields on human body, for example, human head, has been considered by many researchers. Some of these researches are in simulation by software and some of them are done by measurement systems (human phantom models). For more information the references [15–18] can be seen. So, at the same frequency of exposure source, the results may be different because of the difference in human body model.

5. Conclusions

The simulations are done at 900 MHz, because it is the standard for the mobile communication systems. The resulting data show that when the human body tissue especially the human head (because of placing the cell phone near the head) is exposed to EM fields; the fields penetrate in all the human head tissues. The E-field strength penetration and SAR deposition depend on tissue material properties (conductivity, permittivity, and permeability). By increasing the conductivity, SAR increases too. In this paper two human head models have been used, one and six layer. The one-layer human head model is simple and easy to use for simulation and measurement system, because the human body equivalent materials are gel or liquid in commercial SAR measurement system. But it has no assurance and the measurements are not reliable, because it does not show a good and real model of human head.So Six-layer head model has been used. In Tables 5 and 7, the local and average SAR for one and six layer is shown. The compression of both local

and average SAR in six-layer models is more than one layer. Furthermore, the commercial models (viz., one layer model) may not be good models for the human body, because the results show that the EM field penetration is higher in a six-layer model. So the design of a better model is unavoidable for the study of the exposure of human body to EM field sources. The result for another mobile antenna, that is, PIFA is repeated and showes similar results. Results show that by PIFA antenna the E-field strengths are very lower. According to (2) the SAR is lower too.

References

[1] M. H. Repacholi, "Low-level exposure to radiofrequency electromagnetic fields: health effects and research needs," *Bioelectromagnetics*, vol. 19, no. 1, pp. 20–32, 1998.

[2] A. G. Pakhomov, Y. Akyel, O. N. Pakhomova, B. E. Stuck, and M. R. Murphy, "Current state and implications of research on biological effects of millimeter waves: a review of the literature," *Bioelectromagnetics*, vol. 19, no. 7, pp. 393–413, 1998.

[3] F. S. Barnes and B. Greenebaumby, *Bioengineering and Biophysical Aspects of Electromagnetic Fields, Handbook of Biological Effect of Electromagnetic Fields*, Taylor & Francis Group, London, UK, 3rd edition, 2007.

[4] P. Vecchia, R. Matthes, G. Ziegelberger, James Lin, and R. Saunders, *Exposure To High Frequency Electromagnetic Fields, Biological Effects and Health Consequences (100 KHz–300 GHz)*, International Commission on Non-Ionizing Radiation Protection, Oberschleissheim, Germany, 2009.

[5] J. C. Lin, "Effects of microwave and mobile telephone exposure on memory process," *IEEE Antenna and Propagation Magazine*, vol. 42, no. 3, pp. 118–120, 2000.

[6] H. Khodabakhshi and A. Cheldavi, "Irradiation of a six-layered spherical model of human head in the near field of a half-wave dipole antenna," *IEEE Transactions on Microwave Theory and Techniques*, vol. 58, no. 3, pp. 680–690, 2010.

[7] D. A. Sánchez-Hernández, *High Frequency Electromagnetic Dosimetry*, 2009.

[8] J. C. Lin, *Advances in Electromagnetic Fields in Living Systems*, vol. 4, Springer, New York, NY, USA, 2005.

[9] C. Gabriel, "The dielectric properties of tissues," in *Radiofrequency Radiation Dosimetry and Its Relationship To the Biological Effects of Electromagnetic Fields*, B. J. Klauengerg and D. Miklavic, Eds., vol. 82 of *Nato Science Series*, pp. 75–84, High Technology, London, UK, 2000.

[10] C. W. Khoo, *Multi-band antenna for handheld transceivers [Ph.D. thesis]*, 2002.

[11] A. Lak, H. Oraizi, and F. Mohsenifard, "Risk from electromagnetic fields," in *Proceedings of the 3rd International Conference on Mechanical and Electrical Technology (ICMET '11)*, Dalian, China, August 2011.

[12] L. Asmae and O. Homayoon, "Simulation and evaluation of specific absorption rate in human body in high frequency electromagnetic fields," in *Advanced Materials Research*, vol. 433–440, pp. 5489–5493, Trans Tech Publications, Zurich, Switzerland, 2012.

[13] M. R. I. Faruque, M. T. Islam, and N. Misran, "Analysis of SAR levels in human head tissues for four types of antennas with portable telephones," *Australian Journal of Basic and Applied Sciences*, vol. 5, no. 3, pp. 96–107, 2011.

[14] "International Standard IEC 62209-1, human exposure to radio frequency fields from hand-held and body-mounted wireless communication devices-human models, instrumentation, and procedures-Part 1: procedure to determine the specific absorption rate (SAR) for hand-held devices used in close proximity to the ear (frequency range of 300 MHz to 3 GHz)," IEC publication, 2005.

[15] A. Andújar, J. Anguera, C. Picher, and C. Puente, "Human head interaction over ground plane booster antenna technology: functional and biological analysis," *Progress in Electromagnetics Research*, vol. 41, pp. 153–185, 2012.

[16] A. Cabedo, J. Anguera, C. Picher, M. Ribó, and C. Puente, "Multiband handset antenna combining a PIFA, slots, and ground plane modes," *IEEE Transactions on Antennas and Propagation*, vol. 57, no. 9, pp. 2526–2533, 2009.

[17] S. Risco, J. Anguera, A. Andújar, C. Picher, and J. Pajares, "Comparison of a monopole and a PIFA handset antenna in the presence of the human head," *Microwave and Optical Technology Letters*, vol. 54, no. 2, pp. 454–459, 2012.

[18] A. Lak and H. Oraizi, "The effect of distance of human head model from EM sources on SAR," *Journal of Basic and Applied Scientific Research*, vol. 2, no. 9, pp. 9446–9453, 2012.

Hindawi Publishing Corporation
International Journal of Antennas and Propagation
Volume 2012, Article ID 516487, 7 pages
doi:10.1155/2012/516487

Research Article

Printed Internal Pentaband WWAN Antenna Using Chip-Inductor-Loaded Shorting Strip for Mobile Phone Application

Yong-Ling Ban,[1] Shun Yang,[1] Joshua Le-Wei Li,[1] and Rui Li[2]

[1] *Institute of Electromagnetics, University of Electronic Science and Technology of China, 2006 Xi-Yuan Avenue, Western High-Tech District, Sichuan, Chengdu 611731, China*
[2] *College of Software Engineering, Chengdu University of Information Technology, Chengdu 610225, China*

Correspondence should be addressed to Yong-Ling Ban, byl@uestc.edu.cn

Received 10 July 2012; Accepted 17 September 2012

Academic Editor: Minh-Chau Huynh

A compact size on-board printed antenna using capacitive coupled-fed excitation to generate multiple resonant modes for penta-band WWAN operation (GSM850/900/GSM1800/1900/UMTS2100) is presented in this paper. The proposed antenna occupies only a small footprint of $15 \times 25\,\text{mm}^2$ on one corner of the circuit board and a protruded ground of $10 \times 15\,\text{mm}^2$ is displaced with close proximity to the antenna portion. The proposed antenna has a very simple structure which is composed of two separate strips: a loop strip with an inserted chip inductor and an L-shaped feeding strip. The loop strip is shorted to the ground and generates a resonant mode at 890 MHz to cover the GSM850/900 band (824–960 MHz) while the feeding strip contributes to the GSM1800/1900/UMTS210 band (1710–2170 MHz) operation. With such a small size, the proposed antenna can achieve compact integration on the circuit board of the mobile phone, thus the proposed scheme is quite suitable for the slim mobile phone application. Good agreements between simulations and measurements are obtained. Details of proposed antenna are presented and some key parameters are studied.

1. Introduction

Mobile phone antennas with compact size, low profile, and wide operation band characteristics have attracted great attention both in academic and industrial field. In recent years, a variety of small size and broadband antennas excited by the capacitive coupled-fed scheme to achieve multiband operation have been reported [1–4]. These reported antennas can be configured to occupy a compact volume inside the mobile phone for multiband operation. However, most of the reported designs did not consider the integration of internal antenna with the system ground plane because an isolation distance is often needed to guarantee the performance of wideband operation. As a result, these antennas often occupy the whole edge of the system circuit ground plane which is not so suitable for the practical application [1, 2]. This phenomenon is also common in some traditional three-dimensional antenna designs [3]. It limits the integration of the internal antenna with the associated electronic components. Recently, several novel designs with protruded ground are proposed [5, 6] which integrate the antenna with the system board well; furthermore, it has been shown that protruded ground can effectively suppress the surface current distribution on the ground plane away from the edge where the antenna is mounted [7]. Thus decreased near field emission can be achieved if the antenna is placed at the bottom of the mobile handset. But most of them are three-dimensioned or have a large area occupation [5, 6]. To miniature the antenna size, chip inductors are widely used to reduce the length of the strip for a special frequency so as to realize compact designs [8–10]. A penta-band solution with protruded ground plane is reported in [11], which is promising to be implemented in the slim mobile phone designs. In this paper, we presented a WWAN internal antenna suitable to be disposed at a small corner on the circuit board to achieve compact integration. The proposed antenna has a size of $15 \times 25\,\text{mm}^2$ which only requires a small

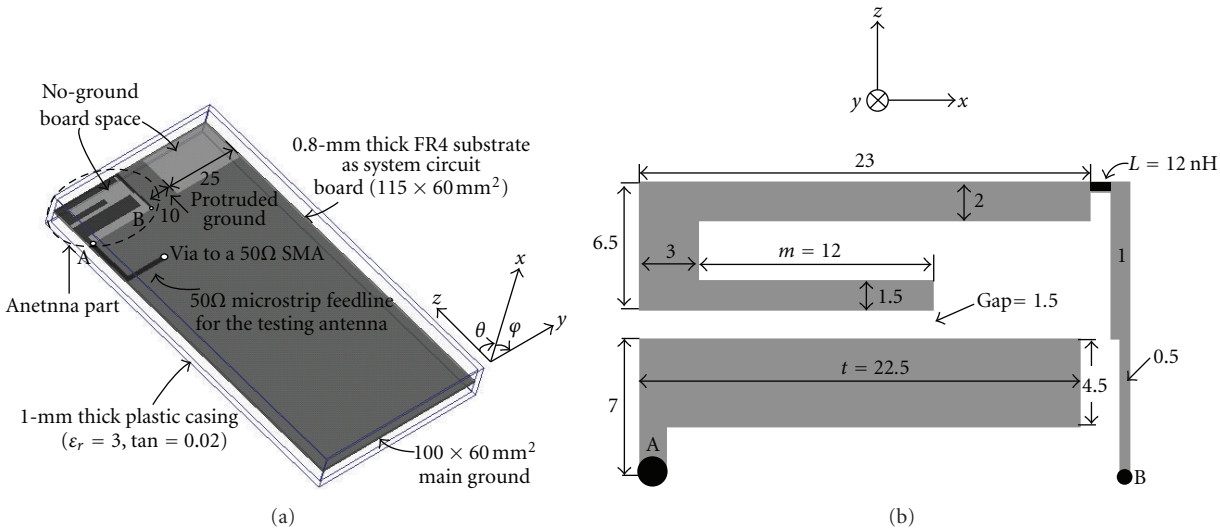

Figure 1: (a) Overall structure of the proposed antenna. (b) Dimensions of the proposed antenna (unit: mm).

foot print of the system circuit plane. A protruded ground area of $10 \times 15\,\text{mm}^2$ is left at the center part of the edge to accommodate associated electronic component such as a universal serial bus (USB) connector, and another no-ground portion at the other side of the circuit board edge near the protruded ground is promising for a another internal antenna deposition. Detailed configurable illustrations and radiation characteristics of the proposed antenna are given in the following sections.

2. Proposed Antenna Configuration

Figure 1(a) shows the geometry of the on-board printed coupled-fed compact antenna. The proposed antenna is printed on a small no-ground board portion of $15 \times 25\,\text{mm}^2$ and it only occupies a small part of the edge on the mobile phone system circuit board. A 0.8 mm thick FR4 substrate of relative permittivity 4.4, loss tangent 0.024, length 115 mm, and width 60 mm is used in this study. 1 mm thick plastic casing of relative permittivity 3.0 and loss tangent 0.02 encloses the whole substrate to simulate the mobile phone casing. As it shows in the figure, a protruded ground portion is placed closely to the antenna and connected to the main ground. The protruded ground has a size of $10 \times 15\,\text{mm}^2$ and it is just suitable to accommodate a USB connector. Also note that on the other side of the protruded ground there is another no-ground board space of size $15 \times 25\,\text{mm}^2$ which can be used to accommodate other internal antenna or electronic components. Furthermore, such a small and symmetrical scheme is promising to develop a compact MIMO (multiple input multiple output) antenna designs [12–14]. Figure 1(b) shows prototype of the proposed antenna which is mainly composed of two parts: an L-shaped feeding strip and a loop shorting strip. The L-shaped feeding strip is directly fed from point A which is further connected to a 50-Ω transmission line as shown in the Figure 1(a). The loop shorting strip is coupled-fed by the L-shaped feeding strip and shorted to the ground plane through a via-hole at point B. A chip inductor

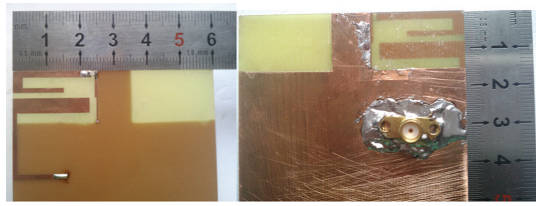

Figure 2: The photos of the proposed antenna.

of $L = 8.2$ nH is inserted at the corner of the loop strip to shorten the path for GSM850/900 band operation. The total length of loop strip is about 60 mm, that is, much shorter than a quarter of the wavelength for 850 MHz which is about 90 mm. As the lower band is mainly generated by the loop shorting strip, the front portion of the loop strip is set to be a variable of m as shown in Figure 1(b). The length of the L-shape monopole is also set as a variable t to tune the upper band operation. Detailed effects of the parameters on the antenna performance will be shown in the following sections.

3. Result and Discussion

Figure 2 shows the fabricated antenna with rulers to demonstrate the antenna size. The simulation is done using the high frequency simulation software (HFSS) version 12 and the measurement in conducted by Agilent N5247A vector network analyzer. Good match between measured and simulated reflection coefficient of the proposed antenna design is shown in Figure 3. The impedance matching for frequencies over the two operating bands is better than 6-dB return loss, which is widely used as the design specification for the internal WWAN mobile phone antennas. According to this criterion, both the simulation and the measured results cover the operation bands (GSM850/900 GSM1800/1900/UMTS2100) perfectly. The simulated input impedance of the proposed antenna on the smith chart is shown in Figure 4 to provide more impedance information.

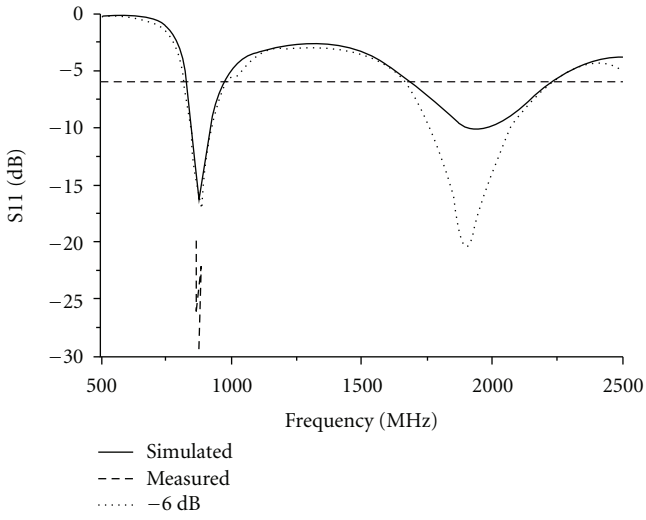

Figure 3: Measured and simulated S11 for the proposed antenna.

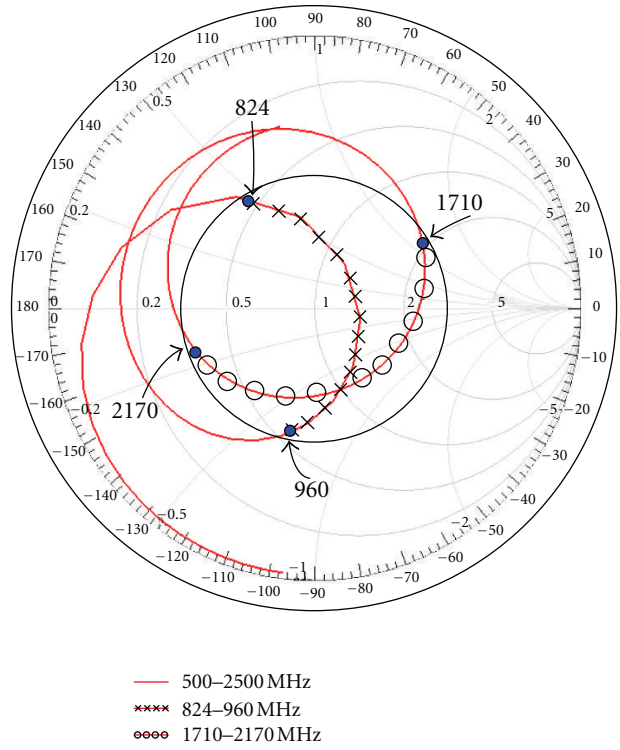

Figure 4: Simulated input impedance on the Smith chart.

A dashed-line circle is drawn in the smith chart to demonstrate the region in which the impedance is well matched.

In order to classify the function of different parts of proposed antenna, the operating principles are analyzed. Figure 5 shows simulation reflection coefficient of the comparison between the proposed antenna and reference antennas. The corresponding Ref1 antenna has only the feed strip while the Ref2 case has no inserted inductor. For the Ref1 case, there is no resonance near 900 MHz and the resonance of the upper band is also some kind of weak due to absence of the bended monopole. And for the Ref2 case, it is seen that both the lower band and the upper band are shifted towards higher frequencies and this phenomenon is especially obvious in the lower band. These results support the idea that the higher band is generated by the L-shaped feeding strip and also slightly affected by the loop strip while the lower band operation is dominantly decided by the loop strip. It also indicates that the inductor can effectively reduce the length of strip for specific resonance which helps to realize the miniature of the antenna design.

Simulated current distributions on the antenna part and ground plane at 890 MHz and 1940 MHz are shown in Figure 6. The directional arrows show the current flowing with varied colors. Corresponding magnitude of different color is shown as label on the left. At the frequency of 890 MHz, the current flows along the loop strip and the magnitude of the current are smallest at the front part while it increases to the largest value at the shorting point. At the same time, the current on the ground plane is well aligned in the same direction which also contributes to the lower band radiation. While at the frequency of 1940 MHz, there is strong current distribution on the feeding strip which shows that the feeding strip is the main radiator at 1940 MHz for the antenna.

Simulated reflection coefficient and current distributions for the case with and without USB mounted on the protruded ground are presented in Figures 7 and 8 to explore the possibility of integrating a USB for the practical applications. To simulate the influence of the USB connector on the antenna performance a cubic conductor with a size of $9 * 8 * 4\,\text{mm}^3$ is placed under the protruded ground. The simulated reflection coefficient demonstrates a slight frequency shifting at the upper band but still covers the upper operation band from 1710 MHz to 2170 MHz; meanwhile there is almost no change to the reflection coefficient in the lower band. The simulated frequency range is set to be from 500 to 3000 MHz on purpose to show the change more clearly. As it can be observed from the reflection coefficient result in Figure 7, there is another resonant mode around 2700 MHz; this resonant mode is generated by the strip between grounding point B and the inserted inductor L as the high frequency current is blocked by the inductor. As the protruded ground is placed closely to the strip which generates the 2700 MHz resonant mode, a USB connector affects the 2700 MHz resonant mode while causing small variance in other bands. This analysis can be further verified in the current distribution at the higher band in Figure 8. It is observed from the simulated current distribution with and without the presence of USB connector, there is a very little change of the current distribution on the antenna and surrounding area. The high frequency current along the loop strip is effectively confined between the grounding point B and the inserted inductor L.

A parametric study of the major parameters on tuning the antenna's lower and upper bands is conducted. Figure 9(a) shows the simulated reflection coefficient of the proposed antenna when the value of the inserted inductor is selected to be 3.9 nH, 8.2 nH, and 15 nH which are available in the lab. In Figure 9(a), it is found that the excited resonant

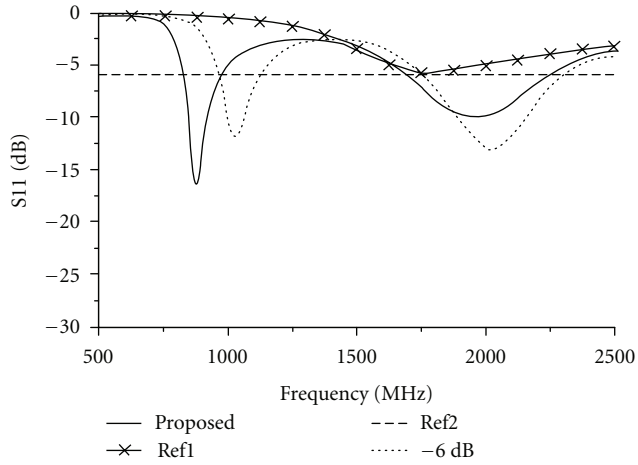

Figure 5: Comparison of the proposed antenna with two reference antennas.

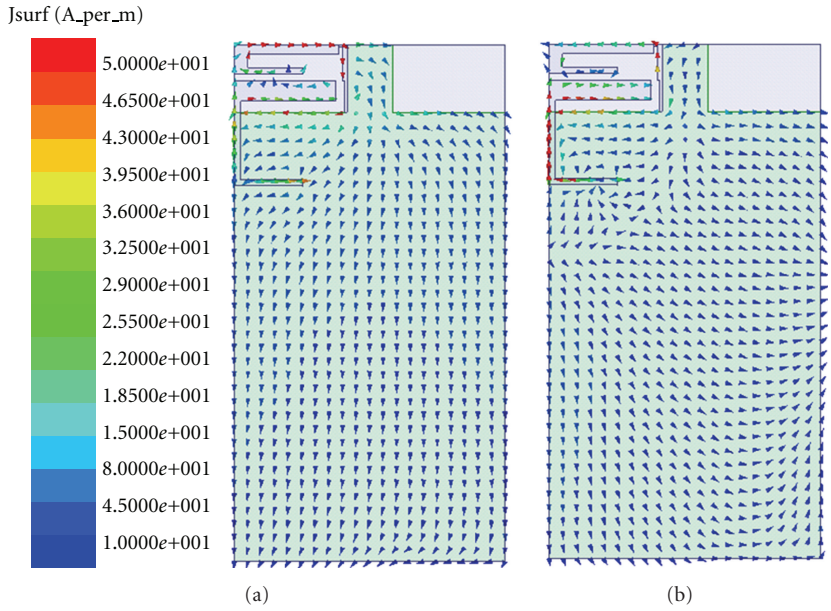

Figure 6: Current distribution at frequency of (a) 890 MHz and (b) 1940 MHz.

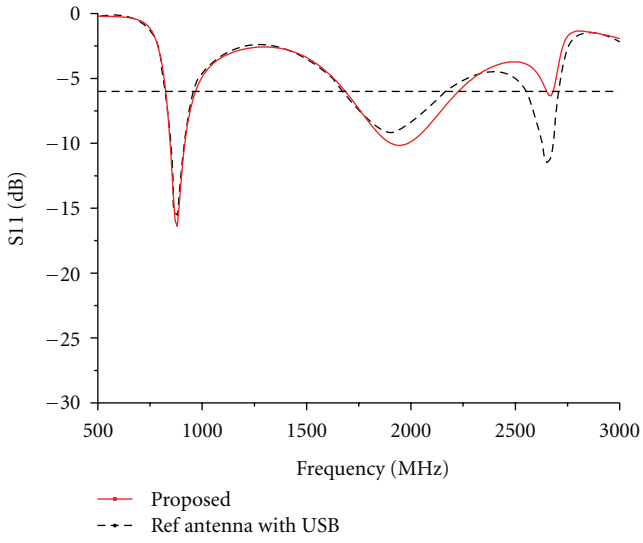

Figure 7: Comparison of reflection coefficient between the antenna with and without USB connector.

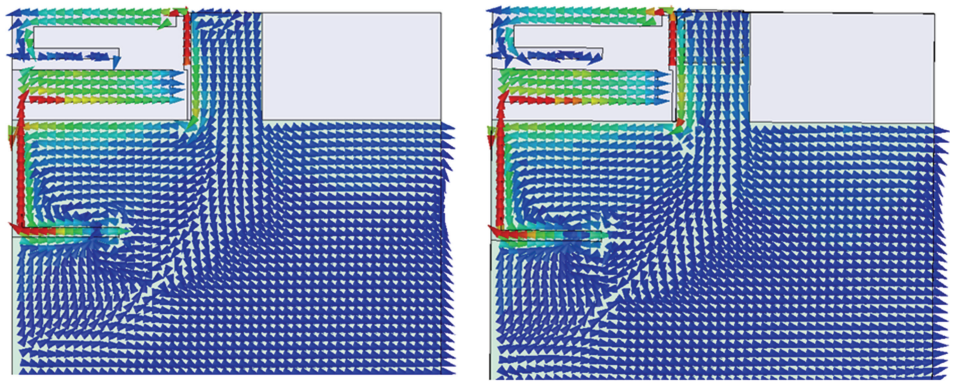

(a) (b)

Figure 8: Simulated current distribution with (a) and without (b) the presence of USB.

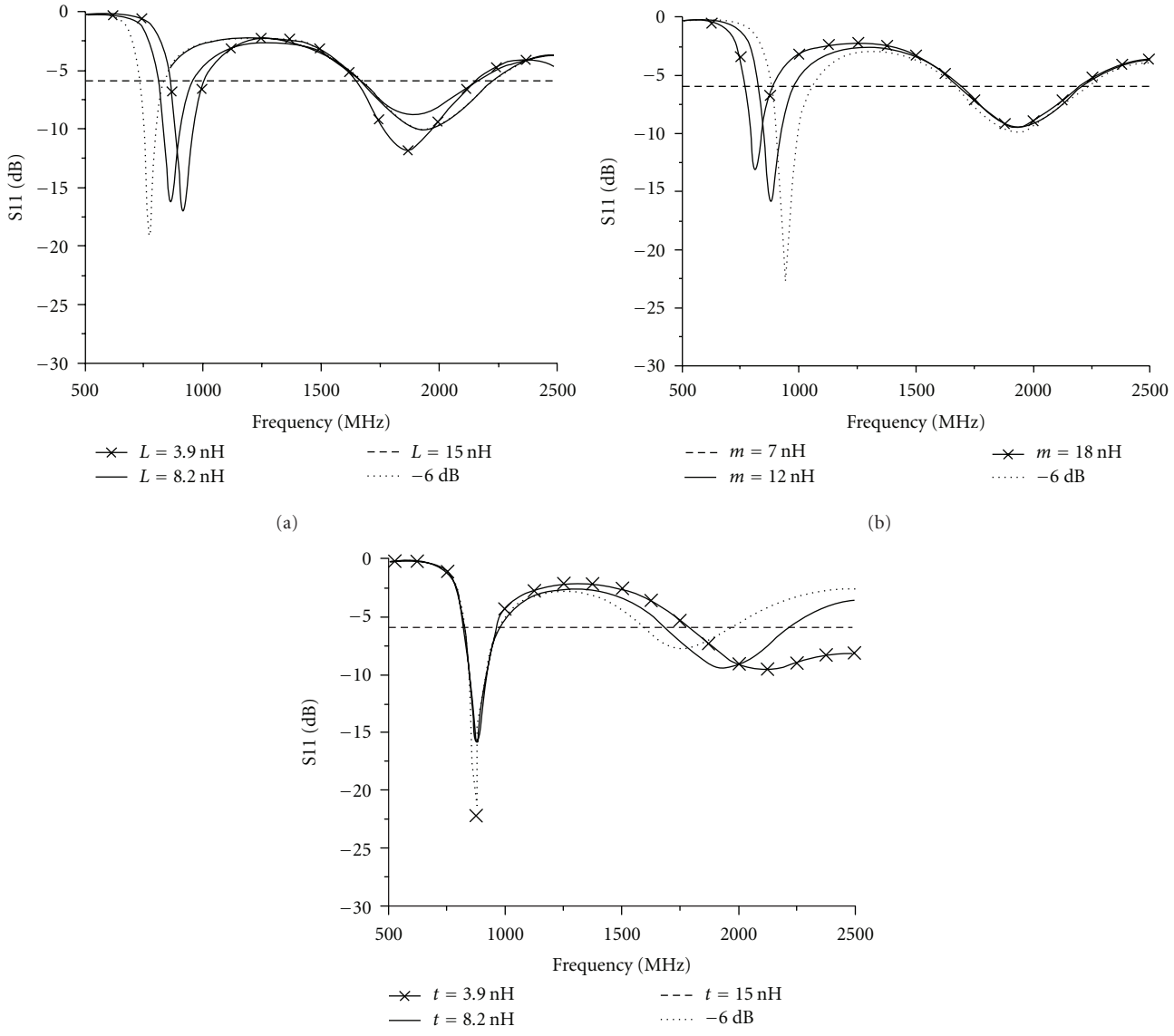

Figure 9: Simulated reflection coefficient for the proposed antenna as a function of (a) the value of the inserted inductor, (b) the length of the coupling strip and (c) the length of the feeding strip. Other dimensions are the same as in Figure 1.

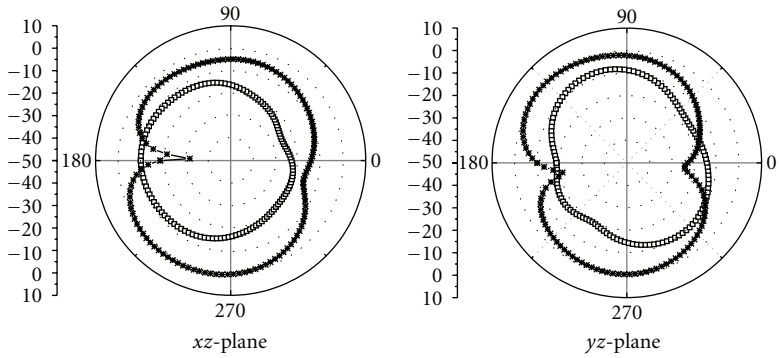

Figure 10: Measured radiation pattern of the proposed antenna at the frequencies of 890 MHz and 1940 MHz (line with rectangle: *E*-phi; line with cross: *E*-theta).

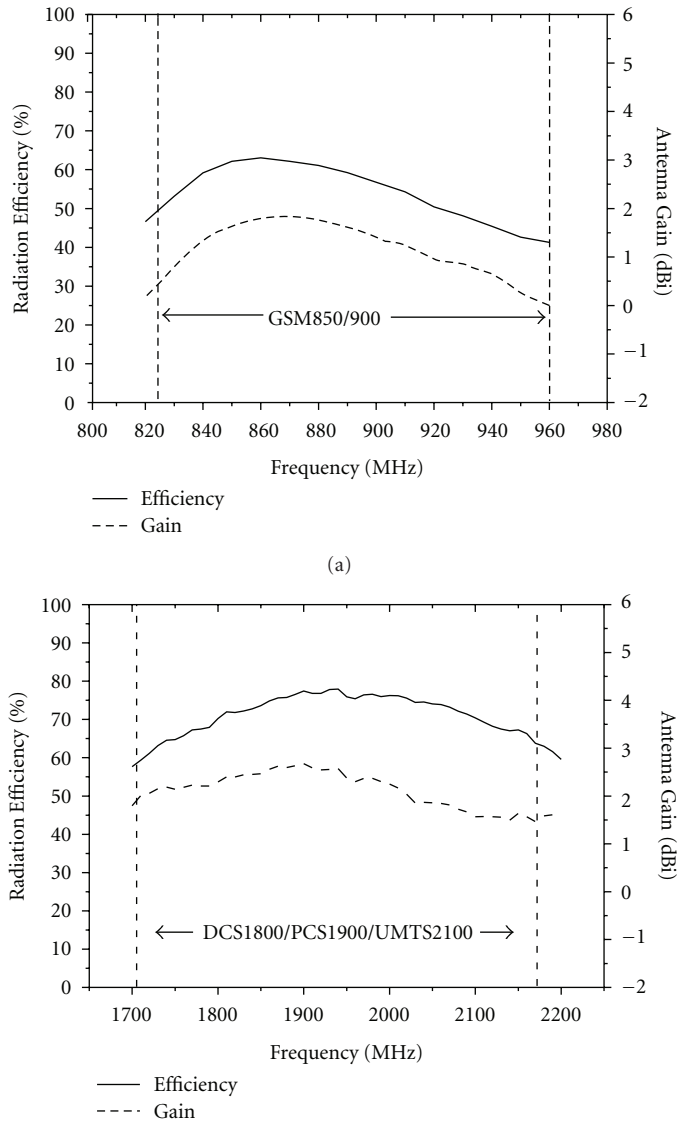

Figure 11: Measured antenna radiation efficiency and antenna gain for the proposed antenna at (a) lower band and (b) upper band.

mode is shifted to the lower frequencies in the lower band when the value of the inductor L is increased. Meanwhile, only small variations are found in the upper band which verifies that the inserted inductor mainly affects the lower band and is effective to reduce strip length for a special resonant mode. Effects of the length of the front portion of the loop strip are studied in Figure 9(b), where simulated reflection coefficient of the proposed antenna is presented when the strip length m varied from 7 mm to 18 mm. There is great similarity between Figures 9(a) and 9(b) that along the change of m there is significant effect on the lower band while subtle effect on the upper band. This is reasonable as the loop is the main radiator of the lower band operation in this scheme. From Figures 9(a) and 9(b), it can be concluded that the inserted inductor and the loop strip jointly determine the resonant mode of the lower band. On the other hand, there is significant change on the upper band and little variation is found in the lower band when the length of the feeding strip is increased from 19.5 mm to 23.5 mm as shown in Figure 9(c). This is also reasonable because the feeding strip controls the upper band resonant mode.

The radiation characteristics of the proposed antenna are also studied. Figure 10 shows the two-dimensional radiation pattern of the presented antenna at the frequencies of 890 MHz and 1940 MHz. For each frequency, it is observed from three different planes, namely, xz-plane, yz-plane, and xy-plane. Dipole-like radiation pattern is found at 890 MHz which means a dumbbell-like shape radiation pattern at the E-plane and a circle one in the H-plane. However, when it comes to the upper band, the radiation characteristic varies more quickly in different directions due to surface current of the ground plane. As it is shown in Figure 6, the current distribution on the ground is quite uniform and contributes to the radiation of the 900 MHz. But at the frequency of 1900 MHz, the length of the system ground plane is comparable to the resonant wavelength, so there are current nulls excited on the system ground plane, which results in nulls and dips in the obtained radiation patterns radiation. Figure 11 shows the measured antenna radiation efficiency and antenna gain. The efficiency ranges from 42% to 63% over the GSM850/900 band and the efficiency varies from 57% to 75% for the GSM1800/1900/UMTS2100 band. The efficiency over the five operation bands is all above 40%, which is acceptable for the practical mobile antenna application. The measured gain is about 0 to 1.2 dBi and 1.6–2.5 dBi over the lower and upper bands, respectively. Good radiation characteristics are generally obtained for the proposed antenna.

4. Conclusion

In this paper, a compact penta-band antenna design for mobile phone application is presented. With the presence of the chip inductor, the resonant strip length for the GSM850/900 band operation is significantly reduced. Due to its small size and simple structure it is promising to be implemented in the slim smart mobile phone designs by using PCB fabrication techniques with low cost. Moreover, Good impedance match and radiation characteristics are found in the five operation bands, making it preponderant for application in the small-size mobile phone for WWAN/LTE operating communication.

References

[1] C. T. Lee and K. L. Wong, "Uniplanar coupled-fed printed PIFA for WWAN/WLAN operation in the mobile phone," *Microwave and Optical Technology Letters*, vol. 51, no. 5, pp. 1250–1257, 2009.

[2] K. L. Wong, M. F. Tu, T. Y. Wu, and W. Y. Li, "Small-size coupled-fed printed pifa for internal eight-band lte/gsm/umts mobile phone antenna," *Microwave and Optical Technology Letters*, vol. 52, no. 9, pp. 2123–2128, 2010.

[3] Y. L. Ban, C. Q. Lei, J. H. Chen, S. C. Sun, Z. X. Xie, and F. Ye, "Compact coupled-fed PIFA employing T-shaped monopole with two stubs for eight-band LTE/WWAN internal mobile phone," *Journal of Electromagnetic Waves and Applications*, vol. 26, pp. 973–985, 2012.

[4] W. Y. Chen and K. L. Wong, "Wideband coupled-fed PIFA for HAC penta-band clamshell mobile phone," *Microwave and Optical Technology Letters*, vol. 51, no. 10, pp. 2369–2374, 2009.

[5] S. C. Chen and K. L. Wong, "Low-profile, small-size, wireless wide area network handset antenna close integration with surrounding ground plane," *Microwave and Optical Technology Letters*, vol. 54, pp. 623–629, 2012.

[6] F. H. Chu and K. L. Wong, "Internal coupled-fed loop antenna integrated with notched ground plane for wireless wide area network operation in the mobile handset," *Microwave and Optical Technology Letters*, vol. 54, pp. 599–605, 2012.

[7] S. C. Chen and K. L. Wong, "Hearing aid-compatible internal LTE/WWAN bar-type mobile phone antenna," *Microwave and Optical Technology Letters*, vol. 53, no. 4, pp. 774–781, 2011.

[8] K. L. Wong and S. C. Chen, "Printed single-strip monopole using a chip inductor for penta-band WWAN operation in the mobile phone," *IEEE Transactions on Antennas and Propagation*, vol. 58, no. 3, pp. 1011–1014, 2010.

[9] Y. L. Ban, J. H. Chen, J. L. W. Li, and Y. J. Wu, "Printed ultrawideband antenna for LTE/GSM/UMTS wireless USB dongle applications," *IEEE Antennas and Wireless Propagation Letters*, vol. 11, pp. 403–406, 2012.

[10] K. L. Wong and C. T. Lee, "Small-size wideband monopole antenna closely coupled with a chip-inductor-loaded shorted strip for 11-band WWAN/WLAN/WiMAX operation in the slim mobile phone," *Microwave and Optical Technology Letters*, vol. 53, no. 2, pp. 361–366, 2011.

[11] Y. W. Chi and K. L. Wong, "Internal compact dual-band printed loop antenna for mobile phone application," *IEEE Transactions on Antennas and Propagation*, vol. 55, no. 5, pp. 1457–1462, 2007.

[12] J. Zhang, J. Ou Yang, K. Z. Zhang, and F. Yang, "A novel dual-band MIMO antenna with lower correlation coefficient," *International Journal of Antennas and Propagation*, vol. 2012, Article ID 512975, 7 pages, 2012.

[13] C. Yang, Y. Yao, J. S. Yu, and X. D. Chen, "Novel compact multiband MIMO antenna for mobile terminal," *International Journal of Antennas and Propagation*, vol. 2012, Article ID 691681, 9 pages, 2012.

[14] Q. H. Zeng, Y. Yao, S. H. Liu, J.S. Yu, P. Xie, and X. D. Chen, "Tetraband small-size printed strip MIMO antenna for mobile handset application," *International Journal of Antennas and Propagation*, vol. 2012, Article ID 320582, 8 pages, 2012.

Hindawi Publishing Corporation
International Journal of Antennas and Propagation
Volume 2012, Article ID 398423, 10 pages
doi:10.1155/2012/398423

Research Article

Compact Dual-Band Dual-Polarized Antenna for MIMO LTE Applications

Lila Mouffok, Anne Claire Lepage, Julien Sarrazin, and Xavier Begaud

Department Comelec Institut Mines Telecom, Telecom ParisTech, LTCI CNRS UMR 5141, 46 Rue Barrault, 75634 Paris Cedex 13, France

Correspondence should be addressed to Lila Mouffok, lila.mouffok@telecom-paristech.fr

Received 15 May 2012; Revised 18 July 2012; Accepted 6 September 2012

Academic Editor: Minh-Chau Huynh

A system of two dual-band dual-polarized antennas is proposed. It operates in two bands, 700 to 862 MHz and 2.5 to 2.69 GHz, thereby making it suitable for LTE applications. The design is composed of two compact orthogonal monopoles printed close to each other to perform diversity in mobile terminals such as tablets or laptops. For each band, two orthogonal polarizations are available and an isolation higher than 15 dB is achieved between the two monopoles spaced by $\lambda_0/10$ (where λ_0 the central wavelength in free space of the lower band). A good agreement is observed between simulated and experimental results. The antenna diversity capability is highlighted with the calculation of envelope correlation and mean effective gain for several antennas' positions in different environment scenarios.

1. Introduction

Deployment of existing and emerging wireless communication systems require a high-data-rate transmission, in order to satisfy the needs of multimedia applications on terminals. Multiple Input Multiple Output (MIMO) applications have been suggested as an effective way to increase the channel capacity by exploiting multipath scattering effects.

MIMO technology is present in many recent wireless standards, such as Long Term Evolution (LTE), and will be implemented in mobile devices [1]. Several research works have proven the efficiency of two-antenna diversity on mobile terminals [2, 3]. However, when the available space is limited, the use of a dual-polarized antenna is more suitable than two separated antennas [4]. A variety of dual-polarized antennas have been reported recently in which good dual-polarized radiation over a wide bandwidth [5] and high isolation between the feeding ports [6] have been achieved. However, these antennas are mainly designed for single-band operation [7] or for frequencies above 800 MHz [8]. Most of the dual-band dual-polarized antennas proposed in literature exploit harmonics frequencies [9] or use techniques to generate additional resonances such as insertion slot [10]. But generally, it leads to a ratio between frequency bands below or equal to 2 and implies a dependence between the two frequency bands. Today, very few designs are reported for dual-band dual-polarized operations for the following bands: 700–862 MHz and 2.5–2.69 GHz. In this paper, we firstly present the design of a dual-band antenna which can provide a dual-polarization for each band, for LTE devices such as a tablet or a laptop. Then, we introduce an enhanced design in which the lower bandwidth has been increased and the mutual coupling between ports has been reduced in the two bands. The lower band is extended towards TV White Space (TVWS) band to provide radio-cognitive capabilities to the terminal [11].

Finally, the diversity performances of the proposed dual-band dual-polarized antennas are evaluated through the envelope correlation (ρ_e) and the mean effective gain in isotropic, indoor, and outdoor environments.

2. Antenna Design

As shown in Figure 1, the proposed structure is composed of two orthogonal monopoles with dimensions of

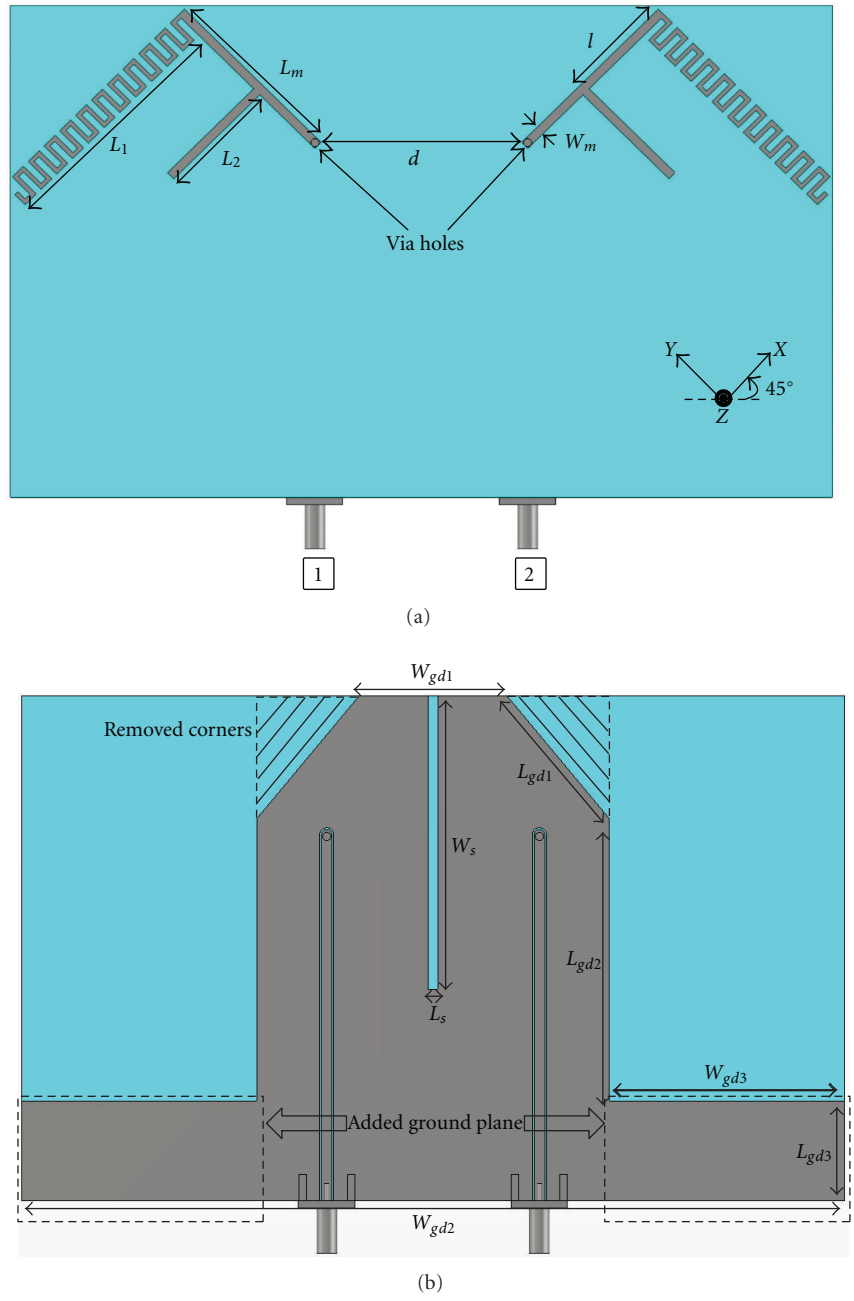

Figure 1: (a) Front view. (b) Back view of one meander bend ending antennas, with added ground plane and slot.

$L_m \times W_m = 27.5 \times 1.5\,\text{mm}^2$. The two monopoles are identical and chosen for their omni-directional radiations pattern, enabling them to receive signals whatever their orientation. They are printed on a $140 \times 83\,\text{mm}^2$ low cost substrate (FR4: $\varepsilon_r = 3.8 \pm 0.1$, $\tan\delta = 0.02$, thickness of 0.7 mm). Each monopole is connected to two bend endings: one bend ending is a meander line whose length is $L_1 = 43.3$ mm operating at 790–862 MHz and the small one whose length is $L_2 = 23.5$ mm operates at 2.5–2.69 GHz. The distance between the two bend endings is $l = 14$ mm. This design allows to obtain independent frequency bands. The two monopoles are spaced by $d = 36$ mm which corresponds to $\lambda_{01}/10$ for the lower band and $\lambda_{02}/3$ for the higher band, where λ_{01} is the free-space wavelength of the lower band central frequency ($f_{01} = 826$ MHz) and λ_{02} the free-space wavelength of the higher band central frequency ($f_{02} = 2.59$ GHz).

The monopoles are fed by two 50 ohms coplanar waveguides (CPW), directly etched in the ground plane, as shown in Figure 1(b), in order to distance the connectors and to avoid perturbations on the measured radiation patterns. Each CPW has a line width of 1.8 mm and a gap of 0.33 mm

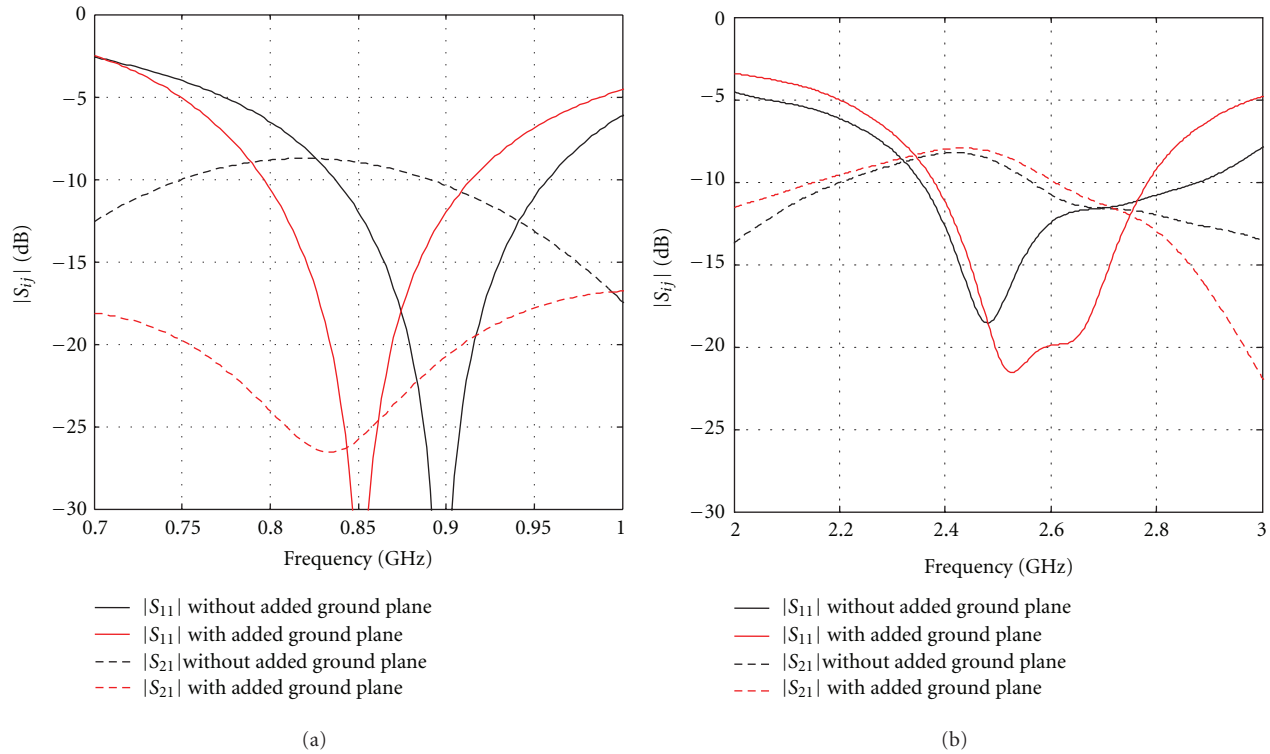

FIGURE 2: Simulated $|S_{ij}|$ parameters of one meander bend ending antennas without slot, with and without added ground plane: (a) lower band, (b) higher band.

with the ground plane. Monopoles are connected to CPW thanks to metallic via holes located as the extremity of each monopole as shown in Figure 1(a).

2.1. Ground Plane Geometry. Since the small bend ending is close to the ground plane extremities, it is sensitive to the path taken by currents along the ground plane. Therefore, a study of the upper part of the ground plane geometry is relevant. It is found that removing corners (shaded part in Figure 1(b)) provides an improvement of higher band matching, leading to optimized dimensions $W_{gd1} = 25$ mm, $L_{gd1} = 25$ mm, and $L_{gd2} = 46$ mm.

Coupling between the two antennas occurs via currents flowing from one antenna to the other one through the ground plane. It can be reduced by altering the ground plane to modify currents' path. Thus, the ground plane is extended without increasing the overall structure size, by adding on the lower part of the substrate, two rectangular shapes on either side with dimensions of each one $W_{gd3} = 40$ mm and $L_{gd3} = 17$ mm (framed part in Figure 1(b)). Simulations have been performed with Transient Solver of CST Microwave Studio. Figure 2 shows a comparison between $|S_{ij}|$ parameters for designs without slot, with and without added ground plane in each band. Because of the structure's symmetry, only $|S_{11}|$ and $|S_{21}|$ are plotted. The matching bandwidth criterion is taken for a return loss less than −10 dB. With added ground plane, a shift of the lower band towards lower frequencies (from 0.9 to 0.85 GHz) is observed in Figure 2(a) without increasing the structure size. The bandwidths of the structure without added ground plane are: 837–957 MHz (13.4%), 2.35–2.86 GHz (19.6%), and for the structure with added ground plane are: 796–914 MHz (13.8%), 2.38–2.78 GHz (15.5%). Regarding the isolation, it is largely reduced thanks to the added ground plane: $|S_{21}|$ becomes below −20 dB in the lower band. Indeed, a resonance has been introduced at the frequency where coupling occurs. However, the coupling remains high ($|S_{21}| < -7$ dB) in the higher band as shown in Figure 2(b).

To improve isolation between ports in the higher band, a slot is etched in the ground plane while keeping the same distance between ports (d), as shown in Figure 1(a). The introduction of the slot produces an open circuit which stops the circulation of current from one radiating element to the other one [12]. The optimized structure has a length $L_s = 34$ mm and a width $W_s = 1.4$ mm. Figure 3 shows a comparison of simulated $|S_{ij}|$ parameters of one meander bend ending antennas with added ground plane, with and without slot in the higher band. The introduction of the slot achieves an isolation improvement of 10 dB in the higher band, while it has no effect in the lower band. The bandwidth is slightly reduced but still covers the desired band. Thus, optimization of the two degrees of freedom which are the slot dimensions and rectangular shapes ground plane dimensions leads to a high isolation in the two frequency bands.

2.2. Radiating Element. In order to increase the bandwidth of the lower band towards the TVWS band, two bend endings

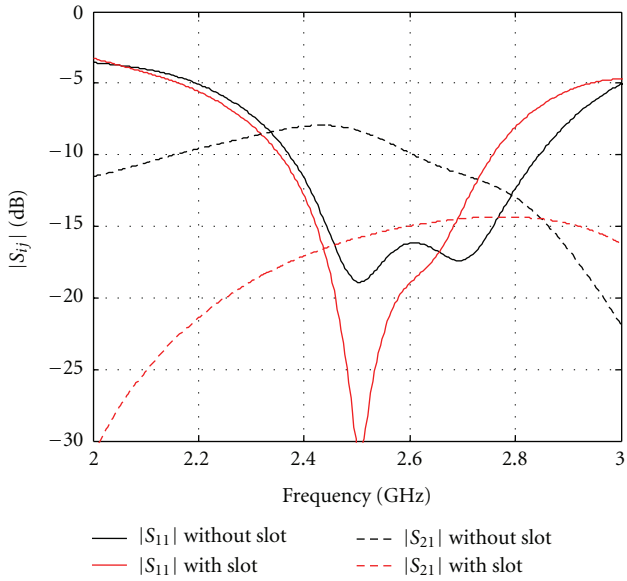

FIGURE 3: Simulated $|S_{ij}|$ parameters of one meander bend ending antennas with added ground plane, with and without slot in the higher band.

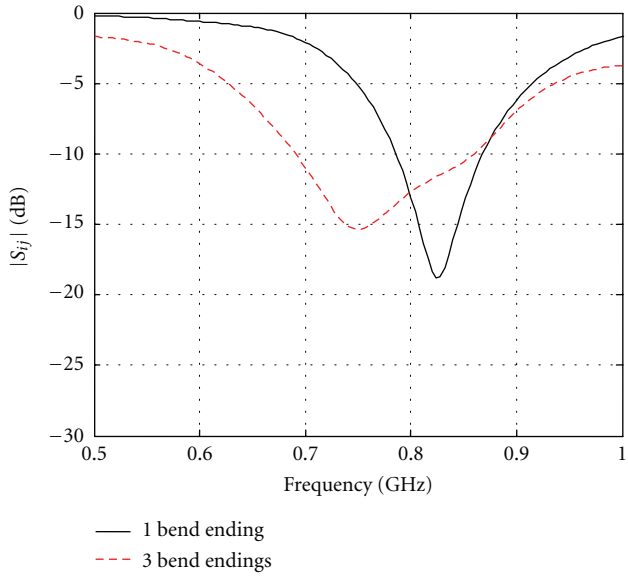

FIGURE 4: Simulated $|S_{11}|$ parameters of one and three meander bend endings antennas with added ground plane and slot in the lower band.

are added below the initial meander line to provide additional resonances close to each other. These two meanders are out of sync to provide a single wide band. Moreover, the three lines are connected to each other to extend the bandwidth towards lower frequencies. After optimization with Transient Solver of CST Microwave Studio, the distance between each meander is $s = 7$ mm as shown in Figure 5 and the overall size of three bend endings antennas with added ground plane and slot becomes $150 \times 90\,\text{mm}^2$.

Figure 4 shows the comparison between S-parameters of one and three bend endings antennas with added ground plane and slot. Matching bandwidth criterion is taken for $|S_{11}| < -10$ dB. It is seen that the bandwidth is enhanced towards lower frequencies. Indeed, the relative bandwidth for the structure with one bend ending is 9.8% (786–867 MHz) and 21.9% (692–862 MHz) for the structure with 3 bend endings. While keeping almost the same electrical length of the structure, the relative bandwidth has been improved by 12%. Indeed, the overall size is $0.35\,\lambda_{\text{low}} \times 0.21\,\lambda_{\text{low}}$ for three meander bend ending antennas (λ_{low}: the free space wavelength at 692 MHz) when it is $0.37\,\lambda'_{\text{low}} \times 0.22\,\lambda'_{\text{low}}$ for one meander bend ending antennas (λ'_{low}: the free space wavelength at 786 MHz).

3. Prototype and Measurement

A prototype of three bend endings antennas with added ground plane and slot described previously has been realized. Monopoles and the ground plane with CPW are located on opposite sides of the same substrate and can be seen simultaneously on Figure 5 because of the transparency of the FR4 substrate. Simulated and measured S-parameters are compared in Figure 6. Simulations results are in good agreement with measurement. The measurement results show that the antenna operates in two bands ($|S_{11}| < -10$ dB): the lower band extends from 700–880 MHz (21.9%) and the higher one from 2.51–2.72 GHz (8%). In these two bands, the two monopoles are satisfactorily uncoupled with an isolation $|S_{21}|$ below -15 dB within the higher band and from 770 to 880 MHz. At the beginning of the lower band, the isolation remains acceptable and is below -10 dB. The simulated total efficiency of the structure, which takes into account all losses, has been evaluated: it varies from 83 to 97% in the lower band and from 74 to 87% in the higher band as shown in Figures 7 and 8.

Figure 9 compares the simulated and measured copolar and cross-polar radiation patterns in the E plane (YZ plane) and H plane (XZ plane), respectively. Because both ports are symmetrical, we only represent radiation patterns for port number 1 while port 2 is loaded by 50 ohms. For both planes and both bands, it is found that the simulated and the measured co-polar radiation patterns are in good agreement. The maximum simulated realized gain is 2.5 dB at 778 MHz and 5 dB at 2.6 GHz. The measured cross-polar level is about 10 dB lower than the copolar level in the lower band but in the higher one, the polarization purity is deteriorated. It is probably due to the proximity of the meander bend endings to the small one.

To further investigate the diversity, the simulated radiation patterns of each radiating element in the XY plane for the two bands are plotted in Figure 10 (one port is excited while the other one is loaded by 50 ohms). Thanks to a good agreement observed in Figure 9 between simulations and measurement, only simulations results are presented. As it can be observed for the lower band, the directions

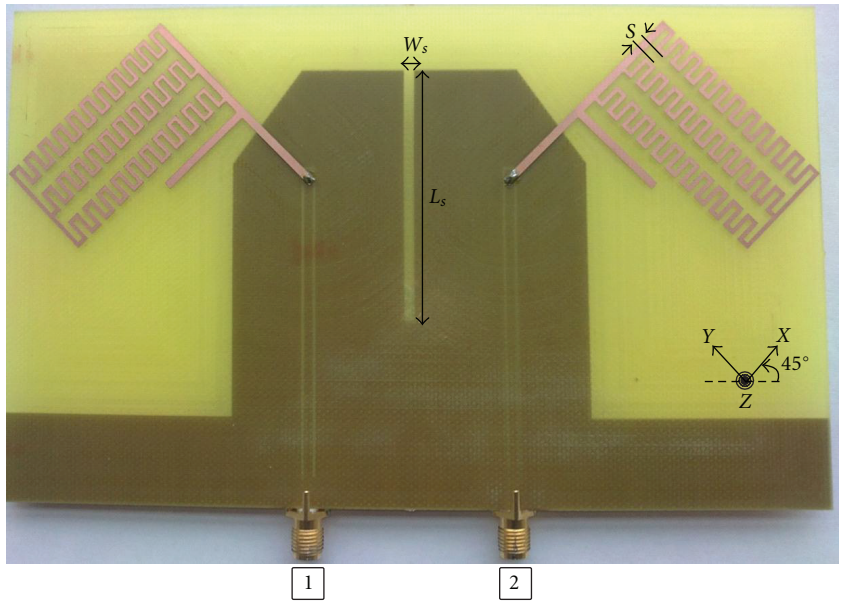

FIGURE 5: A photograph of the prototype with the three meander bend endings antennas.

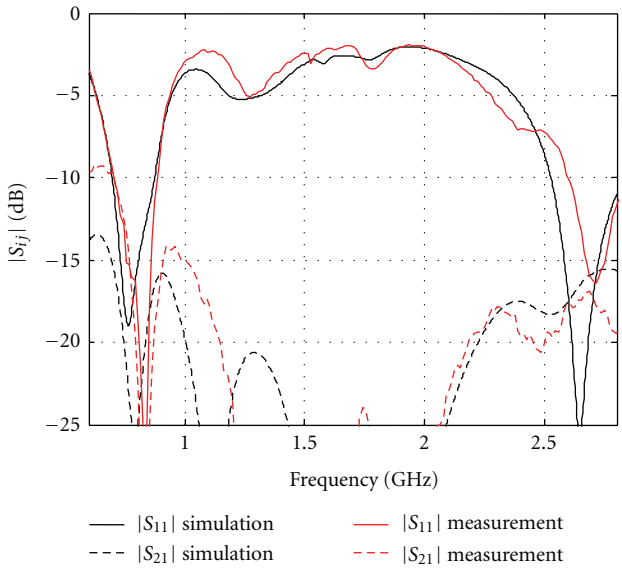

FIGURE 6: Simulated and measured $|S_{ij}|$ parameters of the optimized three bend endings antennas with added ground plane and slot.

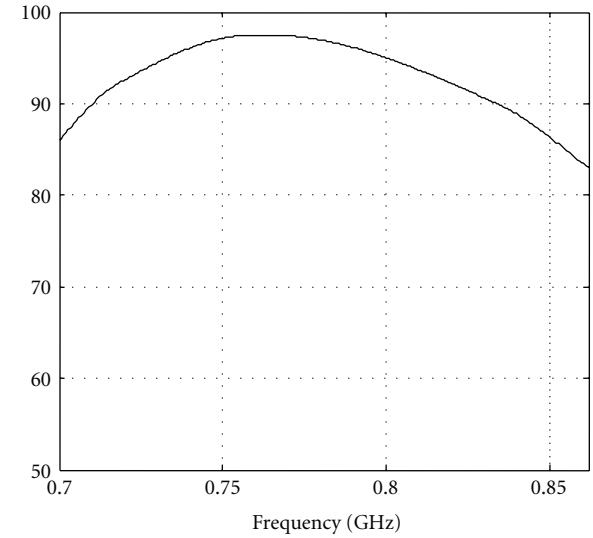

FIGURE 7: Simulated total efficiency in the lower band for the optimized three bend endings antennas with added ground plane and slot.

of the pattern maxima are close to orthogonal, leading to good pattern diversity. Each antenna presents monopole-like radiation patterns. Indeed surface currents are weak on the bend endings. For the higher band, even if patterns are not orthogonal, one monopole presents minimum gain directions where the other one has a maximum gain, except for the directions $\theta = \pm 45°$. This is well-suited to provide high diversity capabilities.

4. Evaluation of the Diversity Performance

The diversity performance of a mobile's antenna system can be affected by the environment in which the device is located [13]. Therefore, in this section, we evaluate the diversity performance of the proposed three bend endings antennas with added ground plane and slot, by calculating the envelope correlation coefficient (ρ_e) and the mean effective gain (MEG) taking into account the propagation environment.

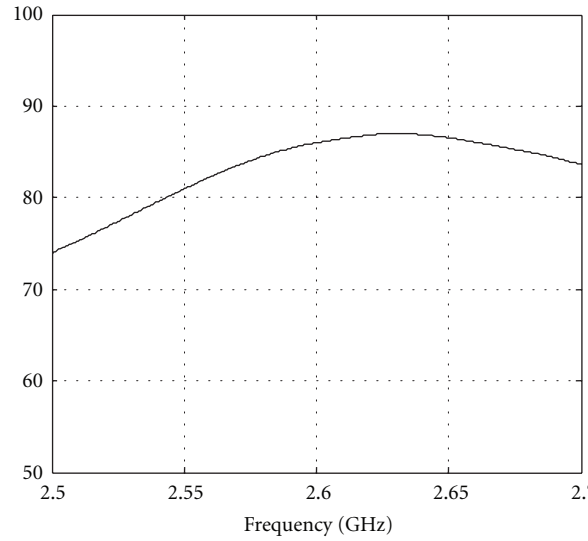

Figure 8: Simulated total efficiency in the higher band for the optimized three bend endings antennas with added ground plane, and slot.

The envelope correlation ρ_e quantifies the similarity between the radiation patterns of the two monopoles. The lower the correlation, the better the diversity performance. Vaughan and Andersen show in [13] that the coefficient can be expressed by

$$\rho_e = \frac{\left| \int_\Omega \left(\mathrm{XPD}\, E_{1\theta} E_{2\theta}^* p_\theta + E_{1\varphi} E_{2\varphi}^* p_\varphi \right) d\Omega \right|^2}{\int_\Omega \left(\mathrm{XPD}\, E_{1\theta} E_{1\theta}^* p_\theta + E_{1\varphi} E_{1\varphi}^* p_\varphi \right) d\Omega \int_\Omega \left(\mathrm{XPD}\, E_{2\theta} E_{2\theta}^* p_\theta + E_{2\varphi} E_{2\varphi}^* p_\varphi \right) d\Omega}. \quad (1)$$

$E_{1\theta}(\Omega)$, $E_{1\varphi}(\Omega)$, $E_{2\theta}(\Omega)$, $E_{2\theta}(\Omega)$ are simulated complex electric fields along θ and φ radiated by the antenna fed by two different ports. The solid angle Ω is defined by $\theta[0:\pi]$ in elevation and $\varphi[0:2\pi]$ in azimuth. $p_\theta(\Omega)$ and $p_\varphi(\Omega)$ are the Angle-of-Arrival (AoA) distributions of incoming waves. The parameter XPD is the cross-polarization discrimination of the incident field and is defined as $\mathrm{XPD} = S_\theta/S_\varphi$ (where S_θ and S_φ represent the average power along the spherical coordinates θ and φ).

The environment depends strongly on the angles of arrival distribution and on XPD. The most common distributions proven by measurements are Gaussian (G) and Laplacian (L) distributions [14]. Thus, we consider different distributions in elevation, while in azimuth plane (XY plane) the distribution is uniform, as demonstrated by two measurement campaigns in the literature [14, 15].

To obtain more realistic results, different environments are considered. Each environment is characterized by typical values of XPD, mean angle of incident wave distribution (θ_i), and standard deviation of wave distribution (σ) [16]. These values were deduced from several measurements [14–16] for different environments: isotropic, indoor, and outdoor. The isotropic environment is defined by XPD = 0 dB, $p_\theta(\Omega) = p_\varphi(\Omega) = 1$, the indoor (In) environment by XPD = 1 dB, $\theta_i = 20^\circ$, $\sigma = 30^\circ$, and the outdoor (Out) environment by XPD = 5 dB, $\theta_i = 10^\circ$, $\sigma = 15^\circ$.

As antennas will be implemented on a mobile terminal, a study of the effect of the antennas orientation on the correlation has been done. Three configurations of rotations have been studied: rotation of antenna around axis A, and around axis B for two initial positions: horizontal and vertical, as shown in Figure 11.

For each configuration, the envelope correlation coefficient for the three meander bend endings antennas with added ground plane and slot has been calculated from simulated radiation patterns. Minimum and maximum values at center frequencies of the two bands 777 MHz and 2.6 GHz are reported in Table 1.

For isotropic environment, a very low correlation is observed, in the two bands as a result of good matching ($|S_{11}| < -10$ dB), a high isolation level ($|S_{21}| < -10$ dB), and orthogonality between radiation patterns especially in the lower band. In addition, polarization diversity is naturally achieved because of the orthogonal positions of both antennas.

For the other cases, maximum values of the correlation envelope coefficient ρ_e are close to 0.5 for outdoor environment, whatever the distribution. Indeed, the incoming waves are mainly along E_θ which implies less diversity in some antenna's position.

When XPD gets close to 0 dB (indoor environment: XPD = 1 dB), E_θ and E_φ values are almost the same. Because these two components are uncorrelated by definition and because each antenna receives preferentially one of each component, the correlation is getting low.

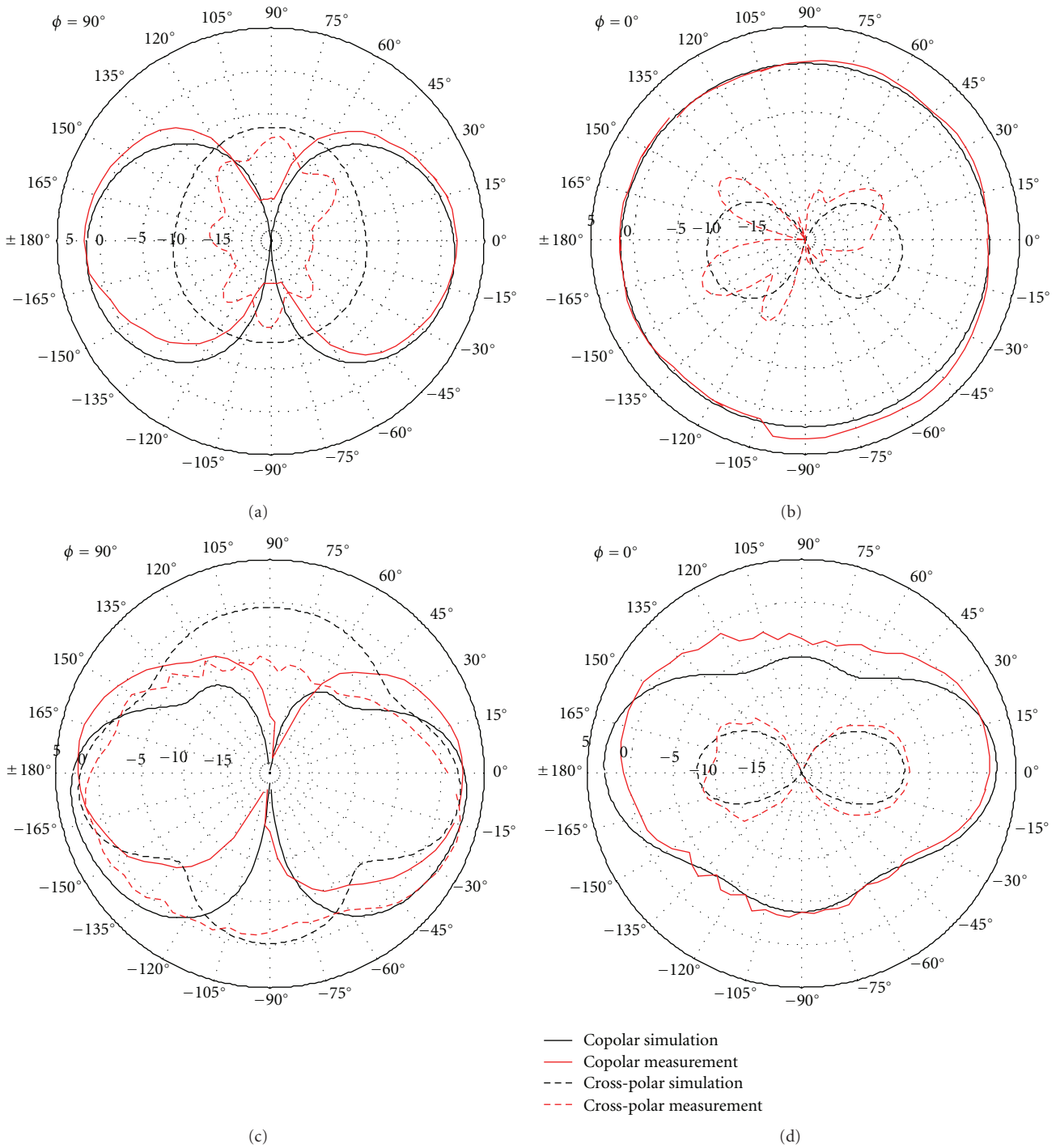

Figure 9: Simulated and measured radiation patterns for port 1 (dB): (a) in the E plane (YZ plane) at 778 MHz, (b) in the H plane (XZ plane) at the 778 MHz, (c) in the E plane (YZ plane) at 2.6 GHz, and (d) in the H plane (XZ plane) at 2.6 GHz.

For rotation around axis A, minimum values of ρ_e are obtained for position at which one antenna receives only E_θ component of the incoming waves while the other one only E_φ component.

For rotation around axis B, for both configurations (b and c), minimum values are obtained when the two radiating elements are positioned on AB plane. Indeed, at these positions, the radiation diversity is exploited as shown in Figure 10, and thus a low correlation is obtained.

Finally, for most configurations, envelope correlation coefficient is less than 0.5 which provides high diversity capabilities [13]. This result has been achieved thanks to the two orthogonal and identical antennas which are spatially separated. It can provide for either or both spatial

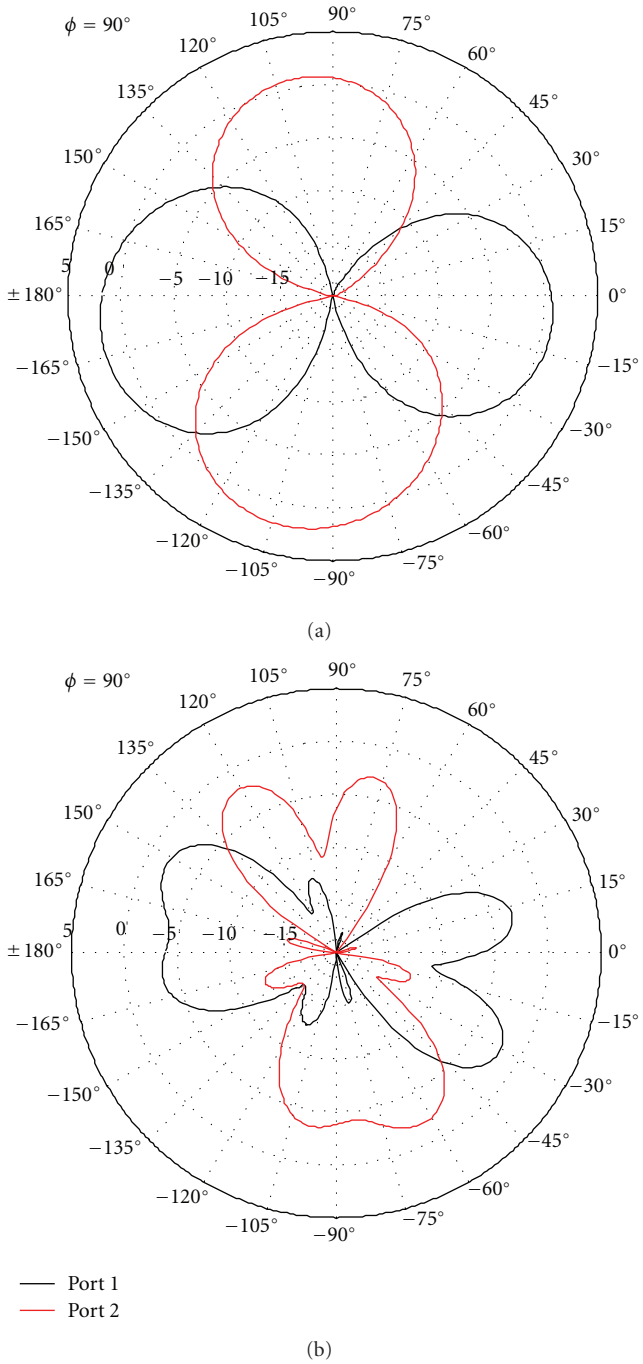

Figure 10: Simulated realized gain (dB) on the XY plane for the two bands: (a) at 778 MHz (b) at 2.6 GHz.

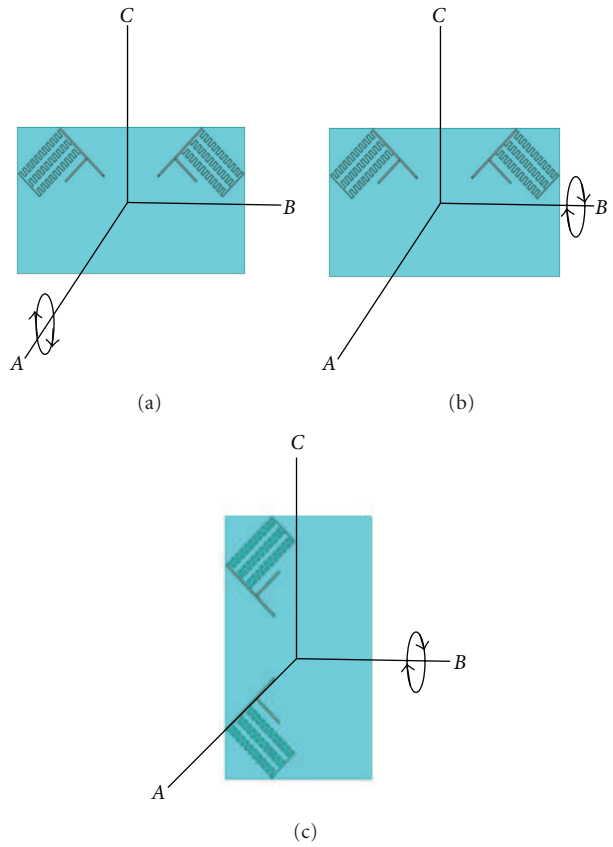

Figure 11: Rotation of antenna: (a) around axis A, (b) around axis B (horizontal antenna position), and (c) around axis B (vertical antenna position).

and pattern diversity. In addition, polarization diversity is available in the Z-direction.

In the following part, we evaluate the MEG which was introduced by Taga [17]. It is defined as the ratio between the mean received power of antennas over the random route and the total mean incident power. When each monopole receives the same quantity of power, the MEG ratio (R) of the two antennas is equal to one, which means that no performance deterioration is expected due to some power imbalance [18].

The mathematical expression is given by the following equation:

$$\mathrm{MEG} = \int_{\Omega} \left(\frac{\mathrm{XPD}}{\mathrm{XPD}+1} G_{\theta} P_{\theta} + \frac{1}{\mathrm{XPD}+1} G_{\varphi} P_{\varphi} \right) d\Omega, \quad (2)$$

where G_{θ} and G_{φ} are the θ and φ components of the antenna power gain pattern, respectively. The calculated mean effective gains of the monopoles from simulated radiation patterns at 777 MHz and 2.6 GHz are presented in Table 2.

The Maximum values of the ratio (R) of MEG_1, determined at port 1, over MEG_2, determined at port 2, are equal to 1, which satisfy an equal contribution of the two monopoles to receive the same quantity of power. The proposed structure is completely symmetric, and the Gaussian and Laplacian angular distributions are taken only along the elevation as presented in [15]. In addition, the incident power in the outdoor environment (or indoor) is concentrated around 10° (or 20°) above the horizon with an aperture of 30° (or 60°), and for these directions both antennas receive an equal amount of power.

Minimum values of ratio (R) are obtained for positions at which the E_{θ} (or E_{φ}) components of the two antennas have different levels in the directions of incident power.

Table 1: Coefficients of correlation for the two bands for all environments of the proposed structure.

Rotation	Distribution	777 MHz		2.6 GHz	
		$\rho_{e\min}$	$\rho_{e\max}$	$\rho_{e\min}$	$\rho_{e\max}$
Whatever	Isotropic	7.10^{-5}		4.10^{-3}	
around *A*	G-In	0.02	0.10	10^{-3}	0.08
	G-Out	0.20	0.42	7.10^{-4}	0.39
	L-In	0.07	0.16	10^{-5}	0.22
	L-Out	0.26	0.49	3.10^{-4}	0.51
around *B* (horizontal position)	G-In	7.10^{-4}	0.10	5.10^{-4}	8.10^{-3}
	G-Out	10^{-3}	0.42	4.10^{-5}	1.10^{-2}
	L-In	2.10^{-3}	0.16	10^{-5}	3.10^{-3}
	L-Out	3.10^{-3}	0.46	10^{-4}	5.10^{-3}
around *B* (vertical position)	G-In	5.10^{-5}	0.05	2.10^{-4}	0.07
	G-Out	10^{-4}	0.40	4.10^{-3}	0.39
	L-In	2.10^{-4}	0.10	8.10^{-5}	0.22
	L-Out	6.10^{-4}	0.49	7.10^{-4}	0.54

Table 2: MEG ratio (R) for the two bands for all environments of the proposed structure.

Rotation	Distribution	777 MHz		2.6 GHz	
		$R_{\min}$	$R_{\max}$	$R_{\min}$	$R_{\max}$
Whatever	Isotropic	1		1	
around *A*	G-In	0.70	1	0.78	1
	G-Out	0.35	1	0.71	1
	L-In	0.63	1	0.46	1
	L-Out	0.30	1	0.58	1
around *B* (horizontal position)	G-In	0.99	1	0.99	1
	G-Out	0.97	1	0.98	1
	L-In	0.99	1	0.99	1
	L-Out	0.96	1	0.98	1
around *B* (vertical position)	G-In	0.94	1	0.80	1
	G-Out	0.84	1	0.63	1
	L-In	0.85	1	0.33	1
	L-Out	0.70	1	0.48	1

For example, if antenna 1 presents a low E_θ component where antenna 2 a high one, an unbalanced power is obtained.

For most configurations, ratio (R) is greater than 0.5 which is acceptable to provide high diversity capabilities [18].

5. Conclusion

In this paper, a compact dual-band, dual-polarized antenna for LTE applications is proposed, with an extension of the lower band towards TV White Space band, to provide radio-cognitive capabilities to the terminal. A design provides dual polarizations in both of the bands: 700–862 MHz and 2.5–2.69 GHz with good impedance matching ($|S_{11}| < -10$ dB).

Measurement results are in good agreement with simulated ones. In addition, good performances are obtained by calculating the envelope correlation coefficient and the MEG ratio for several antennas' positions in different environments: isotropic, indoor, and outdoor. For most configurations, it is found that the system satisfies the condition $\rho_e < 0.5$ and $\mathrm{MEG}_1/\mathrm{MEG}_2 > 0.5$. Thus, the presented design is suitable for MIMO communication applications, and thus enables the SNR value at the terminal side to be maximized.

Acknowledgment

The research leading to these results has received funding from the European Community's Seventh Framework Program (FP7/2007–2013) under Grant agreement SACRA no. 249060.

References

[1] 3rd Generation Partnership Project, Technical Specification Group Radio Access Network, Evolved Universal Terrestrial Radio Access (E-UTRA) Radio Resource Control (RRC), Protocol Specification, 3GPP TS 36. 331.

[2] R. G. Vaughan, "Polarization diversity in mobile communications," *IEEE Transactions on Vehicular Technology*, vol. 39, no. 3, pp. 177–186, 1990.

[3] K. Ogawa and T. Uwano, "Diversity antenna for very small 800-MHz band portable telephones," *IEEE Transactions on Antennas and Propagation*, vol. 42, no. 9, pp. 1342–1345, 1994.

[4] J. W. Wallace, M. A. Jensen, A. L. Swindlehurst, and B. D. Jeffs, "Experimental characterization of the MIMO wireless channel: data acquisition and analysis," *IEEE Transactions on Wireless Communications*, vol. 2, no. 2, pp. 335–343, 2003.

[5] S. Hienonen, A. Lehto, and A. V. Raisanen, "Simple broadband dual-polarized aperture-coupled microstrip antenna," in *Proceedings of the IEEE Antennas and Propagation Society International Symposium*, vol. 2, pp. 1228–1231, Orlando, Fla, USA, August 1999.

[6] P. Brachat and J. M. Baracco, "Printed radiating element with two highly decoupled input ports," *Electronics Letters*, vol. 31, no. 4, pp. 245–246, 1995.

[7] Y. L. Kuo and K. L. Wong, "Dual-polarized monopole antenna for WLAN application," in *Proceedings of the IEEE Antennas*

and Propagation Society International Symposium, vol. 4, pp. 80–83, June 2002.

[8] C. Yang, Y. Yao, J. Yu, and X. Chen, "Novel compact multiband MIMO antenna for mobile terminal," *International Journal of Antennas and Propagation*, vol. 2012, Article ID 691681, 9 pages, 2012.

[9] T. W. Chiou and K. L. Wong, "A compact dual-band dual-polarized patch antenna for 900/1800-MHz cellular systems," *IEEE Transactions on Antennas and Propagation*, vol. 51, no. 8, pp. 1936–1940, 2003.

[10] K. S. Kim, T. Kim, and J. Choi, "Dual-frequency aperture-coupled square patch antenna with double notches," *Microwave and Optical Technology Letters*, vol. 24, no. 6, pp. 370–374, 2000.

[11] SACRA European Project, (FP7/ 2007–2013), http://www.ict-sacra.eu/.

[12] K. J. Kim, W. G. Lim, and J. W. Yu, "High isolation internal dual-band planar inverted-F antenna diversity system with band-notched slots for MIMO terminals," in *Proceedings of the 36th European Microwave Conference (EuMC'06)*, pp. 1414–1417, Manchester, UK, September 2006.

[13] R. G. Vaughan and J. B. Andersen, "Antenna diversity in mobile communication," *IEEE Transactions on Vehicular Technology*, vol. 36, no. 4, pp. 149–172, 1987.

[14] K. Kalliola, K. Sulonen, H. Laitinen, O. Kivekäs, J. Krogerus, and P. Vainikainen, "Angular power distribution and mean effective gain of mobile antenna in different propagation environments," *IEEE Transactions on Vehicular Technology*, vol. 51, no. 5, pp. 823–838, 2002.

[15] F. Adachi, M. T. Feeney, A. G. Williamson, and J. D. Parsons, "Crosscorrelation between the envelopes of 900 MHz signals received at a mobile radio base station site," *Proceedings of IEE on Communications, Radar and Signal Processing Part F*, vol. 133, no. 6, pp. 506–512, 1986.

[16] Z. Ying, T. Bolin, V. Plicanic, A. Derneryd, and G. Kristensson, "Diversity antenna terminal evaluation," in *Proceedings of the IEEE Antennas and Propagation Society International Symposium and USNC/URSI Meeting*, pp. 375–378, July 2005.

[17] T. Taga, "Analysis for mean effective gain of mobile antennas in land mobile radio environments," *IEEE Transactions on Vehicular Technology*, vol. 39, no. 2, pp. 117–131, 1990.

[18] W. C. T. Brown, *Antenna diversity for mobile terminal [Ph.D. thesis]*, University of Surrey, 2002, http://epubs.surrey.ac.uk/2125/.

Hindawi Publishing Corporation
International Journal of Antennas and Propagation
Volume 2012, Article ID 513829, 6 pages
doi:10.1155/2012/513829

Research Article

Band-Notched Ultrawide Band Planar Inverted-F Antenna

H. T. Chattha,[1] M. K. Ishfaq,[2] Y. Saleem,[3] Y. Huang,[4] and S. J. Boyes[4]

[1] *Department of Electrical Engineering, University of Engineering and Technology Lahore, Faisalabad Campus, Faisalabad, Pakistan*
[2] *Department of Electrical Engineering, GC University, Faisalabad, Pakistan*
[3] *Department of Computer Science and Engineering, University of Engineering and Technology Lahore, Pakistan*
[4] *Department of Electrical Engineering and Electronics, University of Liverpool, Liverpool L69 3GJ, UK*

Correspondence should be addressed to H. T. Chattha, chattha43@hotmail.com

Received 25 February 2012; Accepted 9 April 2012

Academic Editor: Minh-Chau Huynh

A novel ultrawide band planar inverted-F antenna with band-notched characteristics is presented in this paper. The planar inverted-F antenna uses two parasitic elements to enhance the bandwidth to cover the ultrawide band. The band-notched feature is added by inserting a W-shaped slot on the top radiating element of the antenna with a band rejection from 5.08 to 6 GHz (measured). Both the measured and simulated results are obtained to draw the conclusions.

1. Introduction

A considerable amount of research has been conducted for developing the ultrawide band (UWB) antennas for its characteristics such as high data rate, being low power, and having wide bandwidths, and simple hardware structure in many real world applications. In 2002, Federal Communications Commission (FCC) of USA allocated a bandwidth from 3.1 GHz to 10.6 GHz to ultrawide band [1]. This band also covers the bands of the previously present wireless networks with standards such as IEEE 802. 11a in USA (5.15–5.35 GHz, 5.725–5.825 GHz), HIPERLAN/2 in Europe (5.15–5.35 GHz, 5.47–5.725 GHz), and Microwave Access (WiMAX) system (5.25–5.825 GHz) [2, 3]. To avoid the interference between these UWB systems and the nearby communication systems such as wireless (WLAN), there is a need to employ some form of filter. In order to save the space and cost and reduce the complexity of the UWB system, this filter should ideally be integrated into the radiating element of the antenna. To tackle this issue, many printed type of antennas with band-notched characteristics have been presented [2–10]. All these antennas have almost omnidirectional radiation patterns; however, some UWB applications require antennas with comparatively higher directivity.

The planar inverted-F antenna (PIFA) is now widely used in mobile and portable radio applications due to its simple design, lightweight, low cost, conformal nature, reliable performance, and attractive radiation pattern [11–14]. The PIFA has higher directivity as compared to the planar monopole antennas which makes it more suitable for certain UWB applications [15]. PIFA was previously known as an antenna having narrow-band characteristics and a reasonable research is already done to enhance its impedance bandwidth [16–18]. Feik et al. have shown in [19] that the fractional impedance bandwidth up to about 25% can be obtained by having different shapes of feed plates. Recently, some UWB PIFA antennas are introduced [20, 21] and one band-notched UWB PIFA is introduced using a spiral slot [22] on the feed plate. However, the UWB PIFAs presented in the [21, 22] have height $h = 7.5$ mm which is relatively high and also it has two PIFA antennas (one on each edge of the ground plane) to cover the whole UWB band which makes it very difficult to integrate with other PCB components. This paper presents a single-element band-notched UWB PIFA for height $h = 4.5$ mm by introducing a W-shaped slot on the top radiating plate.

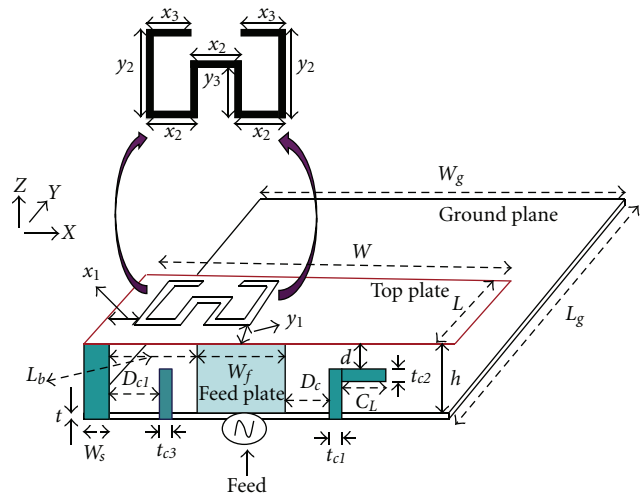

Figure 1: PIFA geometry.

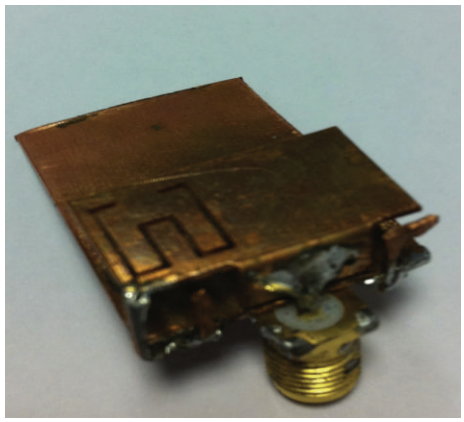

Figure 2: The built PIFA with SMA connector.

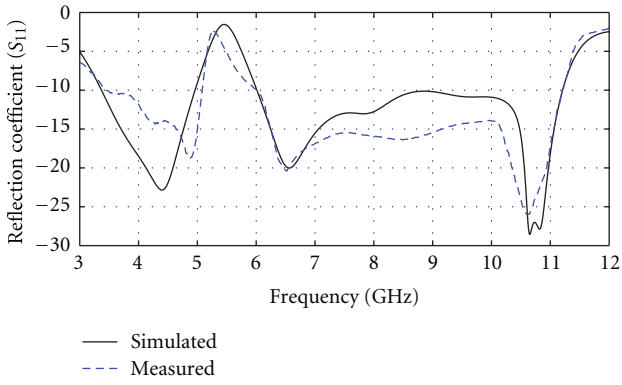

Figure 3: Ref. coefficients S_{11} (dB) versus frequency (GHz).

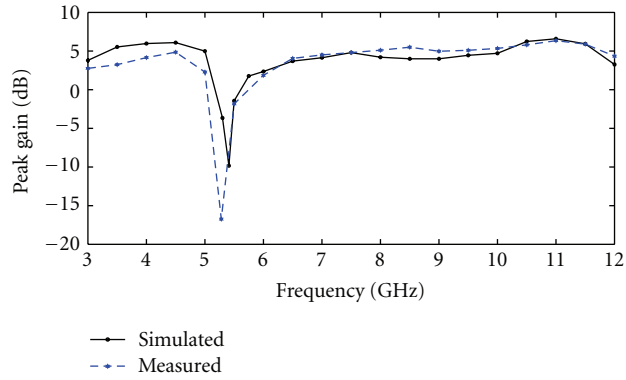

Figure 4: Simulated peak gain (dB) versus frequency (GHz).

2. Antenna Configurations

The structure of the designed PIFA as shown in Figure 1 has a radiating top plate with dimensions of width W and length L and W_g and L_g are width and length of the ground plane. The dimensions of the shorting and feeding plates are $W_s \times (h+t)$ and $W_f \times h$, respectively, having a horizontal distance of L_b between them and h is the height of the antenna having air in the space between the top plate and the substrate. The distance of the parasitic element having a shape of an inverted-L from the feeding plate is D_c. This parasitic element has a thickness of t_{c1}. The horizontal extension of this element is C_L having a thickness of t_{c2}. Second parasitic element rectangular in shape is inserted at the upper edge of the ground plane at a distance D_{c1} from the shorting plate. The width of this element is t_{c3}. The heights of both the parasitic elements are the same and is equal to $(h + t) - d$ having a vertical distance of d between the elements and the radiating plate. The W-shaped slot on the top plate is inserted at a distance x_1 from the side edge and at a distance of y_1 from the upper edge of the top plate. The W-shaped slot is shown separately in Figure 1 to highlight its dimensions. The thickness of the slot is 0.5 mm. The feeding to the PIFA is provided by a coaxial cable with an SMA connector as shown in Figure 2.

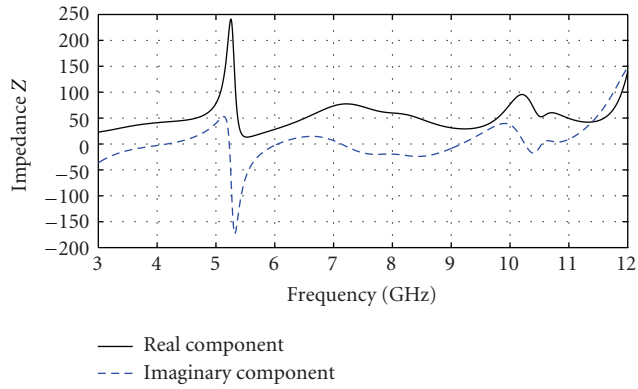

Figure 5: Impedances $Z(\Omega)$ versus frequency (GHz).

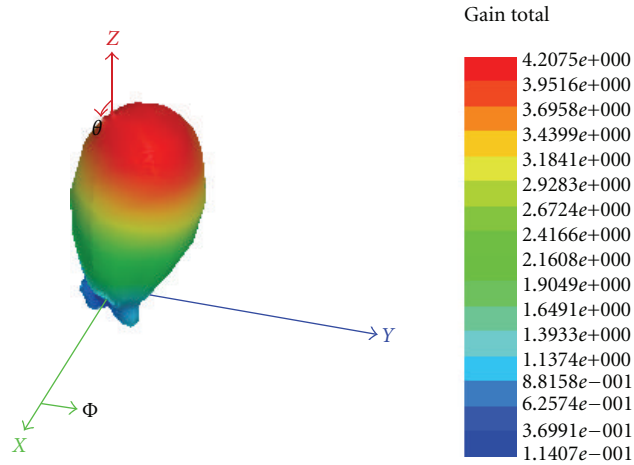

Figure 6: Simulated 3D radiation pattern of PIFA at 7.5 GHz.

3. Results

The optimization of the entire antenna parameters is performed through parametric study in high frequency structure simulator (HFSS) in order to get the maximum impedance bandwidth and feed is provided at the upper edge of the ground plane. The optimized values of all the parameters are found as follows: $W_g = 18.5$ mm, $h = 4.5$ mm, $L_g = 28$ mm, $W = 18.5$ mm, $L = 10$ mm, $W_f = 8.5$ mm, $W_s = 0.5$ mm, $L_b = 5.5$ mm, $D_c = 0.5$ mm, $D_{c1} = 0.07\lambda = 3$ mm, $t_{c1} = t_{c2} = t_{c3} = 0.5$ mm, d $= 0.5$ mm, $(h + t) - d = 5$ mm, $C_L = 2.5$ mm, $x_1 = 1$ mm, $y_1 = 1$ mm, $x_2 = 2.5$ mm, $x_3 = 2$ mm, $y_1 = 1$ mm, $y_2 = 7.5$ mm, and $y_3 = 4.2$ mm.

The simulated and experimental results of the reflection coefficient are shown in Figure 3. It is evident that the bandwidth achieved by these techniques of inserting parasitic elements for $S_{11} < -10$ dB is extremely broad from about 3.4 to 11.2 GHz. The lower frequency and first resonance is controlled by the main structure of PIFA, whereas the insertion of inverted-L-shaped parasitic element creates a second resonance at 6.5 GHz, and the presence of rectangular-shaped parasitic element produces a third resonance around 10.7 GHz (simulated). Due to the insertion of W-shaped slot, band-notched characteristics are introduced with a band rejection from 5.08 to 6 GHz (measured). The simulated and measured results are generally in good agreement. Their differences are mainly due to the cables and connectors which are not being involved in the simulations but exist in the measurements and the manufacturing tolerance in getting the accurate parameters in the manual fabrication of this antenna. Figure 4 shows the simulated and measured peak gain of the band-notched PIFA as a function of frequency in GHz. A sharp decrease in peak gain is observed in the notched frequency band centered at around 5.3 GHz (measured) which confirms that this antenna provides a good level of rejection to signals at frequencies within the notched band. The impedance Z of this PIFA versus the frequency in GHz is shown in Figure 5 to get a better understanding of this antenna.

The simulated 3D radiation pattern (polar plot) of the band-notched PIFA at 7.5 GHz is shown in Figure 6 and the measured 2D radiation patterns of this antenna are shown in Figure 7. Figure 8 shows the simulated time-domain response of the PIFA to an input pulse which affirms the suitability of the PIFA for UWB applications.

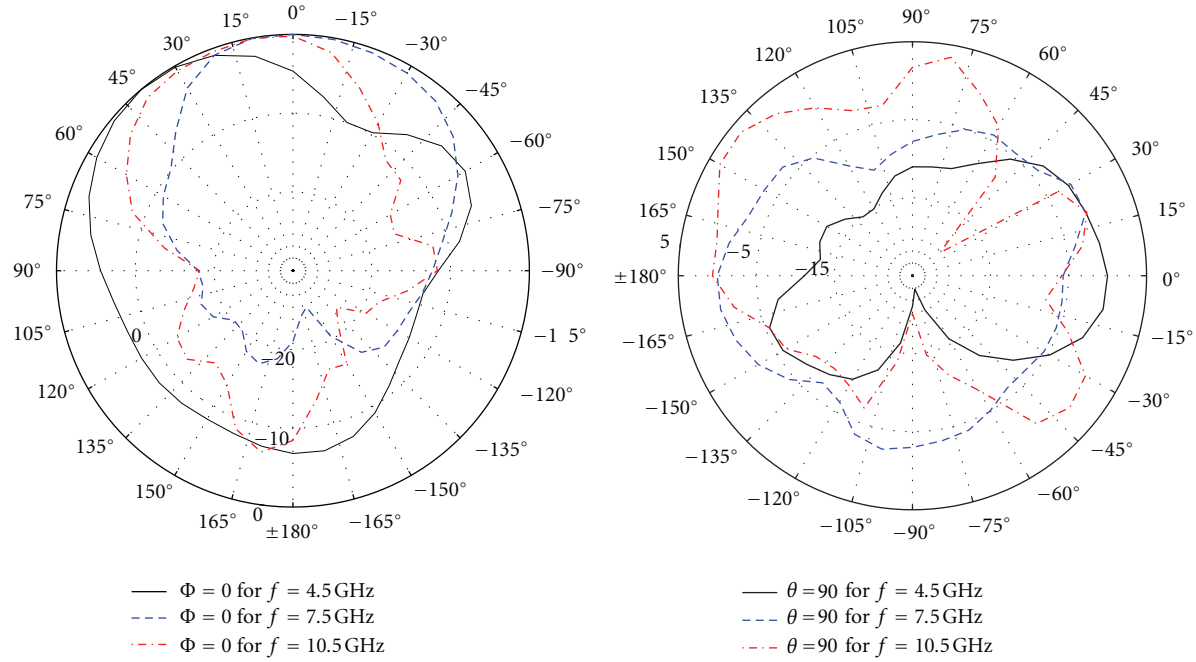

(a) (b)

Figure 7: (a) 2D rad. pattern with total gain in dB for elevation XZ plane ($\Phi = 0^\circ$) for diff. frequencies, (b) 2D rad. pattern with total gain in dB for azimuth XY plane ($\theta = 90^\circ$) for different frequencies.

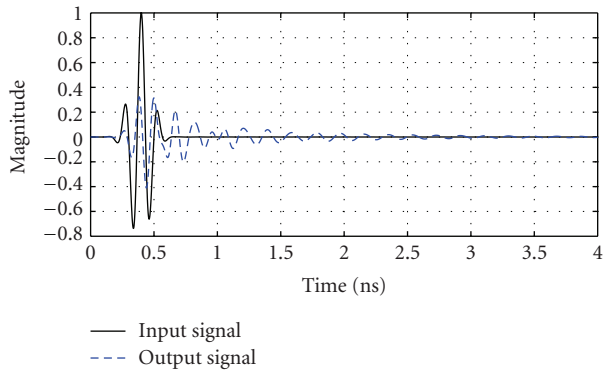

Figure 8: The time domain response of PIFA.

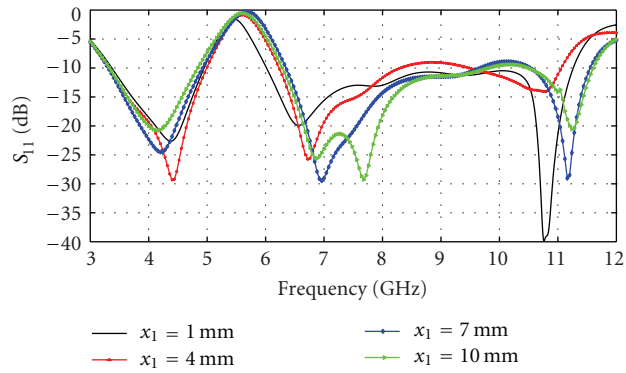

Figure 9: Simulated S_{11} (dB) for values of x_1 versus frequency (GHz).

4. Parametric Study

The parameters of the W-shaped slot are varied to observe its effects on the band-notched characteristics of the PIFA antenna. The distance x_1 from the side edge of the top plate is varied from 1 mm to 10 mm while all other parameters are held constant. Figure 9 shows the variation of x_1 versus the frequency in GHz which makes it obvious that position of the W-slot on the top plate does not significantly affects the notched band of the PIFA but significantly affects the performance of PIFA over the UWB band.

Similarly the length of the outer legs of the W-shaped slot y_2 is varied from 5 mm to 7 mm to observe its effects. Figure 10 shows that varying the length y_2 changes the band which is notched by the insertion of W-shaped slot whereas it does not significantly affect the performance of the PIFA over the UWB band. Therefore, we can vary the length y_2 to change the band to be notched. In the similar way, the length of the inner legs of the W-shaped slot y_3 is also varied from 2 mm to 6 mm to observe its effects on the performance of the W-shaped slot and on the overall performance of the PIFA. It is obvious as shown in Figure 11 that the length y_3 is very critical parameter to decide which band is exactly to be notched. Varying the length y_3 also varies the performance of the PIFA over the UWB band. Therefore, an appropriate and optimized value of y_3 is required to get the exact band

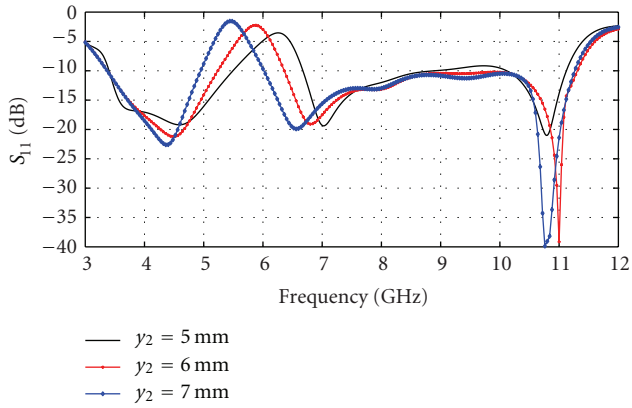

FIGURE 10: Simulated S_{11} (dB) for values of y_2 versus frequency (GHz).

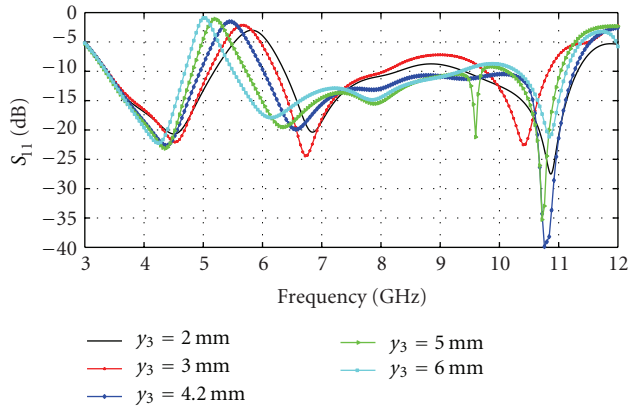

FIGURE 11: Simulated S_{11} (dB) for values of y_3 versus frequency (GHz).

to be notched by the W-shaped slot and also to achieve the reflection coefficient below −10 dB over the UWB band.

5. Conclusions

A band-notched UWB PIFA antenna is presented in this paper. It has been shown that a very wide bandwidth is achieved which almost covers the whole UWB band from 3.4 to 11.2 GHz and a band rejection from 5.08 to 6 GHz is achieved by inserting a W-shaped slot on the top plate.

References

[1] "FCC first report and order on ultra-wideband technology," February 2002.

[2] Y. D. Dong, W. Hong, Z. Q. Kuai et al., "Development of ultrawideband antenna with multiple band-notched characteristics using half mode substrate integrated waveguide cavity technology," *IEEE Transactions on Antennas and Propagation*, vol. 56, no. 9, pp. 2894–2902, 2008.

[3] Q. X. Chu and Y. Y. Yang, "A compact ultrawideband antenna with 3.4/5.5 GHz dual band-notched characteristics," *IEEE Transactions on Antennas and Propagation*, vol. 56, no. 12, pp. 3637–3644, 2008.

[4] J. R. Kelly, P. S. Hall, and P. Gardner, "Planar band-notched UWB antenna," in *Proceedings of the 3rd European Conference on Antennas and Propagation (EuCAP '09)*, pp. 1636–1639, March 2009.

[5] Y. J. Cho, K. H. Kim, D. H. Choi, S. S. Lee, and S. O. Park, "A miniature UWB planar monopole antenna with 5-GHz band-rejection filter and the time-domain characteristics," *IEEE Transactions on Antennas and Propagation*, vol. 54, no. 5, pp. 1453–1460, 2006.

[6] A. J. Kerkhoff and H. Ling, "Design of a band-notched planar nonopole antenna using genetic algorithm optimization," *IEEE Transactions on Antennas and Propagation*, vol. 55, no. 3, pp. 604–610, 2007.

[7] S. J. Wu, C. H. Kang, K. H. Chen, and J. H. Tarng, "Study of an ultrawideband monopole antenna with a band-notched open-looped resonator," *IEEE Transactions on Antennas and Propagation*, vol. 58, no. 6, pp. 1890–1897, 2010.

[8] J. Qiu, Z. Du, J. Lu, and K. Gong, "A planar monopole antenna design with band-notched characteristic," *IEEE Transactions on Antennas and Propagation*, vol. 54, no. 1, pp. 288–292, 2006.

[9] W. S. Lee, W. G. Lim, and J. W. Yu, "Multiple band-notched planar monopole antenna for multiband wireless systems," *IEEE Microwave and Wireless Components Letters*, vol. 15, no. 9, pp. 576–578, 2005.

[10] S. W. Qu, J. L. Li, and Q. Xue, "A band-notched ultrawideband printed monopole antenna," *IEEE Antennas and Wireless Propagation Letters*, vol. 5, no. 1, pp. 495–498, 2006.

[11] K. Hirasawa and M. Haneishi, *Analysis, Design, and Measurement of Small and Low-Profile Antennas*, Artech House, 1992.

[12] K. L. Virga and Y. Rahmat-Samii, "Low-profile enhanced-B and width PIFA antennas for wireless communications packaging," *IEEE Transactions on Microwave Theory and Techniques*, vol. 45, no. 10, pp. 1879–1888, 1997.

[13] P. S. Hall, E. Lee, and C. T. P. Song, "Planar inverted-F antennas, chapter 7," in *Printed Antennas for Wireless Communications*, R. Waterhouse, Ed., John Wiley & Sons, 2007.

[14] Y. Huang and K. Boyle, *Antennas: from Theory to Practice*, John Wiley & Sons, 2008.

[15] H. T. Chattha, Y. Huang, M. K. Ishfaq, and S. J. Boyes, "A comprehensive parametric study of planar inverted-F antenna," *Scientific Research Wireless Engineering and Technology*, vol. 3, no. 1, pp. 1–11, 2012.

[16] D. Liu and B. Gaucher, *The Inverted-F Antenna Height Effects on Bandwidth*, IEEE, IBM T. J. Watson Research Centre, Yorktown Heights, NY, USA, 2005.

[17] F. Wang, Z. Du, Q. Wang, and K. Gong, "Enhanced-bandwidth PIFA with T-shaped ground plane," *Electronics Letters*, vol. 40, no. 23, pp. 1504–1505, 2004.

[18] P. W. Chan, H. Wong, and E. K. N. Yung, "Wideband planar inverted-F antenna with meandering shorting strip," *Electronics Letters*, vol. 44, no. 6, pp. 395–396, 2008.

[19] R. Feick, H. Carrasco, M. Olmos, and H. D. Hristov, "PIFA input bandwidth enhancement by changing feed plate silhouette," *Electronics Letters*, vol. 40, no. 15, pp. 921–923, 2004.

[20] H. T. Chattha, Y. Huang, Y. Lu, and X. Zhu, "An ultra-wideband planar inverted-F antenna," *Microwave and Optical Technology Letters*, vol. 52, no. 10, pp. 2285–2288, 2010.

[21] C. H. See, R. A. Abd-Alhameed, D. Zhou, H. I. Hraga, P. S. Excell, and M. B. Child, "Ultra-wideband planar inverted FF antenna," *Electronics Letters*, vol. 46, no. 8, pp. 549–550, 2010.

[22] H. I. Hraga, C. H. See, R. A. Abd-Alhameed et al., "PIFA antenna for UWB applications with WLAN band rejection using spiral slots," in *Proceedings of the 5th European Conference on Antennas and Propagation (EUCAP '11)*, pp. 2226–2229, April 2011.